AFFDL-TR-67-60

AERODYNAMIC DEPLOYABLE DECELERATOR PERFORMANCE-EVALUATION PROGRAM

PHASE III

P. BLOETSCHER
W. V. ARNOLD

GOODYEAR AEROSPACE CORPORATION

TECHNICAL REPORT AFFDL-TR-67-60

OCTOBER 1967

AIR FORCE FLIGHT DYNAMICS LABORATORY
RESEARCH AND TECHNOLOGY DIVISION
AIR FORCE SYSTEMS COMMAND
WRIGHT-PATTERSON AIR FORCE BASE, OHIO

NOTICE

When Government drawings, specifications, or other data are used for any purpose other than in connection with a definitely related Government procurement operation, the United States Government thereby incurs no responsibility nor any obligation whatsoever; and the fact that the Government may have formulated, furnished, or in any way supplied the said drawings, specifications, or other data, is not to be regarded by implication or otherwise as in any manner licensing the holder or any other person or corporation, or conveying any rights or permission to manufacture, use, or sell any patented invention that may in any way be related thereto.

Copies of this report should not be returned unless return is required by security considerations, contractual obligations, or notice on a specific document.

200 - November 1967 - CO455 - 15-304

AFFDL-TR-67-60

AERODYNAMIC DEPLOYABLE DECELERATOR PERFORMANCE-EVALUATION PROGRAM

PHASE III

F. BLOETSCHER

W. V. ARNOLD

FOREWORD

The work described in this report was performed by Goodyear Aerospace Corporation, Akron, Ohio, under the authority of Project 6065, Task 606507, entitled "Aerodynamic Deployable Decelerator Performance Evaluation Program, Phase I" and Air Force Contract No. AF33(615)-2541.

Mr. S. McFarland and Mr. W. R. Pinnell of the Air Force Flight Dynamics Laboratory, Research and Technology Division, served as contract monitors.

The authors and contributing personnel of Goodyear Aerospace Corporation were W. V. Arnold, project engineer; F. Bloetscher, decelerator evaluation; A. C. Aebisher, field test; I. M. Jaremenko, aerodynamic analysis; W. W. Sowa, thermal analysis; R. E. Aitgelt, data analysis; J. Schlemmer, trajectory analysis; W. A. Barr, decelerator design; and R. G. Slayman, materials.

Goodyear Aerospace wishes to acknowledge the support and technical information supplied by the following Recovery and Crew Station personnel: Mr. S. R. Metres and Mr. W. R. Pinnell.

The contractor's number for the report is GER-12909.

The manuscript was released by the authors June 1967 for publication as an RTD technical report.

This technical report has been reviewed and is approved.

GEORGE A. SOLT, JR.
Chief, Recovery & Crew Station Branch
Vehicle Equipment Division
AF Flight Dynamics Laboratory

ABSTRACT

The Aerodynamic Deployable Decelerator Performance-Evaluation Program (ADDPEP) has aimed to advance the state of the art by developing the most effective analytical and empirical techniques for designing aerodynamic deployable decelerators and for evaluating these engineering techniques through wind-tunnel and free-flight tests. During the third and concluding phase of ADDPEP, two types of decelerators were investigated: large reefed supersonic parachutes and small supersonic parachutes. The areas investigated by tests included analytical and engineering design methods, material capabilities, and fabrication techniques.

Three large parachutes were built that had the same basic configuration: hemisflo, 16-ft-diameter canopy, 10-percent extended skirt, 10-percent porosity. These parachutes were designed for 200,000-lb opening loads. Free-flight tests were performed at deployment Mach numbers of 2.22, 1.20, and 2.70; at altitudes of 18,050, 9370, and 19,700 ft; and at dynamic pressures of 3697, 1514, and 5155 psf, respectively. The tests confirmed the predicted drag area. However, reefing line loads were underestimated; improved analytical methods are needed to predict this hoop-type load under dynamic conditions at the higher Mach numbers.

Three small parachutes were built that had the same basic configuration, designated PARASONIC: 4-ft-diameter, 5-percent total porosity. Wind-tunnel tests confirmed that this PARASONIC design, when constructed of materials that are compatible with the flight environments investigated, has better stability than a HYPERFLO design that was also investigated in both Phases I and II. Free-flight tests were performed at deployment Mach numbers of 2.70, 1.60, and 5.48; at altitudes of 78,000, 56,300, and 117,000 ft; and at dynamic pressures of 329, 328, 229 psf, respectively. The flight tests confirmed the stability predictions and the adequacy of the construction for the performance range investigated.

TABLE OF CONTENTS

TABLE OF CONTENTS

LIST OF ILLUSTRATIONS

LIST OF ILLUSTRATIONS

LIST OF TABLES

LIST OF TABLES

LIST OF SYMBOLS

1. GENERAL

A = area

A^* = area at sonic condition

A_e = exit area

A_i = inlet area

a = skirt camber (in.); velocity of sound (fps); acceleration (ft/sec^2)

b = skirt chord (in.)

C_D = drag coefficient

C_DA = drag area

C_{D_o} = drag coefficient based on nominal surface

C_p = pressure coefficient, external

C_{p_b} = pressure coefficient, external base

C_{p_e} = pressure coefficient, exit throat

C_{p_2} = pressure coefficient, internal static

$C_{p_{2c}}$ = pressure coefficient, external skirt

$C_{p_{2o}}$ = pressure coefficient, internal stagnation

C_{p_3} = pressure coefficient, internal at A_3

D = drag force

D_c = constructed diameter of canopy

D_i = inlet diameter of canopy

D_o = nominal diameter of canopy

D_p = projected diameter of canopy

F = force

F_m = mass acquisition force

F_{ms} = force in meridian strap

LIST OF SYMBOLS

g = gravitational constant (32 ft/sec^2)

K = parachute opening shock factor

K_{RIA} = reefing inlet area coefficient

K_{RLL} = reefing line length coefficient (ii)

L = airload

L_S = suspension line length

M = Mach number

$M_\infty, M1$ = Mach number, free stream

M_2 = Mach number, behind bow shock

M_c = Mach number, in parachute canopy

m = mass (slugs)

N_θ = meridian fabric stress (lb/in.)

N_β = circumferential fabric stress (lb/in.)

n = number of gores, suspension lines, or meridian straps

P = pressure across fabric (psf)

P_a = local static pressure (psf)

P_b = base pressure (psf)

P_s = stagnation pressure (psf)

P_1, p = static pressure (psf)

P_{2_0} = total static pressure (psf)

PAM = pulse amplitude modulation

pps = pulses per second

QE = quadrant elevation angle

q = dynamic pressure (psf)

q_∞ = dynamic pressure, free stream (psf)

R = geometrical radius

R_c = construction radius

LIST OF SYMBOLS

Re = Reynolds number

r_g = radius of gore lobe

S_o = canopy surface area

T = vehicle launch time

t = time

V = air velocity (fps)

v = volume

v_c = critical volume

v_s = specific volume

W = total weight

X, Y = components of parachute radial member

X, Z = canopy gore shaping coordinates

x, y = parachute shape coordinates

α_o = conical angle of attack

β = Mach parameter $\sqrt{M_1^2 - 1}$

ξ = inlet reefing ratio; reefed inlet area/constructed inlet area

ρ = density

ϕ = coordinate angle

2. THERMODYNAMIC

A = geometrical area

A^* = throat area

c^* = characteristic velocity (fps)

c = specific heat of material (Btu/lb-deg-F)

c_p = specific heat of gas (Btu/lb-deg-F)

D^* = throat diameter

g = gravitational constant (32.2 ft/sec^2)

LIST OF SYMBOLS

h_c = heat transfer coefficient (Btu/sq ft-hr-F)

i = (subscript) node number going from 2 through n

K = ratio of specific heats for air (1.4)

k = thermal conductivity (Btu/ft-hr-F)

M_∞ = Mach number, free stream

Pr = Prandtl number

P_o = plenum pressure (psig)

P_1 = static pressure (mm Hg abs)

P_2 = stream pitot pressure (mm Hg abs)

P_t = total pressure

Q_{eff} = effective capacity (Btu/lb)

$\dot{q}$ = heat flux rate (Btu/sq ft-sec)

$\dot{q}_{cw}$ = cold wall heat flux rate (Btu/sq ft-sec)

r = geometrical radius

r_c = radius of curvature

r_g = radius of gore lobe

T = temperature

T_i' = previous node temperature

T_{t2} = total temperature

T_o = plenum air temperature

T_1 = surface temperature

T_2 = stream stagnation temperature

T_s = effective temperature of space

T_{aw} = adiabatic wall temperature

T_{cw} = cold wall surface temperature

T_w = surface temperature

t = thickness of material

LIST OF SYMBOLS

Z = altitude

α = thermal diffusivity (sq ft/hr)

ϵ = emissivity

μ = viscosity (lb-sec/sq ft)

ρ = material density (pcf)

σ = Stefan-Boltzman constant

τ = time

SECTION I

INTRODUCTION AND SUMMARY

1. BACKGROUND

The high speeds and altitudes associated with space flight require new methods of stabilization and deceleration for the recovery of manned escape capsules, of personnel ejected from these capsules, and of rocket boosters, nose cones, and instrument packages. Initial stabilization is required so that heat shields, as well as drag devices of payloads tumbling or disoriented in flight, can be aligned with the flightpath. Initial deceleration is required for the reduction of aerodynamic heating, loading, and velocity in a varying dynamic loading regime. Essentially, this is done by decreasing the weight-to-drag ratio (ballistic coefficient).

If parachutes or sophisticated deceleration devices, such as gliding and homing parachutes, paragliders, and expandable rotor blades, are to be used in the final stage, then the velocity of the payload must be reduced gradually to a dynamic pressure and a speed that will allow reliable deployment of the retardation devices. Missile and wind-tunnel tests show that conventional parachutes are not satisfactory for this first-stage deceleration because of aerodynamic heating and erratic loading under supersonic conditions.

These new requirements of high-speed recovery systems led to the Aerodynamic Deployable Decelerator Performance-Evaluation Program (ADDPEP) by the Air Force Flight Dynamics Laboratory (AFFDL), Research and Technology Division (RTD). The ADDPEP effort was conducted in three overlapping phases from May 1963 to July 1967:

Phase I - May 1963 to September 1964
Phase II - April 1964 to May 1967
Phase III - April 1965 to July 1967

References 1 and 2 are the final reports for Phases I and II. This publication is the final report for Phase III.

2. OBJECTIVES AND DECELERATOR TYPES

The overall objective of ADDPEP was to advance the state of the art by developing the most effective analytical and empirical techniques for (1) designing aerodynamic deployable decelerators and (2) evaluating these engineering techniques through wind-tunnel and free-flight tests. Three types of decelerators were assigned for investigation. These decelerators and their respective goals are:

1. Small supersonic parachute canopy - Goal: to establish the configuration, loadings, design, and structural materials needed to attain a stable performance for flight speeds up to Mach 5 and for dynamic pressures to 500 psf.

2. Large reefed supersonic parachute canopy - Goal: to establish the configuration, loadings, design, and structural materials for withstanding an initial load of 200,000 lb at supersonic speeds, utilizing appropriate canopy reefing. Performance range of interest: from transonic speeds to Mach 3, with dynamic pressures of 10,000 psf.

3. Ram-inflated balloon-type decelerator known as BALLUTE[1] - Goal: to establish the configuration, loadings, design, and structural materials needed to attain a stable performance for flight speeds to Mach 10 and for dynamic pressures to 500 psf.

Areas investigated included analytical and engineering design methods, material capabilities, and fabrication techniques. These were evaluated by wind-tunnel and free-flight tests. The wind-tunnel tests, supported by Goodyear Aerospace personnel, were conducted primarily by AFFDL-RTD personnel at Arnold Engineering Development Center, Tenn.; and also by NASA personnel at Langley Research Center, Va. Other laboratory tests were performed at Goodyear Aerospace, Akron, Ohio, including material, seam, and joint testing, porosity measurements, and heat-tunnel tests. BALLUTEs and small parachutes were flight-tested at Eglin Air Force Base, Florida; and large parachutes, at Holloman Air Force Base, N.M., and White Sands Missile Range, N.M.

3. ADDPEP PHASE I

Goodyear Aerospace conducted Phase I of ADDPEP under Contract AF33(657)-10955. Analytical and empirical techniques were developed to design and build the three types of decelerators (large and small parachute and BALLUTE); and to begin evaluating them through wind-tunnel and free-flight tests on the basis of the aforementioned goals. Moreover, to provide a free-flight basis for evaluating the analytical and empirical techniques, it was necessary to design, develop, build, and evaluate two types of test vehicles that were adaptable for launching by combinations of existing boosters.

4. ADDPEP PHASE II

Goodyear Aerospace conducted Phase II of ADDPEP under Contract AF33(615)-1513. This phase consisted of a continued evaluation of design techniques for two decelerator types: (1) large parachute and (2) BALLUTE. In general, efforts were successful in developing engineering techniques for the design of decelerators capable of performing in severe environments. More specifically:

1. Large parachutes were built that had the same basic hemisflo design: nominal 16-ft diameter canopy, 10-percent extended skirt, and 14-percent porosity.

[1] TM, Goodyear Aerospace Corporation, Akron, Ohio.

These parachutes were designed for 200,000-lb opening loads. Free-flight tests were performed at deployment Mach numbers of 1.50, 1.63, and 1.84; at altitudes of 13,660, 15,539, and 10,538 ft; and at dynamic pressures of 1988, 2118, and 3383 psf, respectively. The tests confirmed that this parachute design has excellent aerodynamic characteristics and adequate strength.

2. Five-foot-diameter BALLUTEs were fabricated from both textile and metal cloths. These were designed for a broad spectrum of deployment conditions ranging from Mach 2.7 at 73,000 ft to Mach 10 at 225,000 ft. The textile BALLUTEs were wind-tunnel and free-flight tested; the metal BALLUTEs were wind-tunnel tested only. Flight tests were limited to Mach 9.7 and dynamic pressures were limited to 355 psf. Wind-tunnel tests were limited to Mach 3 and to 120-psf dynamic pressure. The flight test data supported wind-tunnel data, which indicated that excellent stability and structurally adequate designs can be attained with five-foot-diameter BALLUTEs.

5. ADDPEP PHASE III

Goodyear Aerospace conducted the concluding Phase III of ADDPEP under Contract AF33(615)-2541. This phase consisted of a continued evaluation of design techniques for two decelerator types: (1) large parachute (continued from Phase I and II); and (2) small parachute (continued from Phase I). As in previous phases, the areas investigated include analytical and engineering design, material capabilities, fabrication techniques, and wind-tunnel and free flight tests. The large and small parachute decelerators were evaluated under more severe conditions than those imposed in previous phases. Table I summarizes the characteristics of these decelerators as well as the design test point data. Briefly, the Phase III results are as follows:

1. Three large parachutes (designated LP-7, LP-8, and LP-9) were built that had the same basic configuration as the Phase II design: hemisflo, 16-ft-diameter canopy, 10-percent extended skirt, 10-percent porosity. These parachutes were designed for 200,000-lb opening loads. Free-flight tests were performed at deployment Mach numbers of 2.22, 1.20, and 2.70; at altitudes of 18,050, 9370, and 19,700 ft; and at dynamic pressures of 3697, 1514, and 5155 psf, respectively. The tests confirmed the predicted drag area; however, the reefing line loads were underestimated. Improved analytical methods are needed to predict this hoop-type load under dynamic conditions at the higher Mach numbers.

2. Three small parachutes (designated SP-3, SP-4, and SP-5) were built that had the same basic configuration as the PARASONIC[2] design developed previously during Phase I: 4-ft-diameter, 5-percent porosity. Wind-tunnel tests confirmed that the PARASONIC design, when constructed of materials that are compatible with the flight environments investigated, has a better stability than a HYPERFLO[3] design that was also investigated in both Phases I and III. Free-flight tests were performed at deployment Mach numbers of 2.70, 1.60, and 5.43; at altitudes of 78,000, 56,300, and 117,000 ft; and at dynamic pressures of 329, 328, and 229 psf, respectively. The flight tests confirmed the stability predictions and the adequacy of the construction for the performance range investigated.

Section II of this Phase III final report, dealing with the free-flight test capability for the decelerators considered, describes the two test vehicle/booster systems that were developed previously as part of Phases I and II. Sections III and IV detail, respectively, the evaluations of the large and small parachute design techniques. Each of these three sections concludes with a summary and a statement of conclusions. Section V presents overall Phase III conclusions.

---

[2] TM, Goodyear Aerospace Corporation, Akron, Ohio.

[3] TM, Cook Electric Company, Chicago, Ill.

TABLE I - SUMMARY OF DECELERATOR DESIGNS A

Decelerator type	Principal material	Coating	Reefing line length (ft)	Canopy		Inlet area / Exit area	Load factor (g)	Drag area (sq ft)	Test method
				Surface area (sq ft)	Geometric porosity (percent)				
Large parachute (LP)									Vehicle
LP-7	Nomex	None	13.1	201.10	14	. . .	100.00	100.00	HJ-N
LP-8	Nomex	None	11.0	201.10	14	. . .	100.00	100.00	HJ-N
LP-9	Nomex	None	11.0	201.10	14	. . .	100.00	100.00	HJ-L
Small parachute (SP)									Vehicle
SP-3	Nomex	Dynatherm D-65	None	12.57	5	7:1	2.60	3.14	HJ-N
SP-4	Nomex	Dynatherm D-65	None	12.57	5	7:1	2.40	2.76	HJ-N
SP-5	Nomex	Dynatherm D-65	None	12.57	5	7:1	2.08	2.14	HJ-N

* Booster definitions: HJ = Honest John; N = Nike; L = Lance.

DECELERATOR DESIGNS AND PLANNED TEST POINTS

area / area	Load factor (g)	Drag area (sq ft)	Test methods*	Planned test point data: Mach number	Altitude (ft)	Dynamic pressure (psf)	Total air temperature (F)	Remarks
			Vehicle A					
	100.00	100.00	HJ-N	2.37	13,100	5050	590	Good test; obtained required data
	100.00	100.00	HJ-N	2.37	6,500	6000	620	Lost nose ballast early; obtained data for lower payload weight and velocity than planned
	100.00	100.00	HJ-L	3.00	18,750	6460	805	Good test; obtained all but camera data
			Vehicle G					
	2.60	3.14	HJ-N	2.50	85,300	200	443	Good test; obtained limited airborne data and complete ground data
	2.40	2.76	HJ-N-N	3.35	98,000	200	862	Early booster separation; obtained data for lower velocity than planned
	2.08	2.14	HJ-N-L	5.60	121,200	200	2710	Good test; obtained all but camera data

SECTION II

FREE-FLIGHT TEST CAPABILITY

1. TEST VEHICLE A/BOOSTER SYSTEM

a. General

A basic goal of ADDPEP Phase III (Aerodynamic Deployable Decelerator Performance-Evaluation Program) was to continue advancing the state of the art of large supersonic parachute design methods at high dynamic pressures. During Phase II, parachutes with 16-ft-diameters (D_o) were subjected to a Mach 1.8 regime (Reference 2). The ultimate objective of Phase III was to approach Mach 3 at low altitudes. The requirements for subjecting $t \geq 16$ ft parachutes to the Phase III test regime were fulfilled up to Mach 2.7 by Test Vehicle A, launched by Honest John-Nike (HJ-N) and Honest John-Lance (HJ-L) booster combinations.

b. Design and Configuration

For ADDPEP Phase III requirements, the overall configuration and design of Test Vehicle A remained basically the same as that established for Phase I and employed during Phase II. A photograph and the general configuration are shown in Figure 1. This vehicle is discussed in greater detail in References 1 and 2.

c. Free-Flight Performance

Table II summarizes the Test Vehicle A performance as a test point deployment control for large parachute (LP) tests with the booster combinations utilized.

Table III summarizes the data acquisition (instrumentation) system performance.

2. TEST VEHICLE C/BOOSTER SYSTEM

a. General

Required under ADDPEP Phase III was a series of small supersonic parachute deployments at speeds to Mach 5.5, altitudes to 121,000 ft, and dynamic pressures to 200 psf. Test Vehicle C, launched by Honest John-Nike (HJ-N), Honest John-Nike-Nike (HJ-N-N), and Honest John-Nike-Lance (HJ-N-L) booster combinations, fulfilled these requirements.

b. Design and Configuration

The Test Vehicle C used for Phase III tests contained modifications incorporated during Phase II (Reference 2). A photograph and the general configuration are shown in Figure 2.

SECTION II - FREE-FLIGHT CAPABILITY

TABLE II - PERFORMANCE-DEPLOYMENT CONDITIONS FOR TEST VEHICLE A

Test	QE* (deg)	Booster†	Altitude (ft)		Mach no.		Dynamic pressure (psf)	
			Calculated	Actual	Calculated	Actual	Calculated	Actual
LP-7	47	HJ-N	13,100	18,050	3.37	2.22	5050	3697
LP-8	34	HJ-N‡	6,500	9,370	2.27	1.20	6000	1514
LP-9	40	HJ-L	18,750	19,750	3.00	2.70	6460	5155

*Quadrant elevation angle.

†Booster definitions: HJ = Honest John; N = Nike; L = Lance

‡Tested at lower Mach number and at less payload weight than planned. Launch lug failed. After Nike burnout, nose weight detached.

TABLE III - INSTRUMENTATION PERFORMANCE FOR TEST VEHICLE A

Test	Telemetry instrumentation							Camera operation	
	100-pps monitor	Static press	Diff press	PAM*	Accel	Drag	Shock	500 fps	100 fps
LP-7	1†	1	1	1	1	1	1	2	1
LP-8	1	1	1	1	1	1	1	1	1
LP-9	1	1	1	1	1	1	1	2	2

*Pulse-amplitude modulation.

†Notes:

1. Satisfactory data obtained for test period.
2. Data not useful or not obtained during test period.

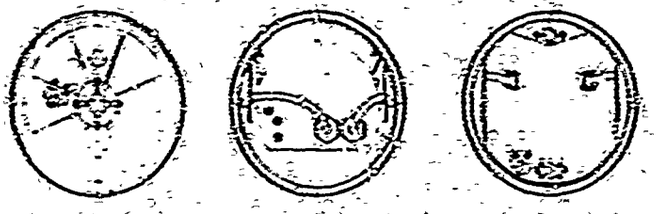

SECTION B–B

SECTION D–D

SECTION F–F

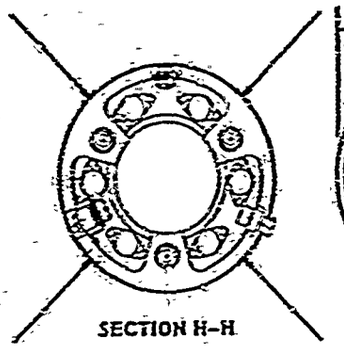

SECTION H–H

SECTION J–J

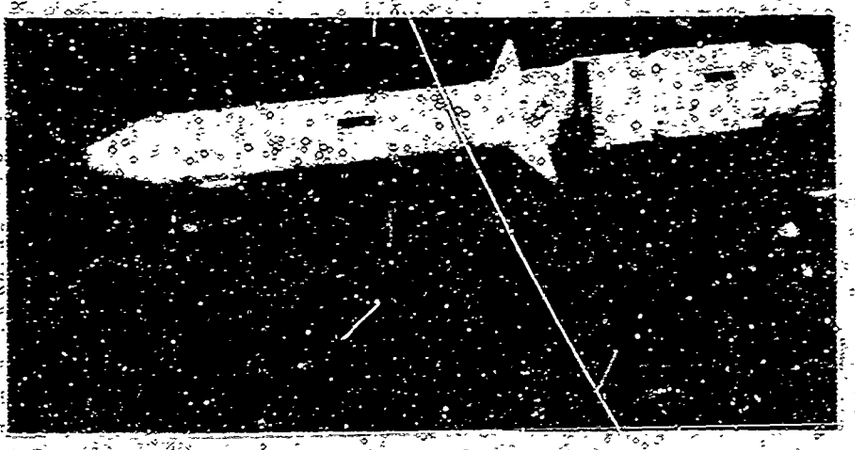

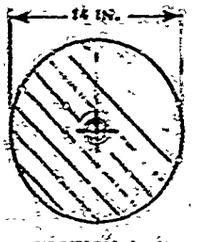

SECTION A–A

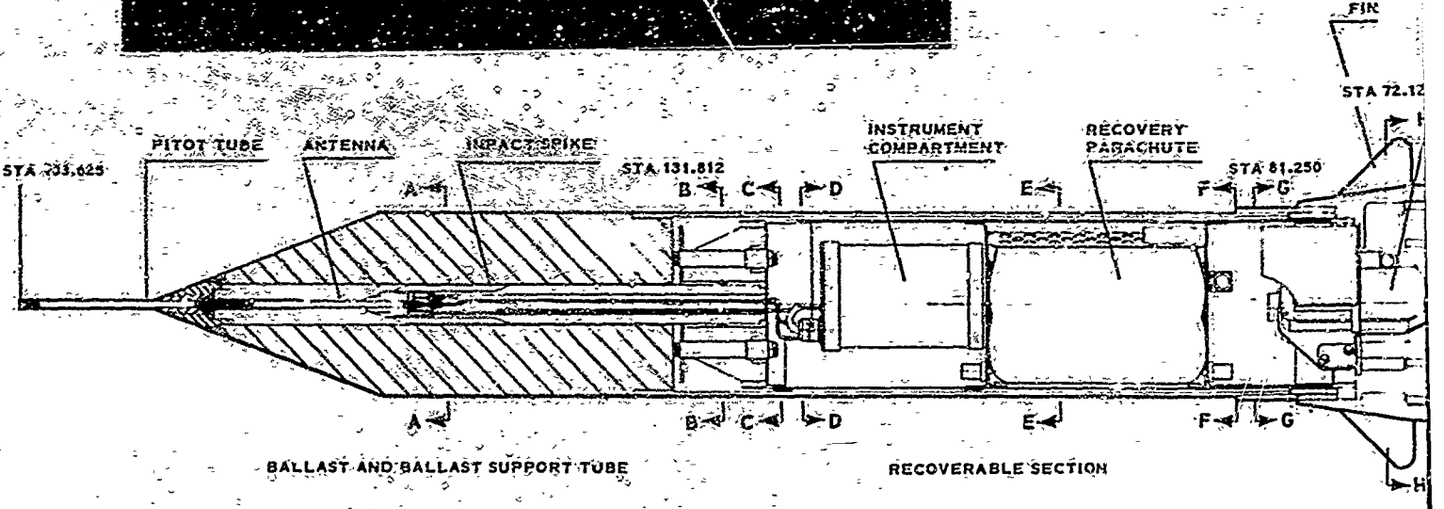

BALLAST AND BALLAST SUPPORT TUBE

RECOVERABLE SECTION

SECTION II - FREE-FLIGHT TEST CAPABILITY

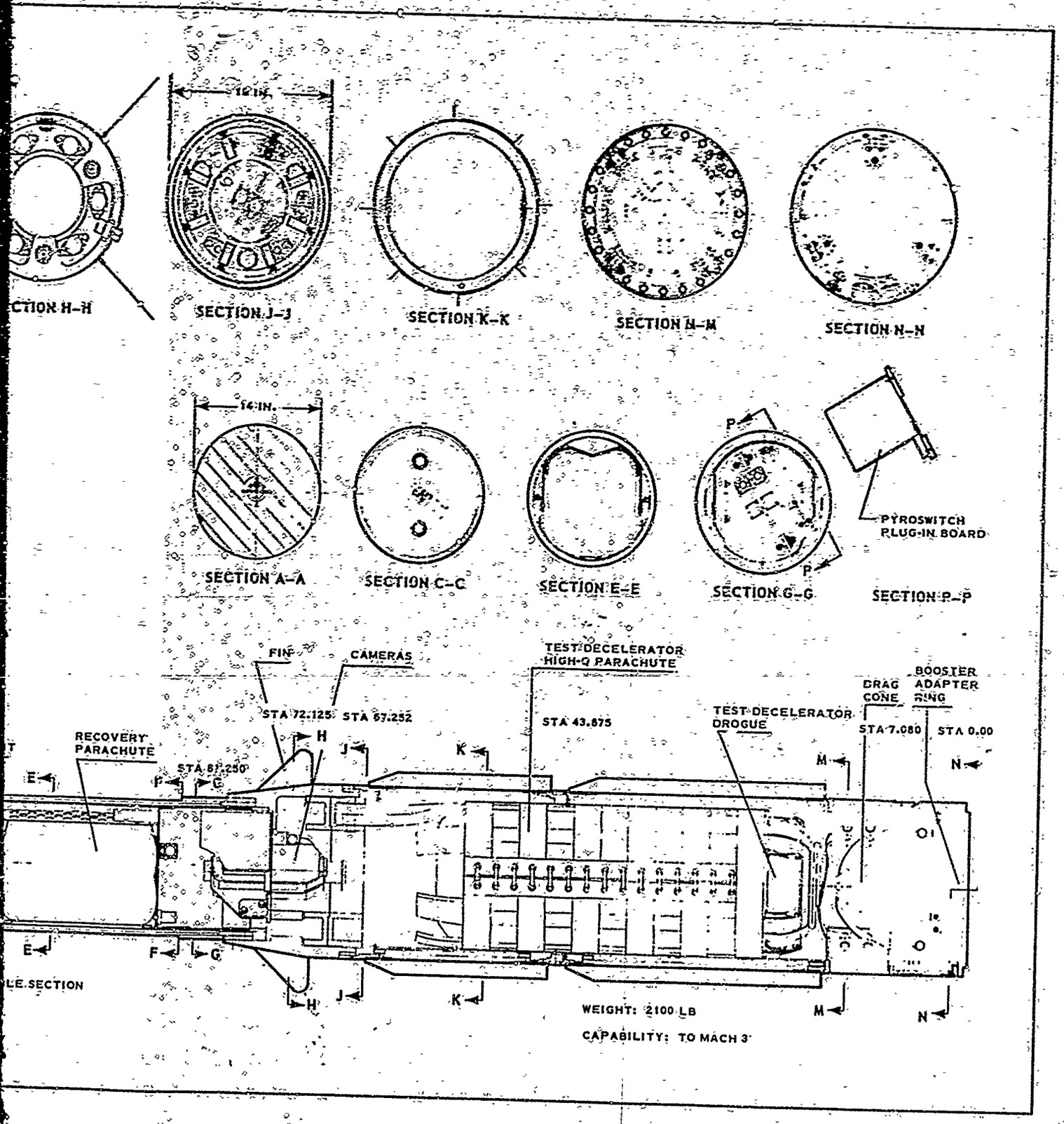

Figure 1 - Test Vehicle A

(Reverse is blank)

SECTI

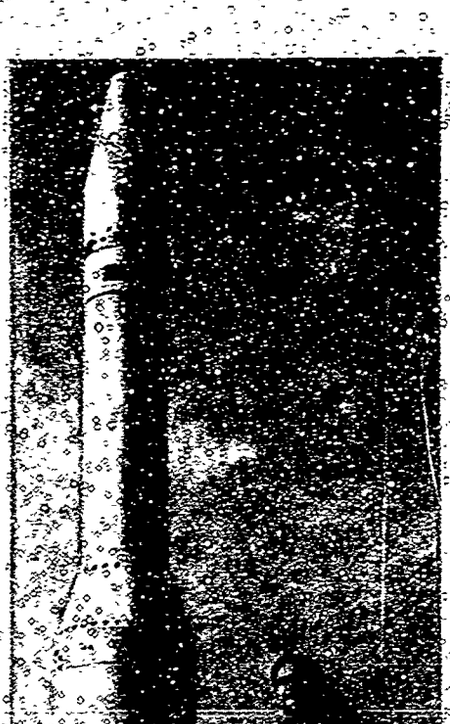

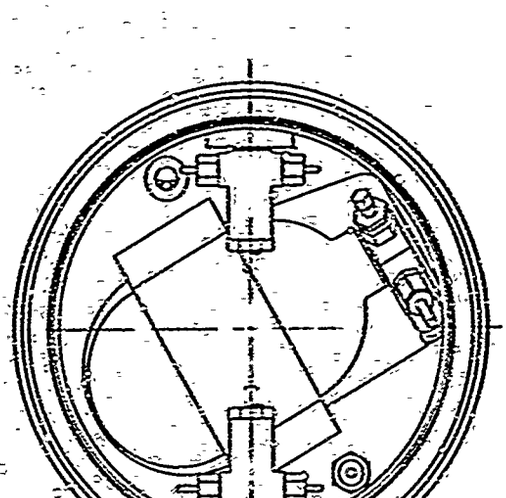

SECTION D–D

RECOVERY PARACHUT
GAS GENERATOR

RECOVERY PA

INSTRUMENT COMPARTMENT

STA 37

BATTERY PACK

STATION 105.6

STA 79.5

D

B

C

B

NOSE PROBE

D

C

FLOTATION SYSTEM

TELEMETRY ANTENNA

DESPIN RESERVOIR

CAMERAS

WEIGHT: 500 LB

CAPACITY: TO MACH 10

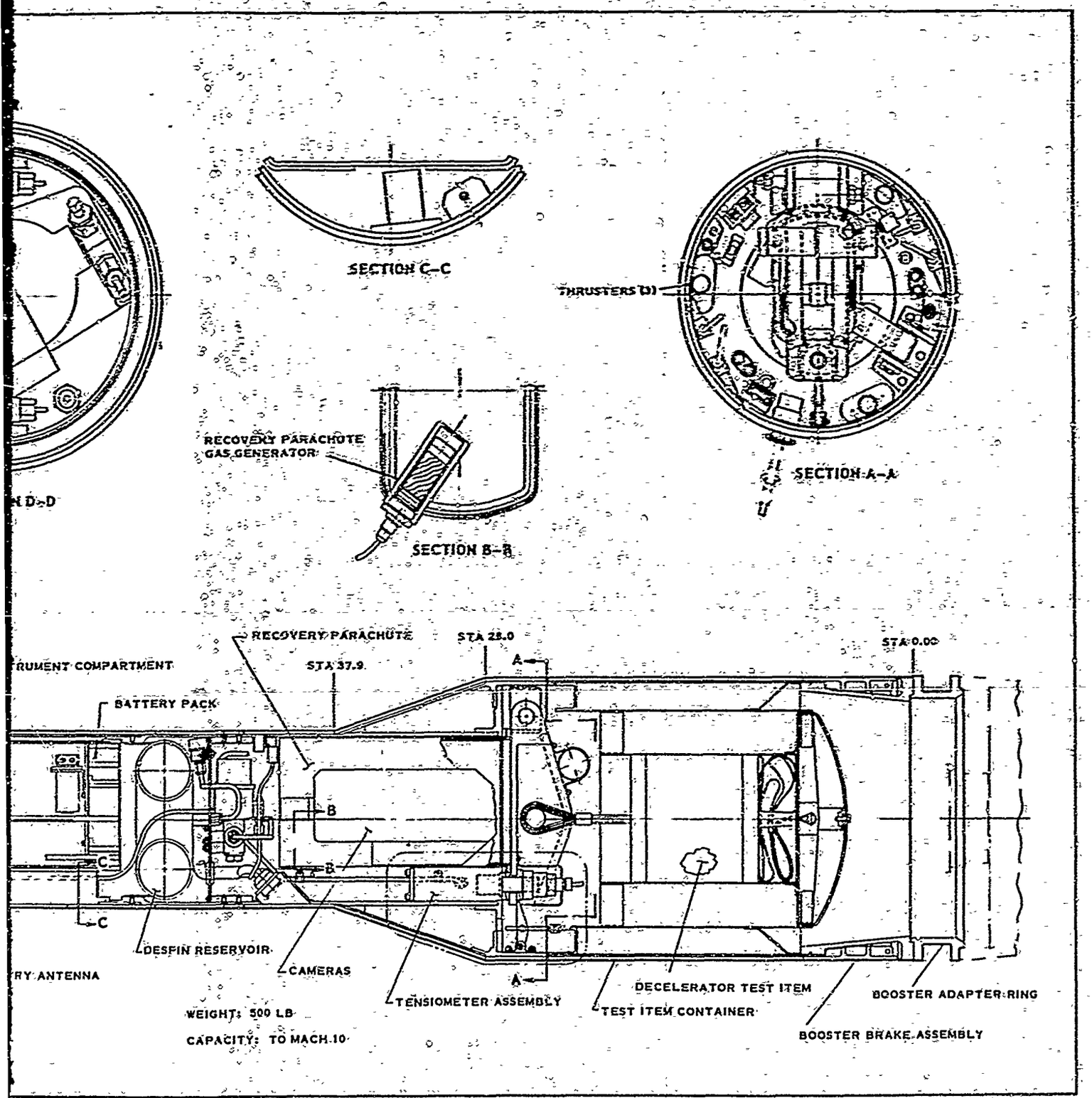

Figure 2 - Test Vehicle C

(Reverse is blank)

SECTION II - FREE-FLIGHT CAPABILITY

c. Free-Flight Performance

Table IV summarizes the Test Vehicle C performance as a test point deployment control for small parachute (SP) tests with the booster combination utilized. Table V summarizes the data acquisition (instrumentation) system performance.

TABLE IV - PERFORMANCE-DEPLOYMENT CONDITIONS FOR TEST VEHICLE C

Test	QE* (deg)	Booster†	Altitude (ft)		Mach no.		Dynamic pressure (psf)	
			Calculated	Actual	Calculated	Actual	Calculated	Actual
SP-3	83	HJ-N	85.3	78.0	2.50	2.7	200	329
SP-4	84	HJ-N-N‡	98.0	56.3	3.35	1.6	200	328
SP-5	84	HJ-N-L	121.2	117.0	5.60	5.5	200	229

*Quadrant elevation angle.

†Booster definitions: HJ = Honest John; N = Nike; L = Lance.

‡Premature ignition of second staged Nike.

TABLE V - INSTRUMENTATION PERFORMANCE FOR TEST VEHICLE C

Test	Telemetry instrumentation						Camera operation	
	Static press	Diff press	PAM*	Accel	Drag	Shock	700 fps	200 fps
SP-3	1†	1	1	1	2	2	3	3
SP-4	1	1	1	1	1	1	1	1
SP-5	4	4	1	1	1	1	3	3

*Pulse-amplitude modulation.

†Notes:

1. Satisfactory data obtained for test period.
2. Data obtained for only portion of test period.
3. Unknown.
4. Data not useful or not obtained during test period.

SECTION II - FREE-FLIGHT CAPABILITY

3. GROUND SUPPORT

a. General

ADDPEP Phase III free-flight support was required in two test areas:

1. Large parachute (LP) free-flight tests and data reduction were performed at Holloman Air Force Base, N.M., and White Sands Missile Range, N.M.

2. Small parachute (SP) free-flight tests and data reduction were performed at Eglin Air Force Base, Fla.

b. Field Operations

Field test operations followed the pattern shown in Figure 3. During the free-flight tests, the Goodyear Aerospace field test crew assumed responsibility for the test and checkout of all vehicle systems, booster interstage hardware, and vehicle refurbishment. The range agency - Holloman, White Sands Missile Range, or Eglin AFB - assumed responsibility for storage, use, and assembly of the booster vehicle; range safety; radar tracking; ground acquisition of telemetered and photometric test data; and data reduction of vehicle flight and test decelerator deployment data.

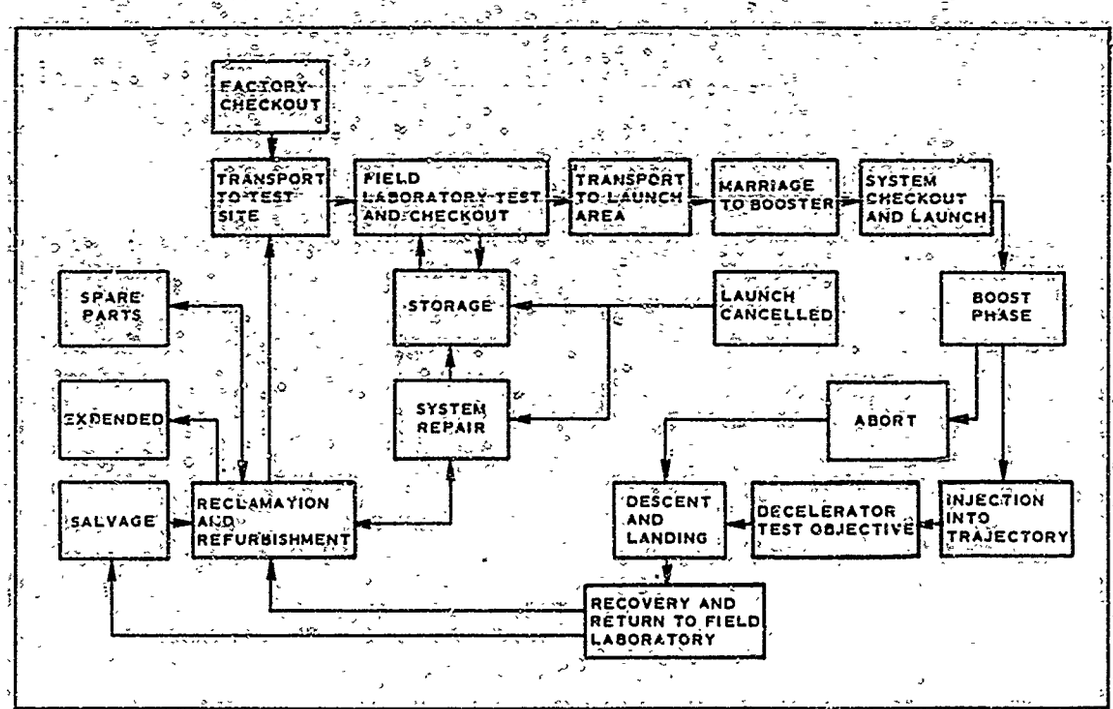

Figure 3 - Field Operations Flow

c. Field Personnel

The field-test crew consisted of three engineers and two technicians; in addition, a part-time pyrotechnics engineer was assigned. Basically, the responsibilities were as follows:

1. Project engineer - program management
2. Instrumentation engineer - on-board data acquisition
3. Development engineer - vehicle systems and assembly
4. Electronics technician - assistance for instrumentation
5. Pyrotechnics engineer - loading and assembly for explosive devices (accomplished on periodic visit basis)

4. SUMMARY AND CONCLUSIONS

The evaluation of the test vehicle systems is summarized as follows:

1. Test Vehicle A/Booster - The test results indicated that vehicle performance can be predicted with confidence. All the data system components were adequate over the performance range. External solder connections to the outside camera became unreliable at Mach 2.2; these were changed to crimp connections. Recovery and reusability of the system as a whole exceeded the design goals. However, the cameras were found to have unacceptable reliability with more than one reuse.
2. Test Vehicle C/Booster - The test results indicated that vehicle performance can be predicted with confidence. Beacon dropout occured just prior to launch on the SP-3 test and at Lance booster ignition on the SP-5 test. The data transmission range was excellent, and the vehicle met design goals for reusability when recovered.

SECTION III

LARGE PARACHUTE DECELERATOR

1. INTRODUCTION

The overall goal of the large supersonic parachute effort under ADDPEP (Aerodynamic Deployable Decelerator Performance-Evaluation Program) was to establish the parachute configuration, loadings, design, and structural materials for attaining an initial opening load of 200,000 lb at supersonic speeds and low altitudes. The performance range for investigation was to extend from transonic speeds to Mach 3, with a dynamic pressure (q) of 10,000 psf. The work on a large supersonic high-q parachute decelerator was initiated during ADDPEP Phase I (Reference 1), continued during Phase II (Reference 2), and concluded during Phase III.

The large parachute (LP) effort has been concentrated on two basic design types: (1) conical and (2) hemisflo. Two conical parachute test items, LP-1 and LP-2, were designed and fabricated during Phase I. Three hemisflo parachute test items, LP-3, LP-4, and LP-5, were designed and fabricated during Phase II. Three identical hemisflo test items, LP-7, LP-8, and LP-9, were fabricated during Phase III.[4] The final hemisflo canopy size chosen was a 16-ft nominal diameter, D_o.

The Phase III test points for LP-7, LP-8, and LP-9 were established with AFFDL-RTD concurrence by considering the desired test conditions, available boosters, and range safety requirements. Trajectory analysis resulted in the achievable test points shown in Table VI.

TABLE VI - DESIRED TEST POINTS FOR LARGE PARACHUTES

Design configuration	Initial conditions					
	Mach no.	Altitude (ft)	Dynamic press (psf)	Flight path angle (σ_g from horiz)	Reynolds no. (10^6)	Booster comb*
LP-7	2.37	13,100	5050	23	11.55	HJ-N
LP-8	2.27	6,500	6000	9	13.42	HJ-N
LP-9	3.00	18,750	6460	21	12.29	HJ-L

*Booster definition: HJ = Honest John; N = Nike; L = Lance.

[4] It was not necessary to build LP-6 since the test point originally anticipated for investigation by this parachute was covered during Phase II by the LP-3, LP-4, and LP-5 tests.

The materials and construction used during Phase II for LP-3, LP-4, and LP-5 were maintained during Phase III. This was possible because all these hemisflo parachutes originally were designed for the maximum aerodynamic loading condition of Mach 3. Only the reefing size changed with changing test conditions. The Phase II test results confirmed the structural design to loads of 155,000 lb and to Mach 1.8.

The hemisflo LP configuration details are given in Reference 2 and are summarized below. The general dimensions are shown in Figure 4.

1. Canopy nominal diameter: D_o = 16 ft
2. Shape: hemisflo ribbon canopy with 10-percent extended skirt
3. Geometric porosity: 14 percent nominal evenly distributed
4. Number of gores: 32
5. Suspension line length (effective): $L_S = 2\ D_o = 32$ ft
6. Reefing: midgore
7. Pocket bands: every other gore; reduces skirt band length approximately 1 in. each

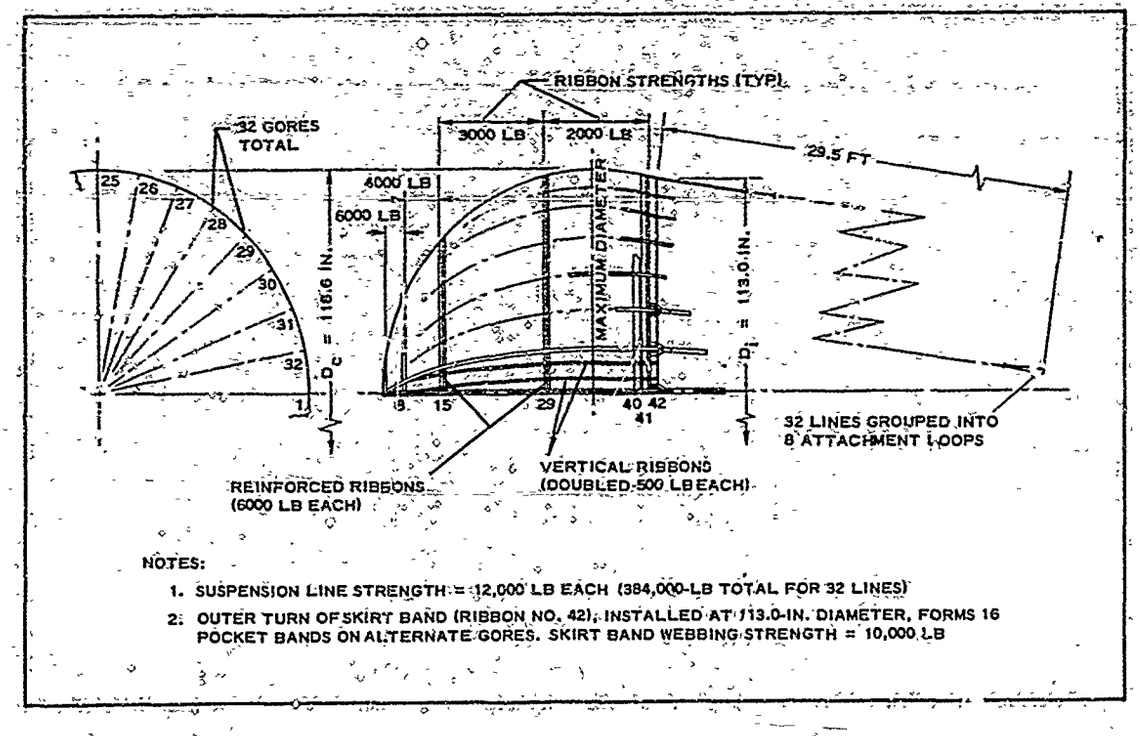

Figure 4 - General Arrangement of 16-Ft D_o Hemisflo Parachute

8. Cutters: 2 on LP-7; none on LP-8 and LP-9

9. Weight: 139 lb

2. EXPLORATORY FREE-FLIGHT TESTS

a. General

During Phase III, the LP-7, LP-8, and LP-9 reefed hemisflo parachutes were deployed by Test Vehicle A, launched by Honest John-Nike (HJ-N) ~ Honest John-Lance (HJ-L) booster combinations. Table VII summarizes the actual test conditions for these three parachutes, as well as for the identical LP-3, LP-4, and LP-5 items that were tested during Phase II. The inflation times for all six large parachute canopies are presented in Table VIII.

TABLE VII - SUMMARY OF LARGE PARACHUTE TEST CONDITIONS, PHASES II AND III

Test item	Event	Range time (hr: min: sec)	Load (10^3 lb)	Conditions		
				Mach no.	q* (psf)	Alt (ft)
Phase II						
LP-3	Test item container separation	16: 10: 28.64	. . .	1.502	1988	13,660
LP-3	Initial line stretch	16: 10: [illegible] 97	50.000	1.341	1590	13,770
LP-3	Maximum load	16: 10: 29.10	[illegible] 500	1.240	1350	13,815
LP-4	Test item container separation	23: 15: 13.75	. . .	1.631	2118	15,539
LP-4	Initial line stretch	23: 15: 14.12	30.000	1.531	19[illegible]	15,842
LP-4	Maximum load	23: 15: 14.23	108.850	1.400	164[illegible]	15,934
LP-5	Test item container separation	13: 00: 10.30	. . .	1.837	3383	10,538
LP-5	Initial line stretch	17: 00: 10.61	40.000	1.725	2950	10,710
LP-5	Maximum load	17: 00: 10.81	152.600	1.560	2410	10,948
Phase III						
LP-7	Test item container separation	22: 00: 14.86	. . .	2.220	3697	18,059
LP-7	Initial line stretch	22: 00: 15.24	26.205	2.160	3436	18,489
LP-7	Maximum load	22: 00: 15.36	112.000	2.110	3250	18,612
LP-8	Test item container separation	22: 34: 13.62	. . .	1.200	1514	9,370
LP-8	Initial line stretch	22: 34: 14.18	20.224	1.080	1232	9,481
LP-8	Maximum load	22: 34: 14.39	27.360	0.908	866	9,517
LP-9	Test item container separation	18: 00: 19.14	. . .	2.700	5155	19,700
LP-9	Initial line stretch	18: 00: 19.45	47.371	2.610	4760	20,000
LP-9	Maximum load	18: 00: 19.55	120.446	2.560	4540	20,085

*Dynamic pressure.

TABLE VIII - INFLATION TIMES OF LARGE PARACHUTE CANOPIES

Test item	Mach no.*	Dynamic pressure* (psf)	Filling time - line stretch maximum load (sec)
LP-3	1.340	1500	0.13
LP-4	1.530	1920	0.16†
LP-5	1.725	2950	0.20†
LP-7	2.160	3436	0.12
LP-8	1.080	1232	0.18
LP-9	2.610	4760	0.10

*At line stretch.

†Line twist observed in these tests was approximately 1.5 turns.

b. Large Parachute LP-7

Test item LP-7 was deployed near the calculated test Mach number of 2.37 but at a higher altitude, which reduced the dynamic pressure to 3697 psf. The Missile roll rates were 1.5 rps, compared to 4 to 5 rps during the earlier LP-4 and LP-5 tests. The reefing line was 13 ft 1.25 in. long as laid out and consisted of a 6000- and a 12,000-lb strength web tacked together. The test parachute was extracted and deployed by means of a 30-in. D_o hemisflo pilot parachute positioned 8 ft 4 in. aft of the test item deployment bag. The pilot chute was permanently reefed by a web 46.75 in. long. Twenty-four suspension line and 8 canopy break ties of 500-lb webbing were used to aid orderly deployment.

The LP-7 deployment was less orderly than in prior tests. This was caused by breaking of the forward restraining loops of the deployment bag; and by tearing of a rear portion of the bag cloth beyond the locking loops. The restraining loop failures allowed the forward half of the bag to invert. As a result, the forward portions of the lines were pulled across portions of the lines still stowed. Because of this rubbing action, while they were under load, damage occurred to the nylon suspension lines. The tear in the rear portion of the bag allowed some canopy growth. During deployment, damage occurred to the skirt band and to one cutter pocket.

The canopy filled rapidly to the reefed condition. Canopy attitude and the amount of line twist (approximately 0.14 turns) were acceptable, based on the earlier LP-4 and LP-5 test results. Several actions occurred at the time of, or immediately following, the inflation to the reefed shape. The exact sequence of the actions could not be determined from

the high-speed camera films; however, the actions could be associated with the period when the canopy had a reefed shape. During this instant, the reefing line, the suspension lines, and the skirt band were broken (skirt band broken in two places).

The maximum load recorded prior to suspension line failure was 112,000 lb. This was considerably less than the values recorded without line failure during the earlier Phase II tests using the same design and construction of the canopy and lines. Postflight inspection of the canopy and lines indicated the lines had been weakened by extensive "nylon-on-nylon" type damage (see Item 8, c, p 44).

Post-test examination concurred that the lines and skirt band were severely scrubbed and damaged during deployment. The two breaks in the skirt band extended into the canopy: one break through 7 ribbons and the other through 13 ribbons. The longer break stopped at the first reinforced ribbon. The damage to the deployment bag indicated a pressure type failure, in which the restraining loops/grommet approach was structurally inadequate at the high dynamic pressures and dynamic effects of line deployment.

Figure 5A shows the LP-7 performance curves, beginning at test item container separation and continuing three seconds. Indicated are the variations in parachute load, velocity, dynamic pressure, and altitude versus time from parachute deployment; data for these curves were obtained from data reduction reports published by White Sands Missile Range (WSMR, References 3 and 4) or from the test vehicle telemetry signal plot.

Figure 5B shows inlet area variation with respect to time on a selective scale. Data for the inlet area plot were generated from onboard motion picture coverage.

c. Large Parachute LP-8

Due to the damage sustained by Test Vehicle A during launch, test item LP-8 was deployed at conditions much less than predicted. The damage allowed the heavy nose ballast to separate after boost and the lightened vehicle to decelerate to Mach 1.2 prior to the deployment of the test item. The reefing line was 11 ft long as laid out and consisted of two 12,000-lb strength webs sewn together. The test parachute was extracted and deployed by a 30-in. D_o hemisflo pilot parachute, reefed permanently by a web 40.375 in. long. The pilot parachute was positioned 8 ft 4 in. aft of the test item deployment bag.

Eight canopy break ties and 24 suspension line ties were used to facilitate orderly deployment. The canopy ties were made using 500-lb webbing. The 24 line ties were made by using 500-lb webbing for the first eight ties; 600-lb webbing for the second 8 ties; and 700-lb webbing for the third 8 ties.

The LP-8 deployment was very orderly and continuous at the reduced test conditions, even though the pilot parachute, line break cords, and canopy break cords were sized for a higher deployment dynamic pressure and

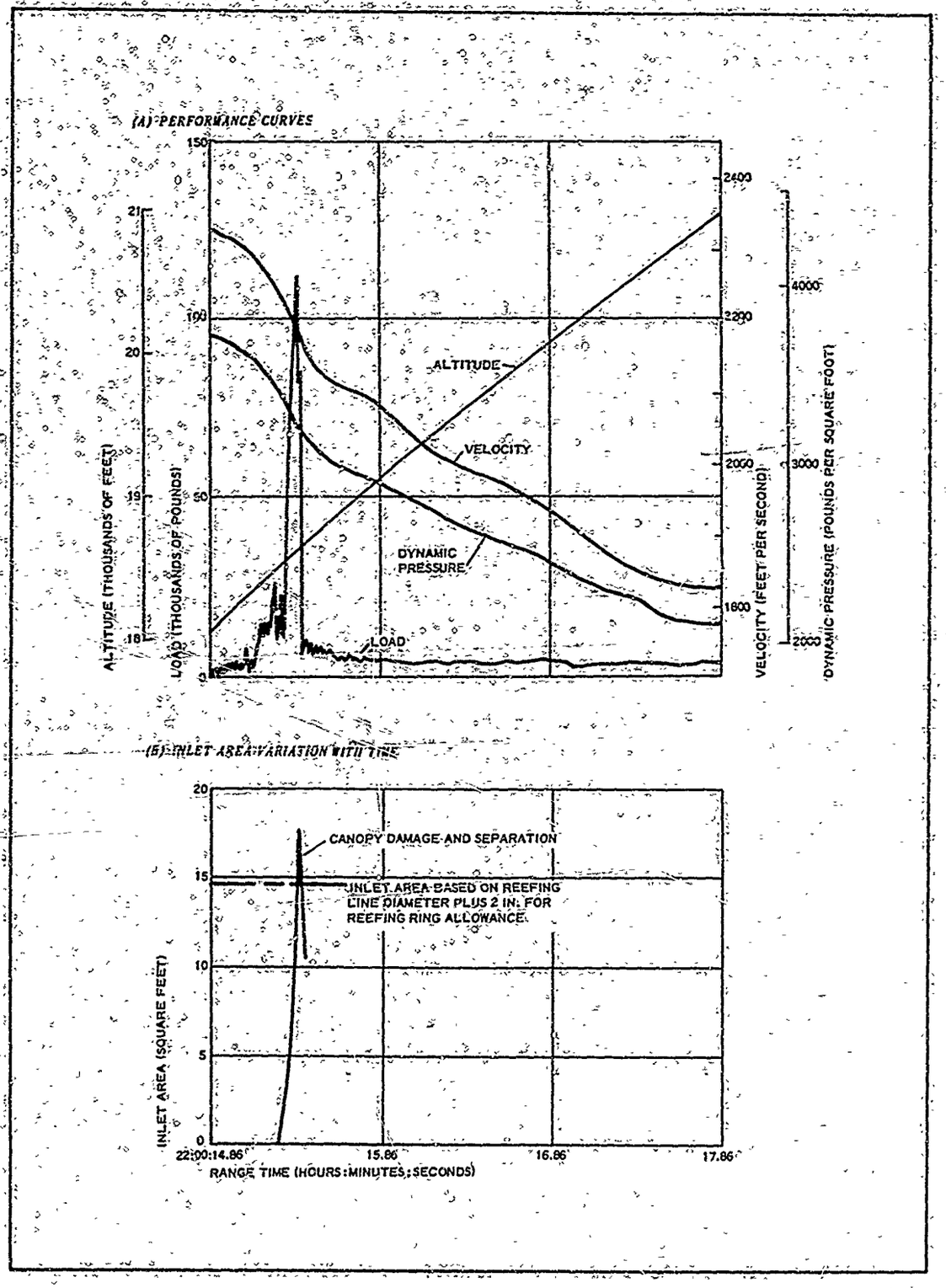

Figure 5 - LP-7 Performance Curves and Inlet Area Variation with Time

payload weight. Missile roll rates were approximately one revolution per second. The new stronger deployment bag operated properly and was undamaged.

The canopy filled to the reefed condition and exhibited excellent stability through the transonic regime. The maximum load recorded was 27,360 lb, a level of 59 g for the much lighter than normal payload weight. Post-test examination indicated no damage to the canopy, lines, deployment bag, and pilot system.

Figure 6A shows the LP-8 performance curves, beginning at test item container separation and continuing for three seconds. Indicated are the variations in parachute load, velocity, dynamic pressure, and altitude versus time from parachute deployment. Data for these curves were obtained from WSMR reduction reports (References 5 and 6) or from the test vehicle telemetry signal plot.

Figure 6B shows inlet area variation with respect to time on a selective scale. Data for the inlet area plot were generated from on-board motion picture coverage.

d. Large Parachute LP-9

Test item LP-9 was deployed at conditions near the anticipated Mach number and altitude, which resulted in a dynamic pressure of 5155 psf. A peak force of 120,446 lb was measured before suspension line failure; this value also was below the values measured in Phase II without suspension line failure. As in the LP-7 test, postflight examination of the suspension lines indicated they had been weakened by extensive "nylon-on-nylon" type damage (see Item 8, c, p 44).

The reefing line was 11 ft long as laid out and consisted of two 12,000-lb strength webs sewn together. The test item was extracted and deployed by means of a 30-in. D_o hemisflo pilot parachute permanently reefed by a web 40.375 in. long. The pilot parachute was positioned 8 ft 4 in. aft of the test item deployment bag. The LP-8 break tie arrangement was repeated for orderly deployment.

Useful on-board camera coverage was not obtained due to heat affecting the exterior camera and the film jamming in the interior camera during the LP-9 deployment. However, the load traces indicated a smooth continuous action with a rapid filling time, followed by an abrupt load drop-off to approximately 25,000 lb.

Post-test examination indicated reefing line failure near Gore 8. The reefing rings were retained by their attachments to the skirt band under the loads occurring during the breaking of the 24,000-lb strength reefing line webbing. The skirt band was broken in Gores 8 and 19. Canopy damage from Gores 9 through 19 took a form different than earlier tests when the radials located on one side of the ribbons became detached from the radials on the other side of the ribbons. Between Ribbons 8 and 29, the verticals spaced the ribbons. From Ribbons 30 to 42 (skirt band), damage to the verticals was extensive, the ribbons were free to slide, and some failed. Other gores had sewing and vertical damage. Near

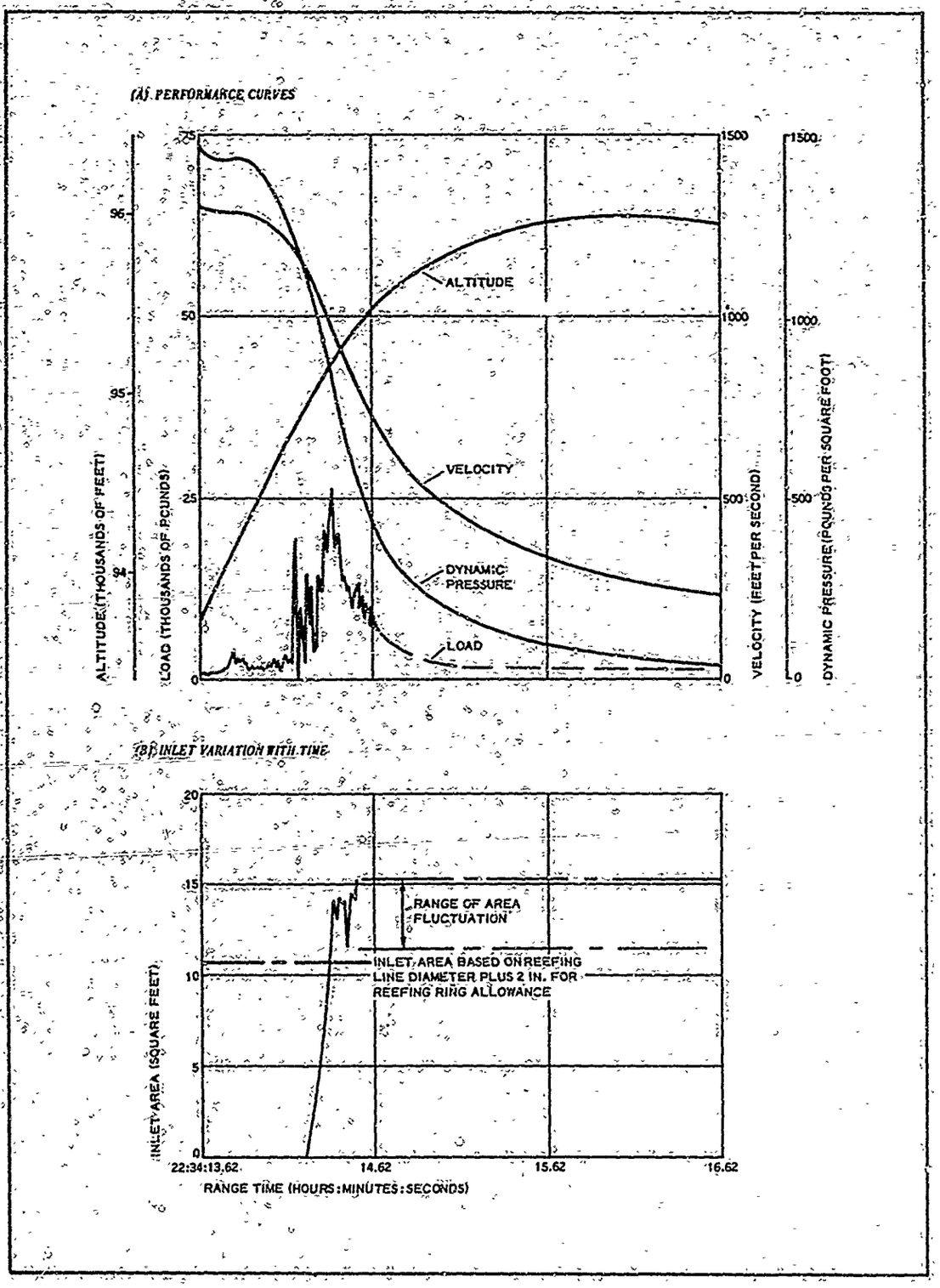

Figure 6 - LP-8 Performance Curves and Inlet Area Variation with Time

Gore 19, several ribbons were broken. The lines were damaged farther from the canopy than in the LP-7 tests, since the line protection sleeves had been extended to 5 ft forward of the skirt.

The LP-9 deployment bag (described later in this section in Item 8, Design and Fabrication) was completely undamaged except for tearing off one small lining flap that covered the locking loops on one bag half. The flap system, which replaced the bag restraining loops on the earlier LP-3 through LP-7 tests, was undamaged, as were the bag grommets and lining at these higher dynamic pressures. The small pilot chute was undamaged as in earlier tests.

Figure 7 shows the LP-9 performance curves, beginning at test item container separation and continuing for three seconds. Indicated are the variations in parachute load, velocity, dynamic pressure, and altitude versus time. Data for these curves were obtained from WSMR reduction reports (References 7 and 8) or from the test vehicle telemetry signal plot.

The performance data for the tests of LP-3 through LP-9 are discussed in the following aerodynamic analysis.

3. AERODYNAMIC ANALYSIS

a. General

The configuration, size, and structural materials for the large high-q parachutes, as established during ADDPEP Phase II, were selected for Phase III. The basic aerodynamic task for Phase III was to determine the reefing size required for a peak longitudinal opening load near 200,000 lb for each set of deployment conditions. Three approaches were investigated for determining longitudinal opening loads; these were based on available wind-tunnel data, free-flight data, and analytical methods.

In addition to establishing the peak longitudinal loads, it became increasingly apparent that the reefing line loads had to be determined. These were needed to prevent early disreefing and skirt band failure, which could lead to locally overloading groups of suspension lines. One of the analytical approaches investigated predicted reefing line load values that can be compared with empirical values.

b. Reefing Based on Wind-Tunnel Tests

References 9 through 11 give wind-tunnel results for steady-state drag coefficients for small and large parachute models. Figure 8 compares these results and the free-flight ADDPEP test results, excluding the opening shock loads; peak load coefficients for the flight tests are also included for reference. (Note that the peak opening loads in Figure 8 are based on WSMR data reduction reports, References 3 through 8 and 12 through 17.) A comparison of the drag coefficient values versus the inlet reefing ratio in Figure 8 indicates that wind-tunnel data are not directly applicable for determining full-scale values after the opening shock. The peak free-flight drag coefficient and the corresponding values after opening can be compared by using the top two curves.

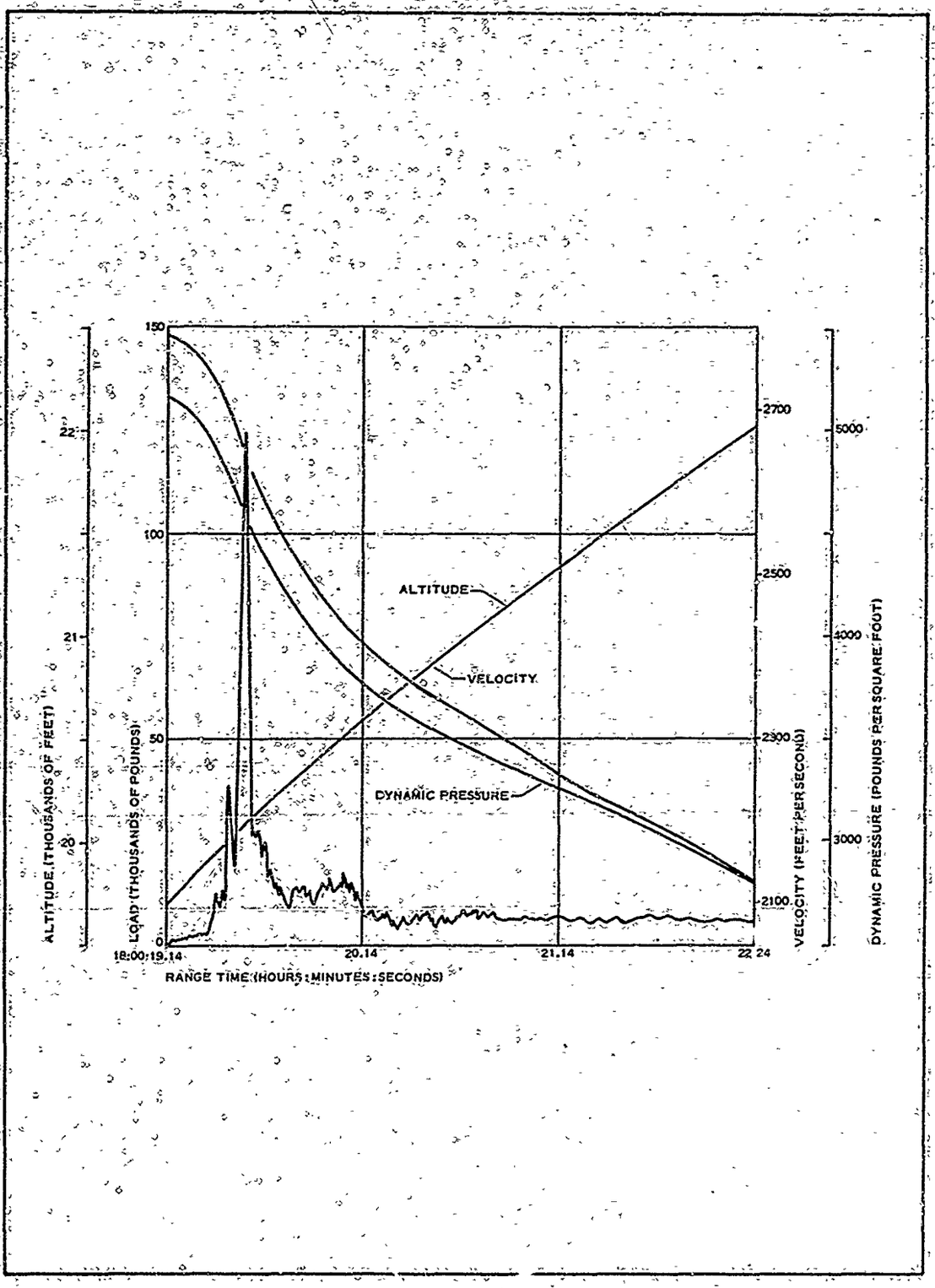

Figure 7 - LP-9 Performance Curves

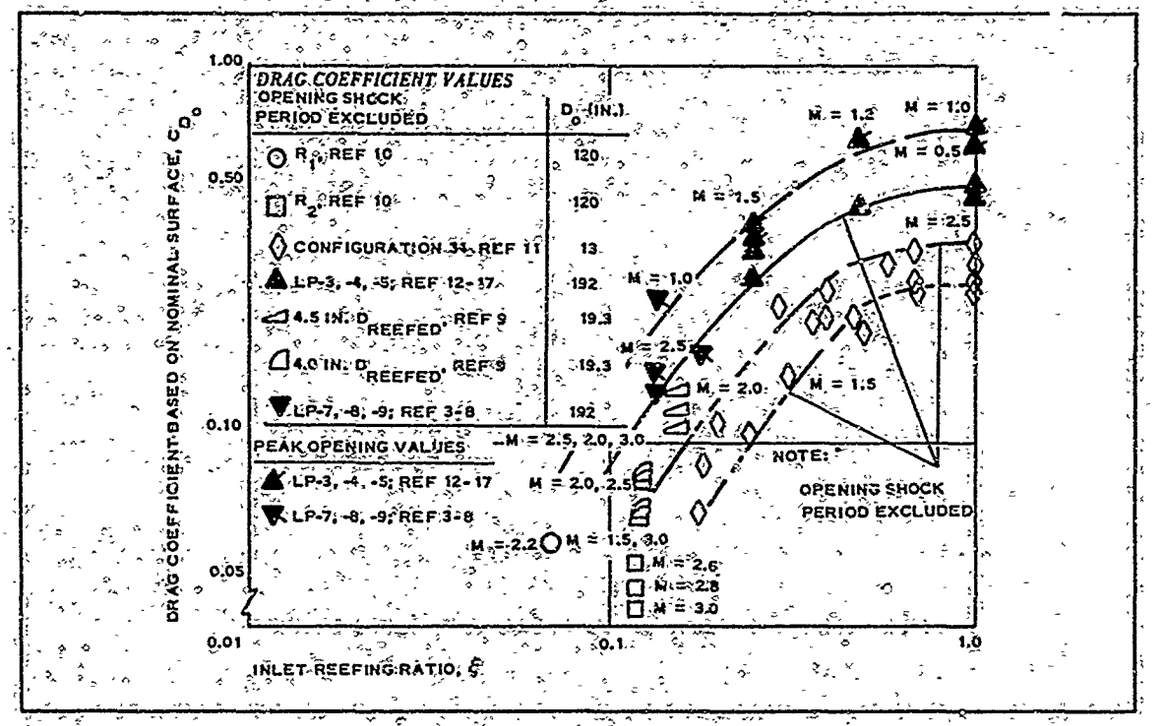

Figure 8 - Comparison of Small-Scale and Free-Flight Data

c. Reefing Based on Free-Flight Data

During Phase III, the LP-8, LP-7, and LP-9 parachutes were deployed at Mach 1.2, 2.2, and 2.7, respectively, with accompanying deployment dynamic pressures of 1514, 3697, and 5155 psf. Table VII shown earlier summarizes the test conditions for the three tests. Figures 9A through 9D show the following values versus range time for LP-7, LP-8, and LP-9:

9A. Mach number

9B. Dynamic pressure

9C. Deceleration and load (strain link)

9D. Nominal surface drag coefficient and load/dynamic pressure

Range times are presented for ease of correlation with the WSMR data reports. The earliest times listed correspond to test item container separation.

The curves of Figures 9C and 9D indicate the type of loadings through the flight regime. The first small load peaks correspond to line stretch. They are usually followed by small second load peaks and then the opening shock loads.

The measured opening times decreased with increasing flight Mach numbers (see Table VIII). This trend was not observed in Phase II (LP-3, LP-4, and LP-5). However, the opening times for LP-4 and LP-5 were affected by 1.5 turns of line twist caused by initial missile roll rates of 4 to 5 rps. This can be compared with minor line twist for LP-3, LP-7, LP-8, and LP-9 that was caused by lower initial missile roll rates of approximately 1 rps.

Figure 10 shows the load measured by the strain link and load/dynamic pressure versus Mach number for LP-3, LP-4, LP-5, LP-7, LP-8, and LP-9. The initial peaks correspond to line stretch loads; and the later peaks, to reefed and disreefed opening loads.

Table IX presents the dimensional and loading parameters. Each loading parameter is based on conditions at the opening peak loading that correspond to its dimensional parameter.

The values presented in Columns 4 through 7 are from the reduced range data. The Column 8 values of load/dynamic pressure (L/q) are from interpretation of the curves after the opening shock. The values for LP-4, LP-5, and LP-8 are evident for the reefed condition; however, LP-8 values are for a lighter weight payload and they are not directly applicable. Values for the disreefed parachute after the opening shock are provided by LP-3 and LP-4 data.

By comparing the values of Columns 7 and 8, an opening shock factor can be determined as given in Column 9. The trend is to lower opening shock values with increasing Mach number and dynamic pressure. It should be noted that the largest opening shock value occurred at the lowest Mach number and dynamic pressure despite the smallest reefing size; i.e., LP-8.

In an attempt to correlate test data and predict reefing sizes for other deployment conditions, the L/q values at maximum load, as occurring at reefed opening, were divided by reefing line length (RLL) or reefed inlet area (RIA) to establish coefficients. The coefficients are:

$$K_{RLL\ (ft)} = \frac{L/q \text{ at } L_{max}\ (\text{sq ft})}{RLL\ (\text{ft})} \qquad (1)$$

$$K_{RIA} = \frac{L/q \text{ at } L_{max}\ (\text{sq ft})}{RIA\ (\text{sq ft})} \qquad (2)$$

The values of these coefficients, at their reefing dimensions and inlet reefing ratios (ξ), are listed in Table X and plotted in Figure 11. The resultant curves can be used to calculate reefing size for a maximum opening load over a range of deployment conditions; the larger reefing sizes correspond to transonic values, and the lower sizes to the supersonic regime (Mach 2 to 3). This plot indicates that the coefficient values based on the reefed inlet area are less sensitive to reefing changes. The same curves can be used for other sizes of this configuration by using the reefing ratio values.

(A) MACH NUMBER VERSUS TIME

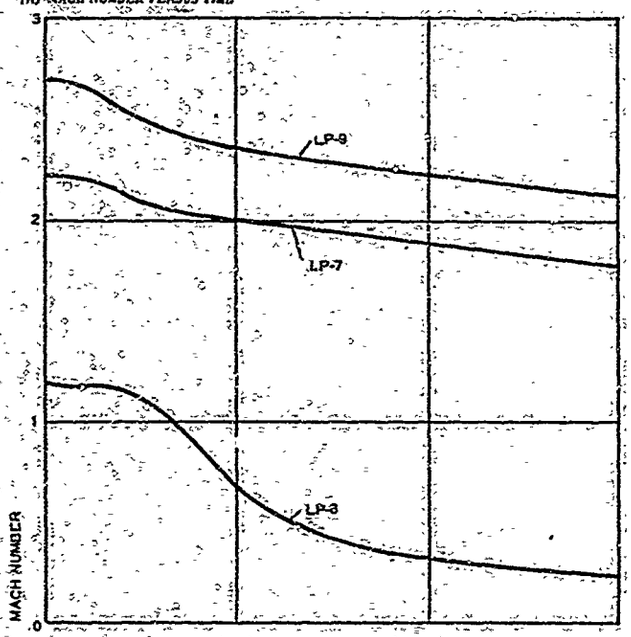

(B) DYNAMIC PRESSURE VERSUS TIME

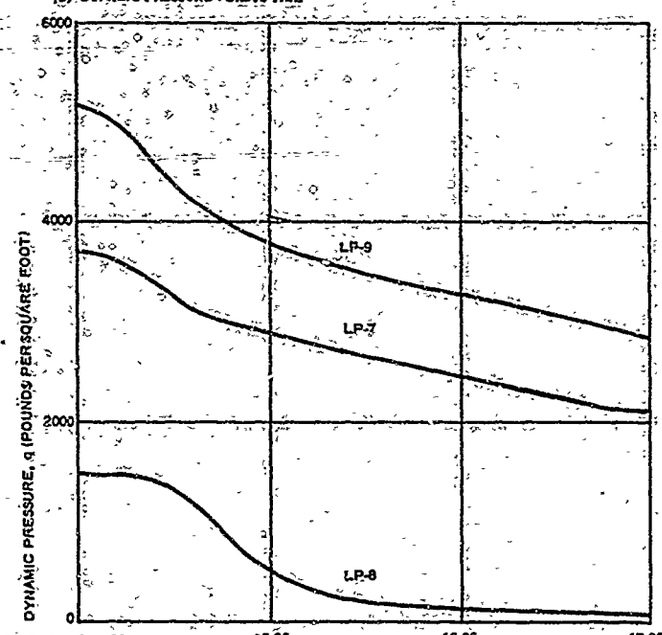

(C) DECELERATION AND LOAD

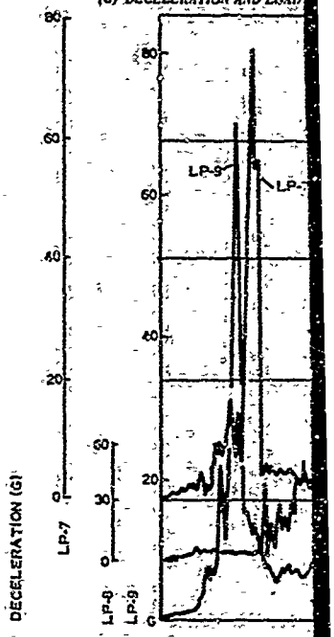

(D) NOMINAL SURFACE DR

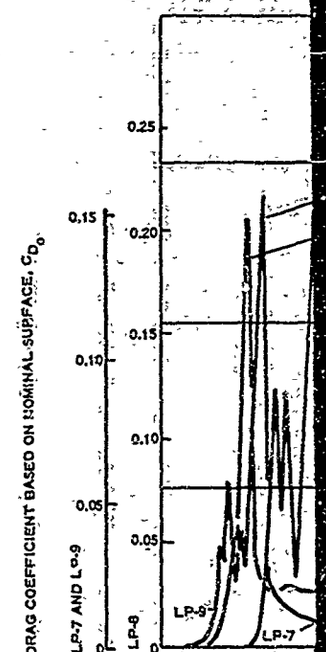

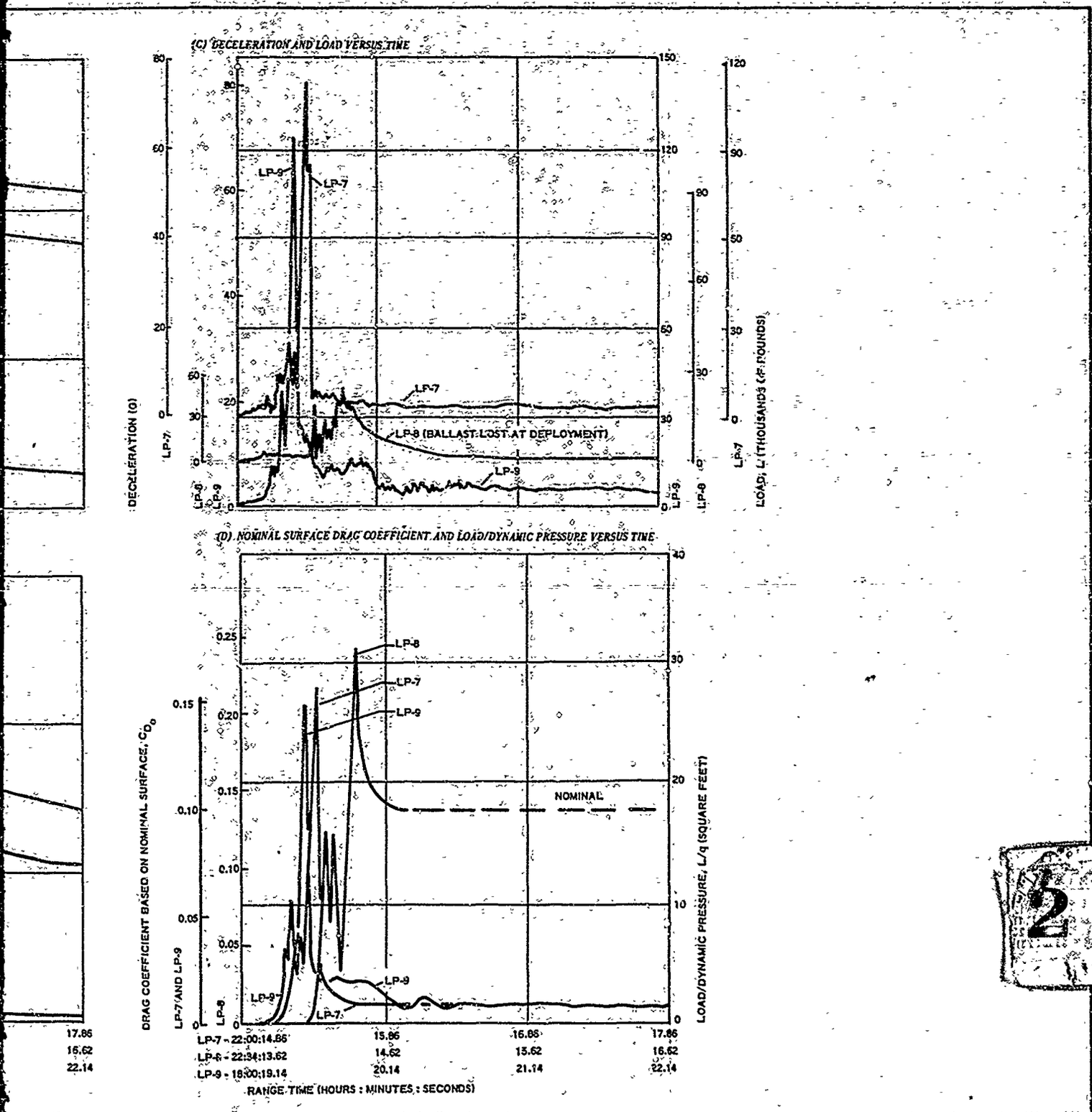

Figure 9 - Performance Data for LP-7, LP-8, LP-9

(Reverse is blank)

SECTION III - LARGE PARACHUTE DECELERATOR

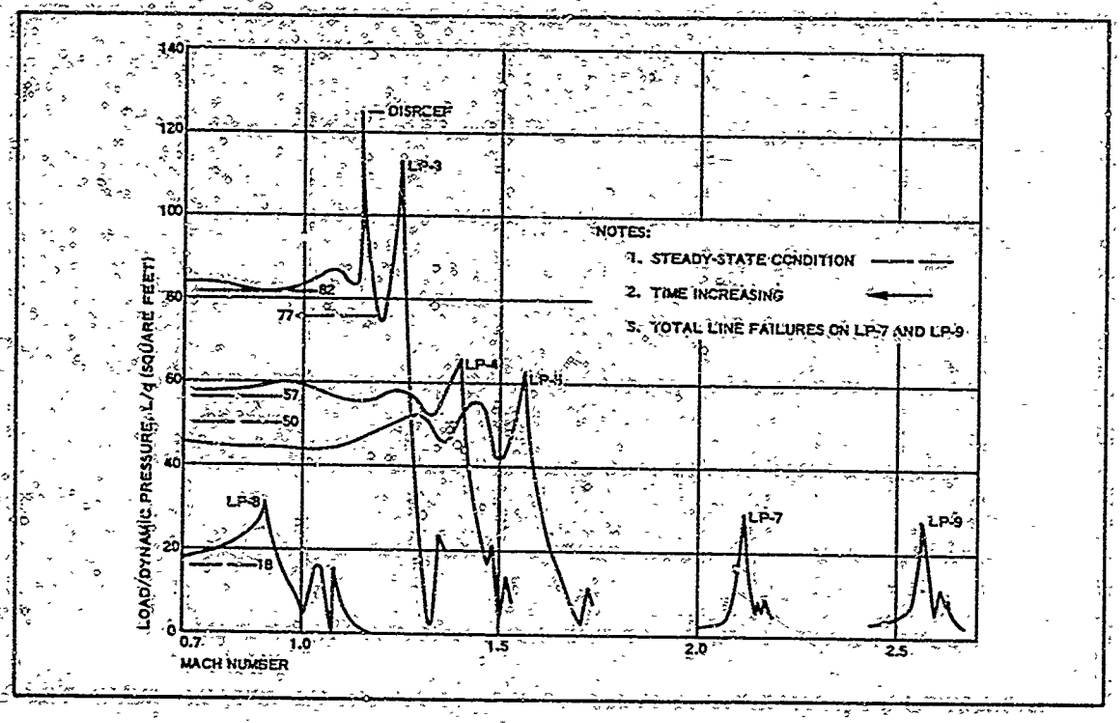

Figure 10 - LP-3, LP-4, LP-5, LP-7, LP-8, and LP-9: Load/Dynamic Pressure versus Mach Number

TABLE IX - LARGE PARACHUTE DIMENSIONAL AND LOADING PARAMETERS

1 Test item	2 Reefing line length, RLL (ft)	3 Reefed inlet area, RIA (sq ft)	4 Test altitude at L_{max} (ft)	5 Test Mach at L_{max}	6 Test q at L_{max} (psf)	7 Test L/q at L_{max} (sq ft)	8 Test L/q after opening (sq ft)	9 Test shock factor, K*
LP-2	20.50	33.60	13,815	1.240	1,350	114.0	77	1.480
LP-3	+	+	13,840	1.130	1,100	125.0	82	1.530
LP-4	14.83	17.55	15,934	1.400	1,642	67.0	57	1.175
LP-4	+	+	16,700	0.460	150	108.0	80	1.350
LP-5	14.83	17.55	10,948	1.560	2,410	63.0	50	1.260
LP-7	13.10	13.66	18,612	2.110	3,250	28.2‡	. . .	. . .
LP-8	11.00	9.63	9,517	0.908	866	31.6	18	1.750
LP-9	11.00	9.63	20,085	2.560	4,540	26.6‡	. . .	. . .

*Column 7/Column 8.

+Disreefed.

‡Reefing and suspension lines broke at this value.

TABLE X - LARGE PARACHUTE MAXIMUM-LOADING COEFFICIENTS

1 Test item	2 Test L/q at L_{max} (sq ft)	3 Reefing line length, RLL (ft)	4 Coefficient, K_{RLL}* (ft)	5 Reefed inlet area, RIA (sq ft)	6 Coefficient K_{RIA}*	7 Inlet reefing ratio, ξ‡
LP-3	114.0	20.50	5.56	33.69	3.40	0.48
LP-4	67.0	14.83	4.51	17.55	3.82	0.25
LP-5	63.0	14.83	4.25	17.55	3.59	0.25
LP-7	28.2	13.10	2.15	13.66	2.07	0.195
LP-8	31.6	11.00	2.88	9.63	3.28	0.138
LP-9	26.9	11.00	2.41	9.63	2.76	0.138

*Column 2/Column 3.

‡Column 2/Column 5

‡Column 5/70 sq ft.

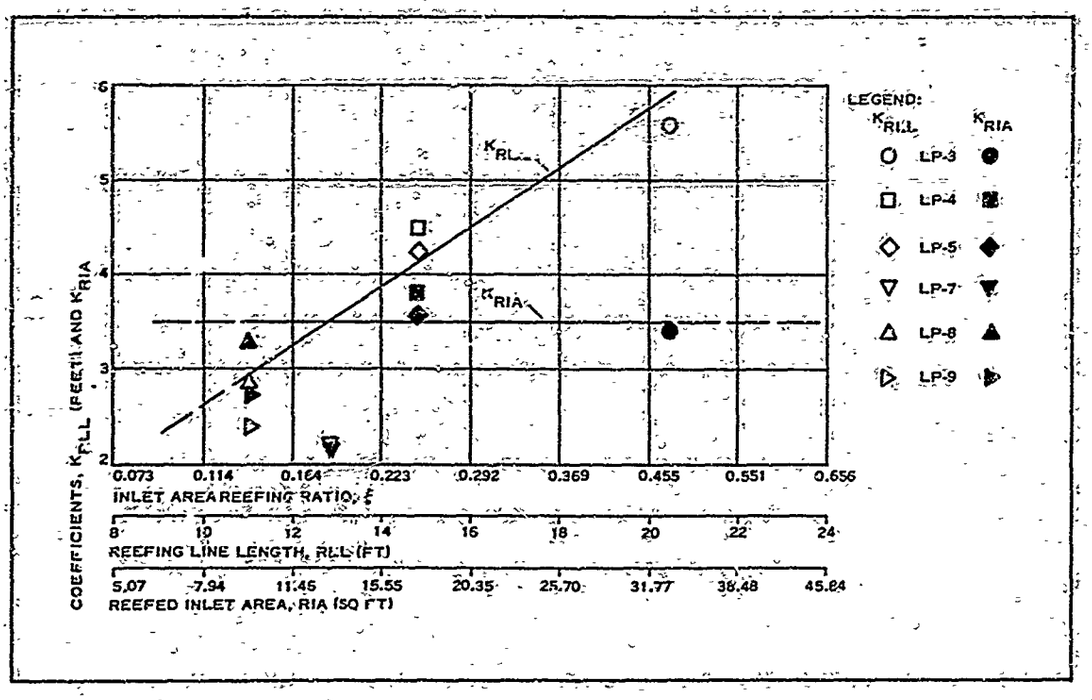

Figure 11 - Reefing Line Length (RLL) and Reefed Inlet Area (RIA) versus Coefficients (K)

d. Reefing Based on Analytical Methods

(1) Approach

The ADDPEP Phase II report presents an approach for determining opening loads based on flow into the canopy, canopy volume change, and flow exiting the canopy (Reference 2, pp 33-35). This approach determined the total drag; i.e., the drag of the shape plus the mass acquisition force during the filling process by geometric increments of canopy growth.

The filling times, which became outputs of the calculations, were much less than those measured during flight. The mass acquisition force calculated approached the drag values for the shape using the inlet-to-exit relationships assumed and the corresponding rapid filling times. Correcting the inlet and/or exit flows to obtain filling times more consistent with the longer values measured reduced the calculated mass acquisition forces.

(2) Shape Drag Calculations

The shape drag calculations are presented for LP-5 in Reference 2 (pp 35-46). A time was chosen after the opening period and when the decelerations were changing at a low rate. Figure 12 summarizes the force values calculated from reduced data for the conditions at a range time of 17:00:10.90 (12.622 sec along trajectory).

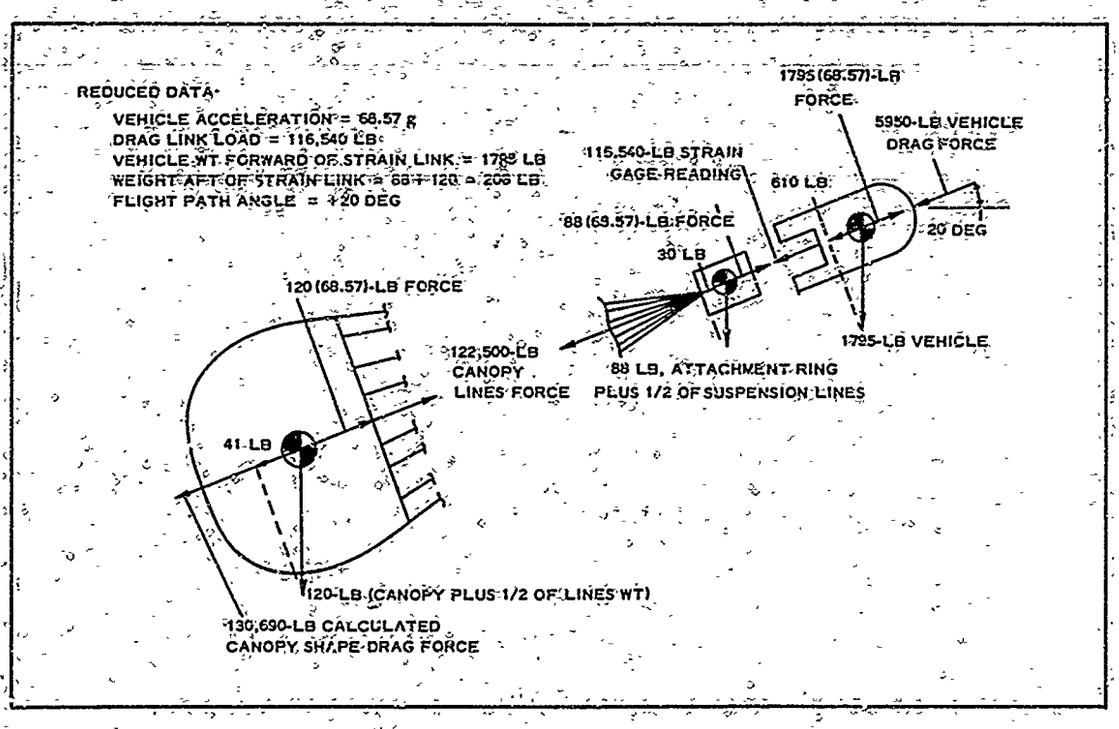

Figure 12 - Summary of Shape Drag Calculation Forces

Vehicle drag was calculated as the force to establish vehicle equilibrium under the remaining loads:

$$\text{Vehicle drag} = \text{vehicle inertia force} - \text{strain link tension} - \text{vehicle weight component}$$

$$= 1795(68.57) - 116,540 - 610$$

$$= 5950 \text{ lb} \tag{3}$$

Canopy lines force at the midpoint of the lines for balancing the loads was calculated, along with canopy drag force, D; and nominal surface drag coefficient, C_{D_o}:

$$\text{Canopy force at line midpoint} = \text{interia force of weight aft of link} - \text{weight component} + \text{strain link tension}$$

$$= 88(68.57) - 30 + 116,540$$

$$= 122,500 \text{ lb} \tag{4}$$

$$\text{Canopy drag force, D} = \text{canopy inertia force} - \text{weight component} + \text{canopy line force}$$

$$= 120(68.57) - 41 + 122,500$$

$$= 130,649 \text{ lb} \tag{5}$$

$$\text{Nominal surface drag coefficient, } C_{D_o} = \frac{\text{canopy drag force, D}}{(\text{dynamic pressure, q})(\text{canopy surface area, } S_o)}$$

$$= \frac{130,649}{(2068.6)(201.06)}$$

$$= 0.314 \tag{6}$$

The 0.314 calculated value for the coefficient, at a high load after the peak of opening, falls correctly near the curves shown earlier in Figure 8 for the flight values excluding the opening shock.

(3) Opening Drag Calculations

The opening drag calculations can be made in the same manner as above by the inclusion of the mass acquisition terms. The test results from LP-9 are presented here as an example. The calculation is simplified, as compared to the previous example, by breaking the loads into only two parts instead of three and ignoring the flight path angle weight components because of the small flight angle. Figure 13 summarizes the force values

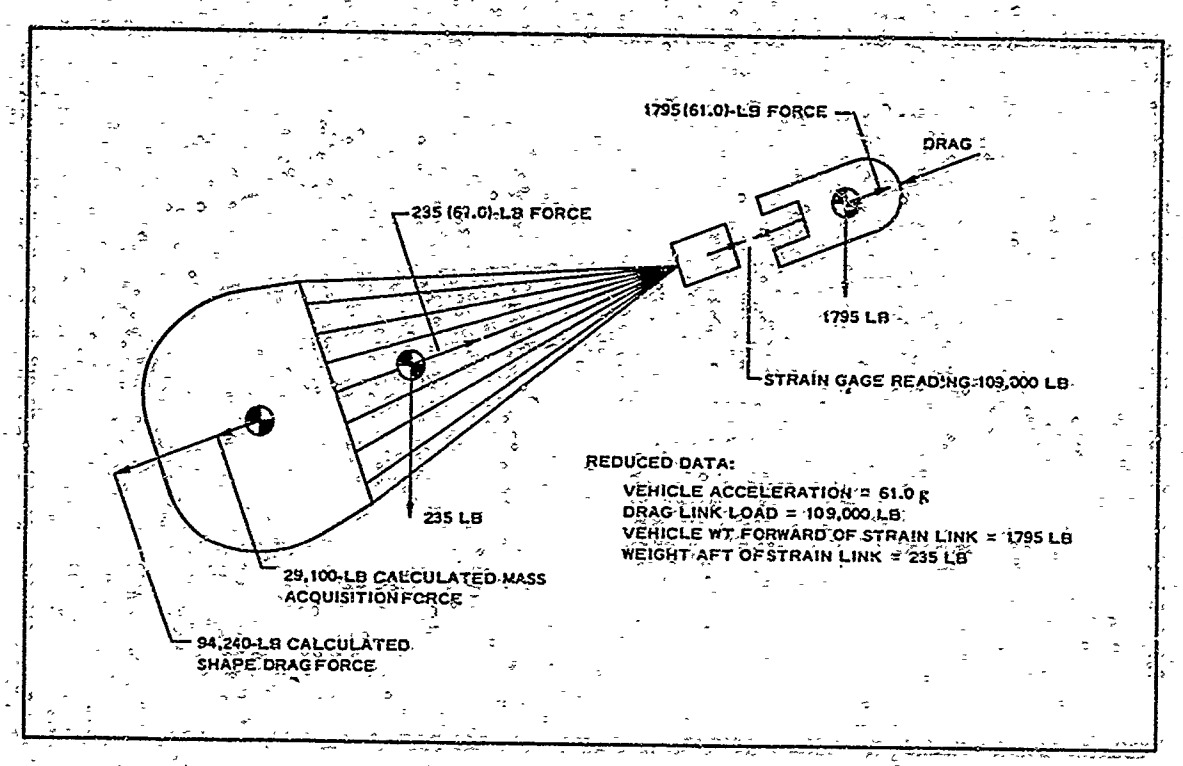

Figure 13 - Summary of Opening Drag Calculation Forces

calculated about the strain gage from reduced data for the conditions at a range time of 18:00:19.537 (17.937 sec along trajectory).

The drag at the first reefing line contact is based on the area of the inlet disc formed by the reefing line. The unstretched reefing line circumference is 10.71 ft. It is assumed that this line stretched to 1.2 times its unstretched length, or to 12.87 ft. The corresponding reefing line radius is 2.06 ft. The inlet radius is considered to extend 1 in. outside of the reefing line. Thus, the inlet radius is 2.14 ft, and the inlet area is 14.4 sq ft.

Detailed study of the load curve shows an abrupt decrease from the peak value, signifying the start of parachute failure at the 19.537-sec point of range time. From analysis, the velocity at this point is 2652 fps, and the corresponding dynamic pressure is 4480 psf, as indicated earlier in Figure 7.

The mass acquisition force can be calculated. The opening time interval extends from 19.481 to 19.536 sec, an elapsed time of 0.055 sec. The acquired mass is based on the volume of gas assumed to have been acquired during the interval. This volume and mass are calculated in the following paragraphs.

At the time that the reefing line is loaded, the canopy and suspension lines are considered to be in line, as shown in Figure 14. The indicated dimensions are based on the longitudinal members elongated to 1.1 times

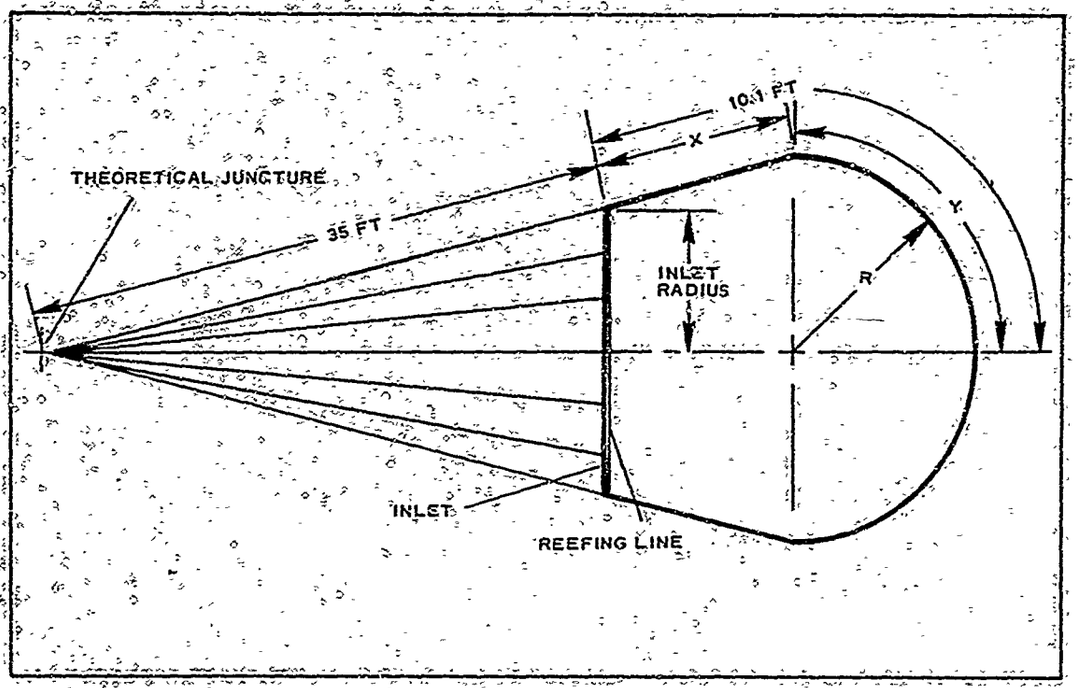

Figure 14 - Geometric Nomenclature

their unstretched length. The following calculation shows the manner in which R is determined:

$$\frac{35 \text{ ft}}{2.06 \text{ ft}} = \frac{35 + X}{R}$$

$$X = 17R - 35$$

$$Y = 1.572R$$

$$X + Y = 10.1$$

$$17R - 35 + 1.572R = 10.1$$

$$18.572R = 45.1$$

$$R = 2.43 \text{ ft} \qquad (7)$$

The corresponding spherical volume is $(4.189)(2.43 \text{ ft})^3 = 60.0$ cu ft.

It is assumed that the sphere of air is brought to a complete stop relative to the canopy. Using Equation 134 of Reference 18 (p 167), the stagnation pressure (P_s) is:

$$P_s = p_\infty \left(1 + \frac{K-1}{2} M^2\right)^{K/K-1}$$

$$= 17,970 \text{ psf} \tag{8}$$

where $p_\infty = 993$ psf; $K = 1.4$; and $M = 2652/1044 = 2.54$

The specific volume of the stagnant air mass (v_s), assuming a reversible adiabatic compression is:

$$v_s^{1.4} = \frac{p_\infty v_\infty^{1.4}}{P_s}$$

$$= 3.10 \text{ cu ft/lb} \tag{9}$$

Where $v_\infty = 24.40$ cu ft/lb. The overall sphere of air weight thus becomes $60/3.10 = 19.35$ lb. The corresponding mass of the sphere is $19.35/32.06 = 0.604$ slugs.

The mass acquisition force (F_m) is:

$$F_m = V\frac{\Delta m}{\Delta t}$$

$$= 29,100 \text{ lb} \tag{10}$$

Where $V = 2652$ fps, assuming negligible obstruction from vehicle and suspension lines; $\Delta m = 0.604$ slugs; and $\Delta t = 0.055$ sec.

Finally, the force resulting from acceleration of the mass to the rear of the strain link is calculated for the following weight:

Item	Weight (lb)
Strain link connection	75
Parachute alone	141
Parachute virtual weights	19
Total weight behind strain link	235

The force (F) to accelerate this weight is:

$$F = ma$$

$$= \frac{Wa}{g}$$

$$= 14,340 \text{ lb} \tag{11}$$

Where W = 235 lb and a = 61.0 g at the instant of reefing line loading. The canopy shape drag at the same instant can be solved by equating the values about the strain link:

Canopy shape drag + mass acquisition force = parachute inertia force + strain link force

$$\text{Canopy shape drag} + 29,100 = 235(61.0) + 109,000$$

$$\text{Canopy shape drag, } D = 94,240 \text{ lb} \tag{12}$$

$$\text{Shape drag coefficient at maximum load} = \frac{D}{qS_o}$$

$$= \frac{94,240}{4480 \times 201.06}$$

$$= 0.105 \tag{13}$$

The 0.105 falls correctly near the shape drag curves shown earlier in Figure 8.

Checking the strain link value versus the vehicle inertia force to determine the vehicle drag:

Vehicle drag force = vehicle weight × acceleration load factor - strain link force

$$= 1795 \times 61.0 - 109,000$$

$$= 109,500 - 109,000$$

$$= 500 \text{ lb} \tag{14}$$

Based on this low vehicle drag value, a measurement error or errors are evident in the load factor or dragline load. The vehicle drag at these conditions should be approximately 9200 lb.

(4) Opening Reefing Line Loads

Phase III testing experience, with premature disreefing and resulting skirt-band failure (LP-7 and LP-9), emphasized the need for determining the magnitude of the generated hoop loads on the reefing line. This analysis, described in Appendix I, offers a new basis for future predictions of the high values likely to be encountered at high q's, i.e., greater than 5000 psf.

4. LARGE PARACHUTE GEOMETRY

The basic configuration of the Phase III LP-7, LP-8, and LP-9 large parachutes, as well as the Phase II LP-3, LP-4, and LP-5 items, is a 16-ft D_o hemisflo ribbon type, with 10-percent extended skirt and 14-percent geometri porosity. The parachute profile dimensions are given

in Figure 15, and the ribbon arrangement and dimensions for a typical gore with the desired porosity are found in Figure 16 and Table XI. The parachute dimensions were derived by geometric computation. Layouts and calculations determined the ribbon arrangement with the desired porosity (Phase II report, Reference 2).

5. STRUCTURAL LOADS AND MATERIAL SELECTION

a. General

During Phase II, all structural elements of the large parachute were analyzed for an opening shock load of 200,000 lb. Hence, material selections and sizes for LP-7, LP-8, and LP-9 remained essentially the same as for LP-3, LP-4, and LP-5 by controlling the reefing within this opening load limit. This meant that the suspension lines, ribbon patterns, skirt band, and reefing line were the same, except as the LP-8 and LP-9 reefing lines were modified following the LP-7 test.

b. Reefing Lines

Part of the reefing line load can be determined from the canopy geometry and the drag load. The remainder of this load is associated with absorbing the energy attained during opening.

It is reported in Reference 2 (Phase II) that, for a 200,000-lb drag load, the corresponding geometric reefing line load is 5700 lb. However, it is also reported in Reference 2, based on the LP-3 tests, that a reefing line strength considerably greater than 5700-lb strength is required to withstand the drag and opening loads. Accordingly, after the LP-3 test, the reefing line design was modified for the LP-4 and LP-5 tests by changing the reefing line webbings from two 6000-lb rated webbings to one 6000-lb and one 12,000-lb rated webbing.

This design was also chosen for LP-7 because the design drag load remained the same as for LP-5. Nontheless, the LP-7 reefing line failed. Therefore, the LP-8 and LP-9 reefing line design was modified to consist of two 12,000-lb rated webbings joined together (shown in Figure 17). This design was tested to 18,850-lb ultimate static load, as compared to 24,000 lb, with failure occurring at the load pins. The reefing failed on the LP-9 test.

The maximum reefing ring load, based on a 24,000-lb reefing line webbing strength, is 4720 lb, which is less than the test value of 6200 lb for the reefing ring attachment (Reference 2).

6. THERMODYNAMIC ANALYSIS

The thermal analysis of the large parachutes is detailed in the Phase II report (Reference 2). Because this analysis included Mach 3 operation at 8000-ft altitude, no alteration or expansion of the analysis was necessary for Phase III. No significant thermal effects were predicted with the materials chosen. No evidence of aerodynamic heating damage was observed in post-test examination of the large parachutes.

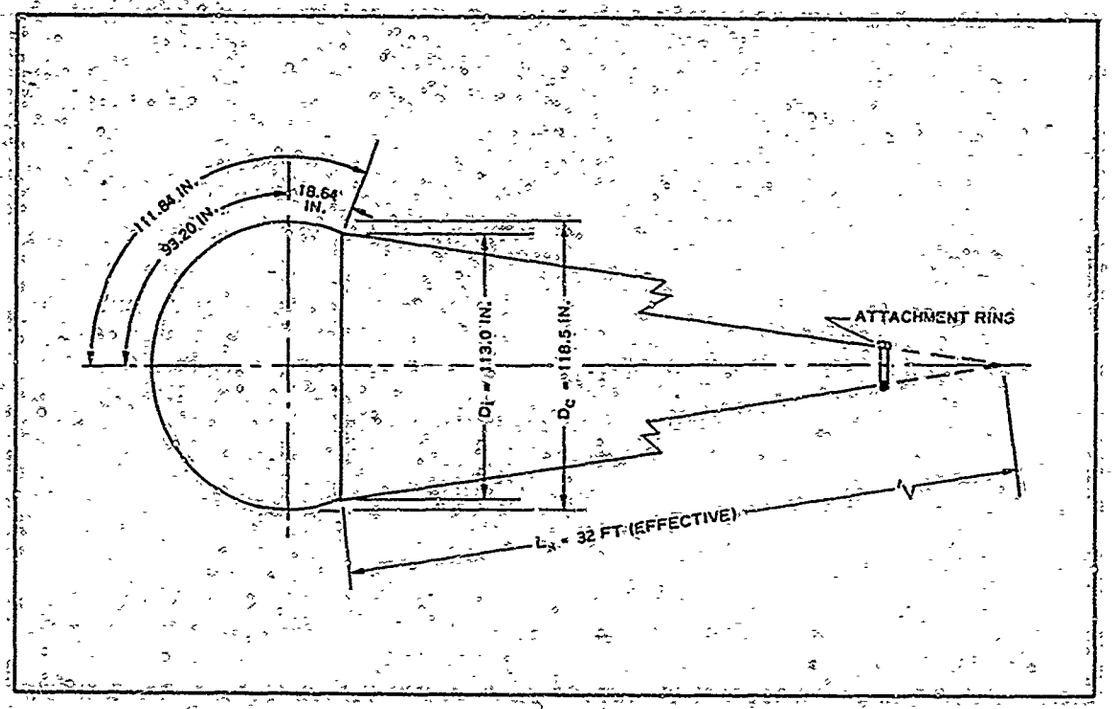

Figure 15 - Sixteen-Foot D_o Hemisflo Profile Dimensions

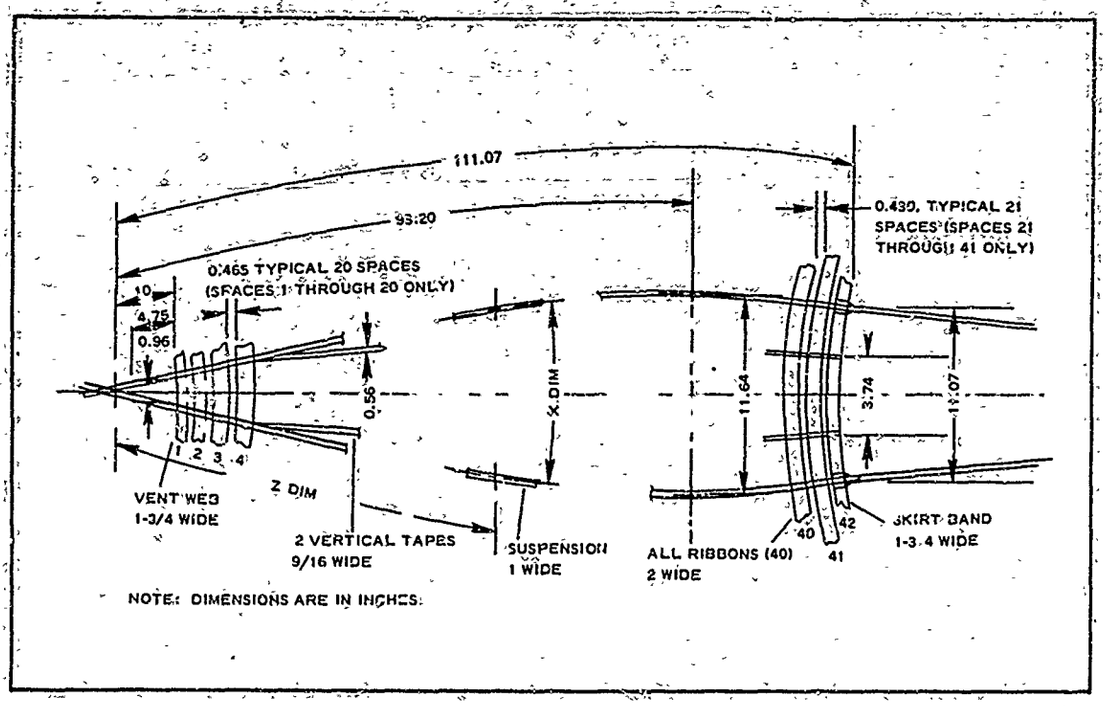

Figure 16 - Ribbon Arrangement for Typical Gore

TABLE XI - RIBBON AND WEB DIMENSIONS FOR TYPICAL GORE

Ribbon	Z*	Circumference (32 X)	X*	Ribbon	Z*	Circumference (32 x)	X*
1	10.95	73.87	2.31	22	62.65	326.70	10.21
2	13.42	88.00	2.75	23	65.08	333.58	10.43
3	15.88	103.00	3.22	24	67.51	340.30	10.63
4	18.34	117.77	3.68	25	69.94	346.42	10.83
5	20.81	132.32	4.14	26	72.37	351.65	10.99
6	23.28	146.50	4.58	27	74.80	356.40	11.14
7	25.74	160.47	5.01	28	77.23	360.65	11.27
8	28.20	174.45	5.45	29	79.66	364.00	11.38
9	30.67	187.50	5.86	30	82.09	366.90	11.47
10	33.14	200.92	6.28	31	84.52	369.38	11.54
11	35.60	213.62	6.68	32	86.95	371.13	11.60
12	38.07	226.34	7.07	33	89.38	372.25	11.63
13	40.53	238.78	7.46	34	91.81	372.73	11.65
14	43.00	250.78	7.84	35	94.24	372.62	11.64
15	45.46	261.00	8.16	36	96.67	371.84	11.62
16	47.93	271.80	8.49	37	99.10	370.46	11.58
17	50.39	282.41	8.83	38	101.54	368.41	11.51
18	52.86	292.95	9.15	39	103.98	365.80	11.43
19	55.32	302.00	9.44	40	106.43	362.48	11.33
20	57.79	310.67	9.71	41	108.87	358.68	11.21
21	60.22	319.34	9.98	42 inner	111.07	354.45	11.08
				42 outer	111.07	333.45	. . .

*Canopy gore-shaping coordinates.

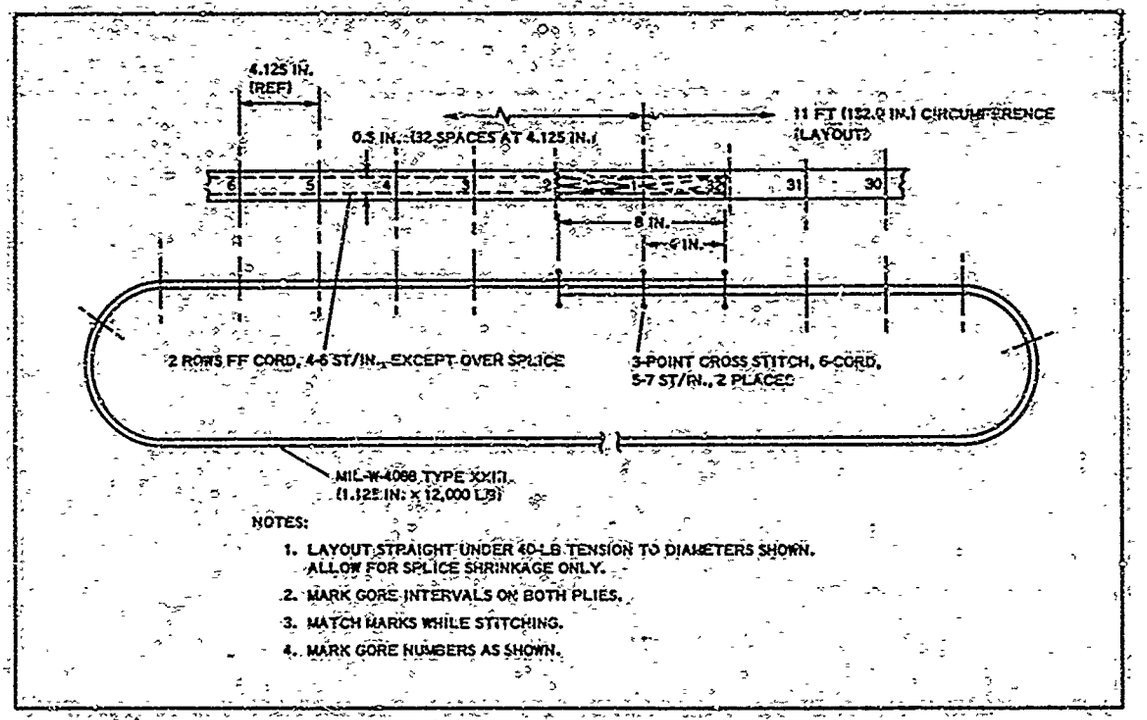

Figure 17 - LP-8 and LP-9 Reefing Line Construction

7. MATERIAL, SEAM, AND JOINT TESTING

During Phase II, the basic material strengths and the joint and seam fabrications used in design and construction were determined by tests in accordance wtih Federal Specification CCC-T-191. The designs resulting from development testing are documented in the design drawings (Reference 2).

For Phase III, the only additional testing was that required for qualifying new lots of material or for changes in construction. Examples include the new heavier reefing line (Figure 17) and the use of different size MIL-T-5038 tapes as canopy break ties in the deployment bag (discussed in the following Item 8 of this section). Loop tests of the reefing line, fabricated of two MIL-W-4088 Type XXIII webbings, developed an ultimate load of 37,700 lb against its material rated strength of 48,000 lb.

8. DESIGN AND FABRICATION

a. General

The Phase III large parachutes retained most of the construction details of the Phase II parachutes (Reference 2). This continuity was possible because the original parachute was designed for operation at Mach 3.0 and 10,000-psf dynamic pressure, the most severe conditions to be encountered during Phase III. However, some structural changes were incorporated as a result of the Phase II testing. These included improving

the vertical-to-skirt band attachments and using additional sewing to attach the teflon sleeve to the suspension lines near the canopy.

Apart from these structural changes, color was added to specific line and canopy areas to aid data interpretation and correlation with post-test inspections (see Figure 18).

b. Drogue Parachute and Deployment Bag

For the LP-7 test, the pilot or drogue chute size was reduced from 48 to 30 in. D_o to control the drag force. For the LP-8 and LP-9 tests, drag force was controlled by further reefing of the drogue. Additional information and supporting calculations are given in Appendix II. Since the drogue parachute was in excellent condition after the tests, no changes were incorporated to the drogue design.

During the LP-7 test, some damage occurred to the deployment bag of the drogue parachute. Hence, for the LP-8 and LP-9 tests, the deployment bag was modified by incorporating additional sewing between the longitudinal webbing and the rear lateral hcop.

The LP-9 tests indicated the drogue and drogue bag were suitable for the test conditions of Mach 2.7 and 5155-psf dynamic pressure.

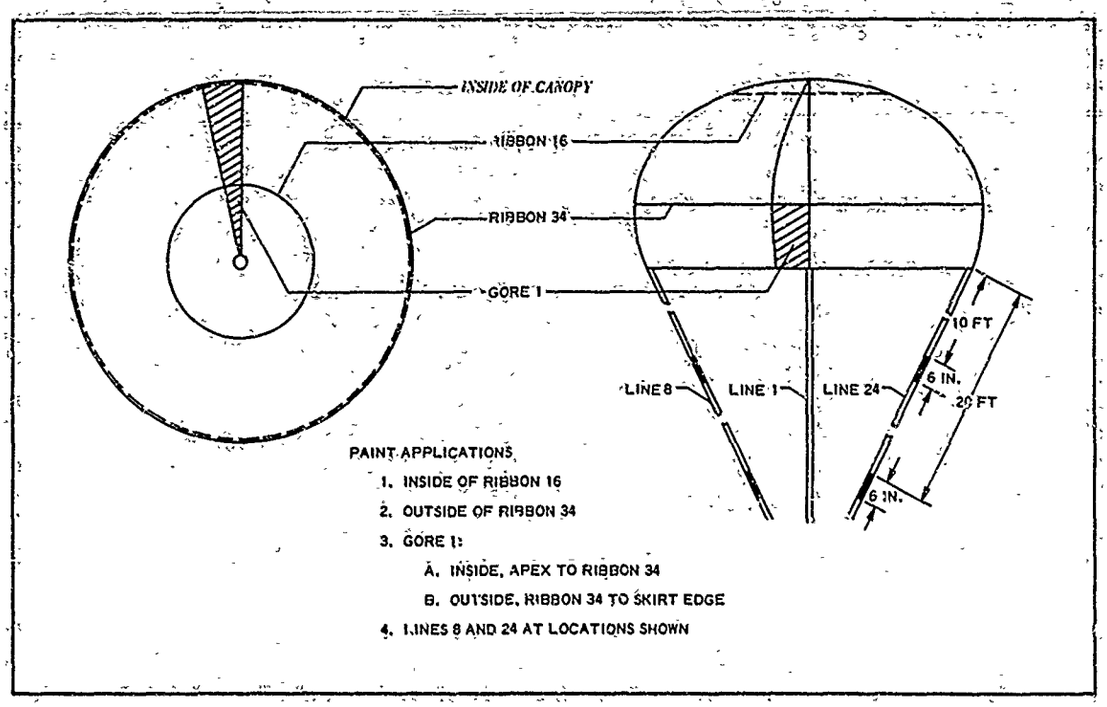

Figure 18 - Large Parachute Marking Pattern

c. Test Item Parachute and Deployment Bag

The LP-7 test showed the test item deployment bag would have to be strengthened to withstand the loads generated by the increased internal pressure in the bag caused by the increased dynamic pressures. From the onboard films, the high pressures appeared to have failed the forward bag-restraining loops; this allowed the bag halves to fold back and permitted the forward portion of the suspension lines to be dragged across the lines still stowed. The rear portion of the lines appeared to have deployed in a less orderly manner than the forward portion. Post-flight inspection showed that the rear half of the bag, behind the locking loops, was split longitudinally allowing a portion of the canopy to be prematurely exposed. One of the four bag loops holding the locking loop was also broken.

Inspection of the nylon suspension lines revealed considerable overall damage, such as that caused by nylon rubbing across nylon at high speed and under heavy loads. Damage from rubbing was also evident on the inlet band. The inlet band is a continuous 19,000-lb nylon web wrapped around twice, once to form the skirt band and once to form the pocket bands. The outside (pocket band) wrap was rubbed through behind one cutter pocket and was damaged and failed in other areas. Two complete breaks occurred and two canopy gore rips resulted. One break stopped at the first reinforced ribbon, and the other involved only two ribbons.

Other canopy damage was associated with the reefing rings and with the butterfly reinforcements. One ring was torn loose, and the sewing was pulled at other rings and on one side of the butterflies. The reefing line was cut in one place and broken in another.

The test item deployment bag, suspension line protection sleeves, and reefing line strength were modified on the basis of post-test inspection and film data of LP-7. The bag design changes were made to improve its strength and provide increased protection to the lines and canopy during deployment (see Drawing 530A005-017-111). These modifications included:

1. Changing the nylon bag material from MIL-C-7219 Type III cloth, 7.25 oz/sq yd (325 by 275 lb/in.) to Stern and Stern Pattern 2823, 20.5 oz/sq yd (1200 by 1200 lb/in.)

2. Adding an interior cotton lining to the bag to cover the nylon bag cloth, longitudinal webs, interior flap, restraining flap, and locking loop flap.

3. Adding Teflon cloth to cover the bag locking loops and canopy locking loop.

4. Replacing the No. 2 grommets with the larger No. 3 size and cutting instead of burning the holes for the grommets. (Test data are presented in Appendix III.)

5. Using one length-oriented flap instead of several restraining loops to restrain the bag after opening. (The flap allows the bag to increase to a 56-in. perimeter upon cutting lacing.)

Packing included these new procedures:

1. Locating 1.5 folds of the suspension lines on the canopy side of the locking loop.

2. Increasing the suspension line tie strengths with the strongest ties nearest the canopy. The ties and break values, based on static pull tests, were (a) 500-lb tie material (MIL-T-5038 Type V, 9/16 in.), first third of lines (nearest the confluence point); (b) 600-lb tie material (MIL-T-5038 Type IV, 1/2 in.), second third of lines; (c) 700-lb tie material (MIL-T-5038 Type IV, 5/8 in.), last third of lines (nearest the canopy).

Other design changes included (1) increasing the length of the teflon sleeves around the suspension lines to 5 ft; and (2) removing the reefing line cutters to allow using a permanent reefing line of two thicknesses of 1z, 600-lb webbing (see Item 5, b.).

These design chang· were incorporated into the LP-8 and LP-9 test units. The LP-8 test conditions were much less severe than anticipated (see Table IX), and no damage resulted to the deployment system or the test item. Under the LP-9 test conditions, which was the most severe of the series (see Table IX), the deployment system withstood the loads with minimum damage. However, inspection of the tested item canopy and lines indicated reefing line failure, major canopy damage, and extensive overall suspension line damage.

Based on these observations, it is concluded that reefing line improvements or alleviation of reefing loads are required for the higher dynamic pressures. The suspension line damage and failure at low load values indicates that more protection or different suspension line materials are requir·d. The teflon sleeves and new deployment bag appear to have reduced local line damage associated with the lines rubbing on the bag or locking loop during deployment. The line damage may be associated with the nylon lines rubbing against each other during deployment. If this is true, it may be necessary to use sleeves for the total length of the lines or to change the suspension line material. From a weight and cost standpoint, a switch from nylon plus teflon sleeves to Nomex lines may be indicated. Nomex appears to have the capability of withstanding the high loading rates associated with the test conditions, based on the behavior of the canopy verticals and ribbons.

9. DEPLOYMENT SYSTEM AND PACKING PROCEDURE

The system established during Phase II for deploying the large parachute test items is described step-by-step in Reference 2. This system was continued successfully throughout Phase III.

Packing refinements that resulted from the LP-7 test findings are reported earlier in this section in Item 8, d. The LP-9 data review showed that this revised packing procedure was allowing the parachute to deploy to line stretch intact, but that suspension line damage was still occurring. The near-perfect condition of the deployment bag indicated that friction between the suspension lines and canopy and the deployment bag was a negligible cause of chute damage at the LP-9 test conditions (Mach 2.7 and 5155-psf dynamic pressure).

10. SUMMARY AND CONCLUSIONS

a. Configuration

Three free-flight tests were conducted on large parachute (LP) decelerators whose basic configuration was established by Phase II tests (Reference 2) and earlier wind-tunnel tests. The free-flight tests indicated strong inflation characteristics in the transonic and supersonic regime (to Mach 2.7) when the inlet was reefed to low inlet area ratio values (ξ = 0.15 to 0.20).

b. Aerodynamic Loadings

As in Phase II, the free-flight data gave higher shape drag coefficients than measured in wind-tunnel tests (see Figure 8). Therefore, reefing line lengths were based on the flight test results. The calculations for LP-7, LP-8, and LP-9 reefing sizes were based on extrapolations of the coefficient curves of LP-3, LP-4, and LP-5 (presented in Figure 11). As can be seen from the final data points on Figure 11, good straight line correlations were obtained over the range of tested reefing sizes.

The measured opening times decreased with increasing flight Mach numbers and dynamic pressures (see Table VIII). This trend was not observed in Phase II; however, the opening times for LP-4 and LP-5 now appear to have been lengthened due to 1.5 turns of line twist compared to small twist values for LP-3, LP-7, LP-8, and LP-9.

Based on the values calculated for opening shock in Table IX, the opening shock values decreased with increasing Mach number and dynamic pressure. It should be noted that the largest opening shock value occurred at the lowest Mach number, dynamic pressure, and reefing size (LP-8).

Because of the strong inflation characteristics of the LP-8 configuration, which resulted in failing the reefing lines of LP-7 and LP-9, an analytical approach was undertaken that appears to better estimate the hoop loads than using the geometry and the drag force (see Appendix I).

c. Geometry

Review of the free-flight films indicated the LP configuration takes a firm geometry, and no changes are recommended to the canopy from a performance standpoint. Changes to reduce the reefing line forces at the highest Mach numbers by using shorter suspension lines, changes in

canopy porosity, or distribution of porosity were not attempted during Phase III.

d. Structure

Inspection of the parachute after each test confirmed the lack of thermal effects on the structure. In the LP-7 and LP-9 tests, reefing line failures overloaded the canopy and failed weakened suspension lines in groups. The line damage was associated with high-speed rubbing of nylon on nylon. This occurred despite an improved deployment bag and teflon sleeves that extended five feet forward of the canopy. Canopy damage after reefing line failure included breaking the skirt band and some ribbons.

Based on these results, more consideration should be directed toward changing the suspension line material and reducing the reefing line loads at Mach numbers above 2.

e. Deployment System and Packing Procedure

The deployment and packing procedure was satisfactory based on films and inspection of the bag; however, line damage, nylon on nylon, and line breakage occurred on most tests. The procedure was the same as presented in Reference 2, with changes to reduce local line damage and obtain a straight pull on the cutter lanyards (see Item 9 of this section).

The near-perfect condition of the newly designed deployment bag, drogue parachute, and drogue parachute deployment bag after the LP-9 test indicates no changes are required to Mach 2.7 and a 5155-psf dynamic pressure for this system.

SECTION IV

SMALL PARACHUTE DECELERATOR

1. INTRODUCTION

a. General

The goal of the small supersonic parachute effort under ADDPEP (Aerodynamic Deployable Decelerator Performance Evaluation Program) was to establish the configuration, loadings, design, and structural materials necessary to attain stable performance for flight speeds up to Mach 5 and for dynamic pressures to 500 psf. This work was initiated during Phase I (Reference 1) and concluded during Phase III.

b. Background

Prior to the ADDPEP undertaking, wind-tunnel and free-flight tests indicated that a truncated cone-type parachute held promise at supersonic speeds and at low ratios of decelerator size to payload size (References 10 and 19). Wind-tunnel tests of small parachute models indicated that reasonable inflation and attitude stability could be attained with cloth designs and a porous base (or roof) made of Perlon, which is a fine-mesh material. However, free-flight performance data of Perlon parachutes were limited to approximately Mach 2.1 because of the limited temperature capability of this fine-mesh material. While Nomex ribbons also were used to construct porous roofs, wind-tunnel tests at higher Mach numbers showed considerably degraded performance as compared to parachutes made of fine-mesh roof. In the light of these considerations, one of the first efforts under ADDPEP was to develop a Nomex fine-mesh material and associated coatings for the higher temperatures linked with the flight environments at Mach 2.1 to 4.0.

To generate the basic engineering data, two concurrent tasks were conducted. The first, undertaken as an in-house program by AFFDL-RTD personnel, provided full-scale wind-tunnel data on past small parachute designs and on a newly generated ADDPEP design (Reference 10). These parachutes, which had low- and high-temperature roof mesh materials, were tested in wind tunnels over past and contemplated test regimes. The second task, undertaken under ADDPEP, was aimed at (1) establishing free-flight data on past designs using old and new materials; and (2) developing analytical methods for designing small supersonic parachutes.

The AFFDL-RTD wind-tunnel tests established the sensitivity of the small parachute to the free-stream Mach number and to manufacturing tolerances. They indicated that an effective ratio of inlet area to exit area approaching the critical for isentropic flow in a convergent rigid inlet is required to ensure full parachute inflation. The exit area was based on (1) the open percentage of the roof mesh (based on measurements at 0.5 in. of water differential pressure) and (2) the roof-mesh area.

c. Phase I

Two basic small parachute 4-ft D_o configurations were investigated during Phase I. The first, known as HYPERFLO, followed past designs (References 19 and 20). The second, known initially as Composite 1 and later as PARASONIC, was evolved as part of the ADDPEP effort.

Two HYPERFLO parachutes, designated SP-1 and SP-2, were obtained for the Phase I undertaking. The SP-1 test item had a Perlon mesh roof and was designed for a planned Mach 2.08 test. The SP-2 item had a Nomex mesh roof and was designed for a planned Mach 2.74 test. The common design of these two HYPERFLO parachutes was based on the general guidelines established prior to the ADDPEP effort by (1) wind-tunnel tests of small parachute models trailing a simulated payload at Mach 2.3 to 4.65 (Reference 19); and (2) one free-flight test behind a 9-in. missile at Mach 2 [illegible], at 101,200-ft altitude, and at 7.0-psf dynamic pressure (Reference 21). This flight-tested model had a 2.71-ft-diameter canopy (D_o), it used 35-percent porous Perlon mesh for the roof gores, and it had a total roof porosity of 26 percent. During Phase I, the SP-1 and SP-2 units were built but missile malfunctions prevented their successful deployment.

The PARASONIC configuration was evolved from (1) the inflated coordinates of a stable model while under wind-tunnel test in the von Karman Gas Dynamics facility at Arnold Engineering Development Center (Reference 22); and (2) loadings derived by analytical methods. The evolved configuration most nearly met the shape requirements of an isotensoid design over the Mach 2 to 4 regime for the predicted loadings. The measured coordinates for the wind-tunnel model and the nominal coordinates for the evolved configuration are given in Figure 20 of the Phase I report (Reference 1).

Three small parachutes, based on the PARASONIC configuration and designated SP-3, SP-5, and SP-7, were designed during Phase I. They had a four-foot diameter canopy (D_o). Two SP-3 and one SP-7 units were constructed of Nomex. The major differences between SP-3 and SP-7 lay in the strength of the suspension lines and in the porosity of the mesh roofs, which were coated to correspond to the test Mach number requirements.

The design methods, as well as the actual designs, of all the Phase I small parachute test items are described in the final report (Reference 1), the results of wind-tunnel tests are given in References 10 and 20.

d. Phase III

Three new PARASONIC small parachutes, designated SP-3, SP-4, and SP-5, were constructed during Phase III. These were identical in all principal geometric details to the basic PARASONIC design established during Phase I. Such a continuity was possible because the maximum Mach 5.6 planned for the Phase III test item (SP-5) fell within the geometric capability of the parachute as originally designed. The configuration is shown in Figure 19, and the details are listed on the following page:

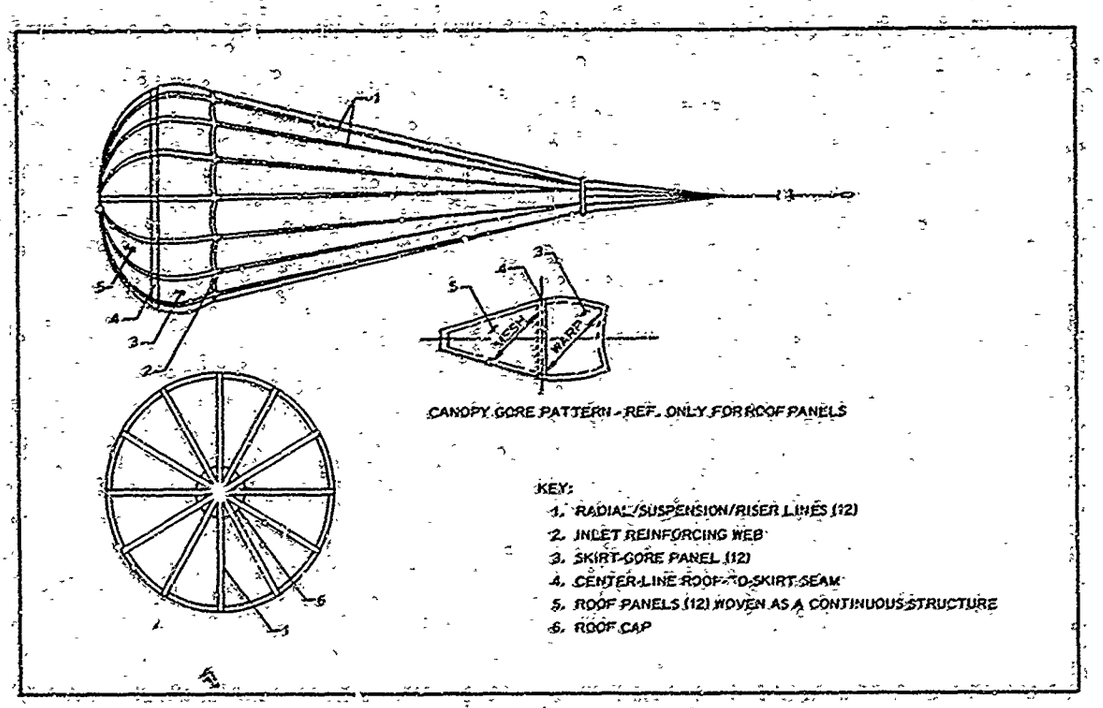

Figure 19 - Configuration for PARASONIC Parachutes SP-3, SP-4, and SP-5

Canopy nominal diameter: D_o = 4 ft

Shape: isotensoid canopy with mesh roof

Ratio of inlet area to exit area: A_{inlet}/A_{exit} = 7.0

Number of gores: 12

Suspension line length (effective): $L_S = 2D_o$ = 61.76 in.

Porosity: nominal 5 percent overall with porous area limited to mesh roof

Material: Nomex-coated to meet heating and porosity requirements

The planned Phase III test conditions for SP-3, SP-4, and SP-5 were established with AFFDL RTD concurrence. Each set of test conditions reflected booster capability, range safety requirements, and results of previous tests. Trajectory analyses produced the desired test conditions that are shown in Table XII. The calculated parameters after deployment are shown in Figures 20A, 20B, and 20C.

As part of Phase III, a new 4-ft D_o HYPERFLO parachute was built that was based on the Phase I SP-1 and SP-2 configuration. This HYPERFLO parachute was wind-tunnel tested along with a PARASONIC unit for comparative purposes. Both were constructed and coated to meet the same high-Mach number flight requirements.

TABLE XII - DESIRED TEST POINTS OF PARASONIC SMALL PARACHUTES

Initial conditions	Design configuration		
	SP-3	SP-4	SP-5
Mach no.	2.50	4.00	5.59
Altitude (ft)	85,000	99,000	121,000
Dynamic pressure (psf)	200	274	201
Flight-path angle (deg from horiz)	76.3	83.2	77.6
Reynolds no. (millions)	2.14	1.70	0.85
Booster comb*	HJ-N	HJ-N-N	HJ-N-L

*Booster definitions: HJ = Honest John; N = Nike; L = Lance

2. WIND-TUNNEL AND FREE-FLIGHT TESTS

a. General

Wind-tunnel tests of the HYPERFLO and PARASONIC parachutes were conducted in the propulsion wind tunnel of Arnold Engineering Development Center. The generally superior stability of the PARASONIC configuration in these tests merited their recommendation for flight tests. Accordingly, the three PARASONIC parachutes (SP-3, SP-4, and SP-5) were flight-tested behind Test Vehicle C on the Eglin Air Force Base test range. The actual test conditions are summarized in Table XIII. In general, these tests demonstrated the capability of the small parachutes to operate up to the conditions of the SP-5 test. The tests also showed that the temperatures predicted by theory were conservative. Significant heating occurred during re-entry of SP-5. Motion pictures indicated that the parachute maintained satisfactory, inflation with some oscillation in the transonic regime. Drag traces were similar to those obtained in the wind-tunnel using the same size PARASONIC parachutes at Mach 2.6 to 3.0 for SP-5.

b. Wind-Tunnel Tests

(1) Parachute

Figures 21A and 21B show the construction geometries of the wind-tunnel tested PARASONIC and HYPERFLO parachutes, as well as their locations behind the forebody.

The 4-ft-diameter HYPERFLO parachute was constructed of Nomex. Only the roof panel was coated with Dyna-Therm. The mesh roof was

(A) ALTITUDE AND MACH NUMBER VERSUS TIME

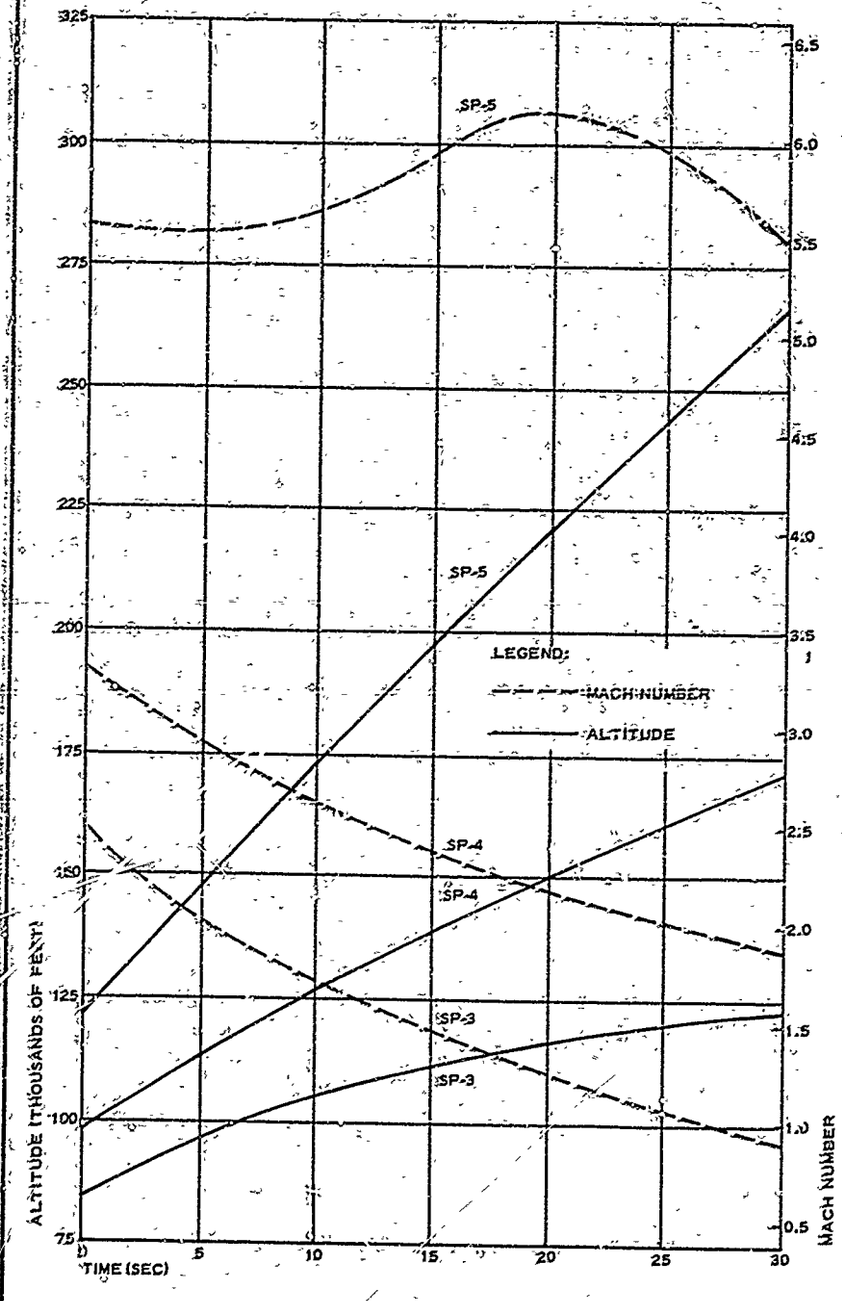

(B) DYNAMIC PRESSURE AND LOAD FACTOR VERSUS TIME

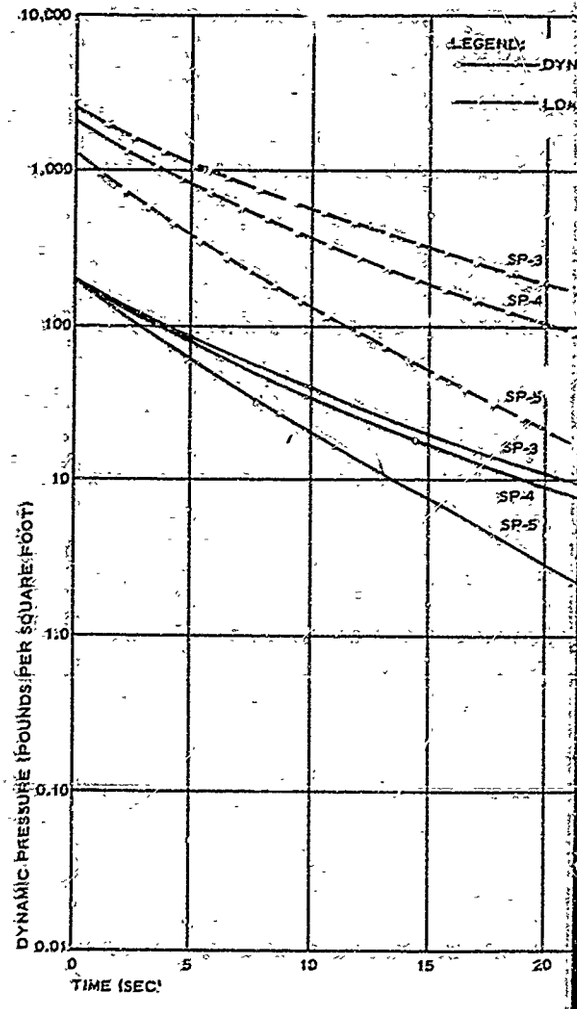

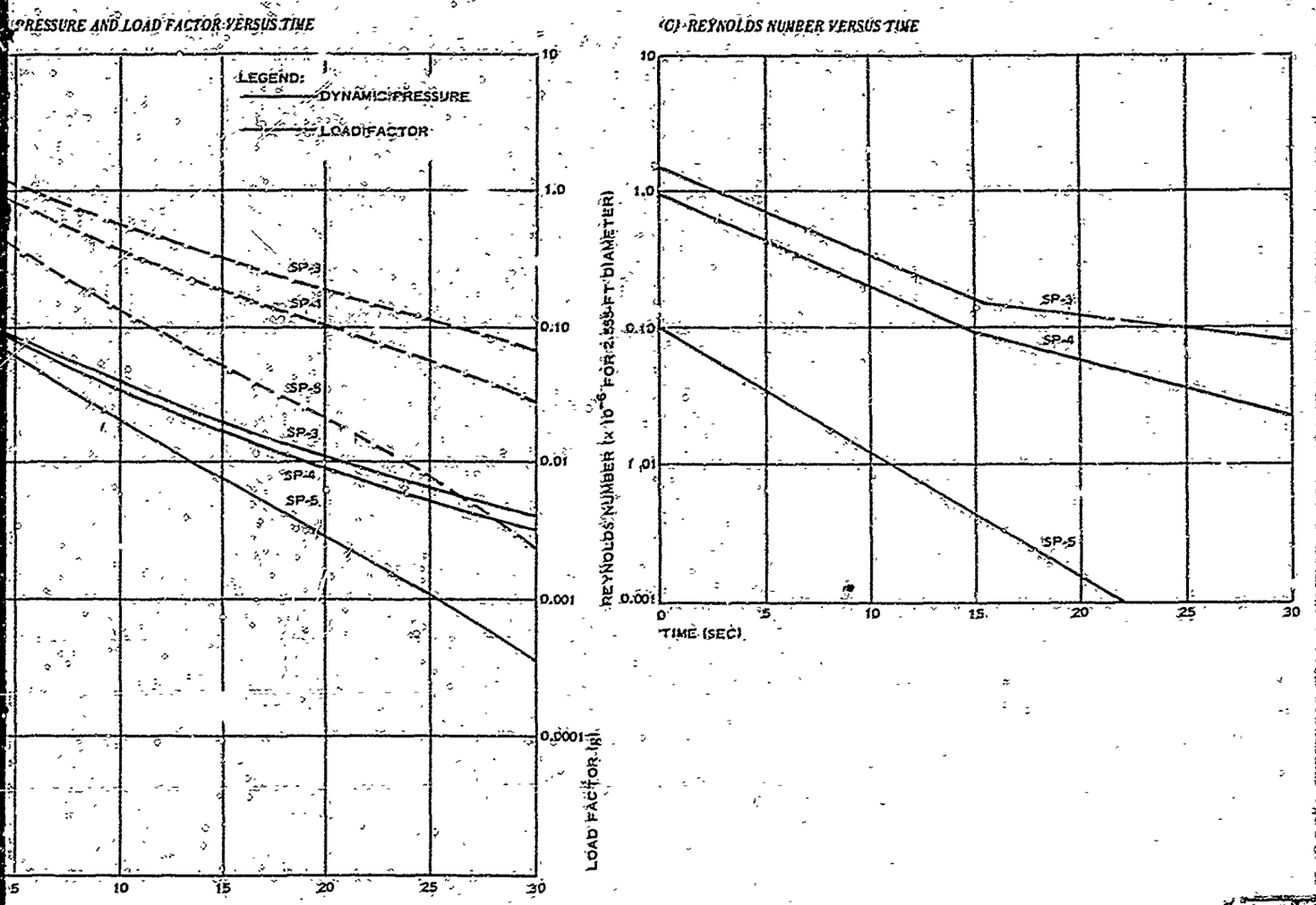

Figure 20 - Calculated Parameters after Deployment for PARASONIC Parachutes SP-3, SP-4, and SP-5

(Reverse is blank)

TABLE XIII - SUMMARY OF SMALL PARACHUTE (PARASONIC) TEST CONDITIONS

Test item	Event	Range time (hr:min:sec)	Load (lb)	Conditions			
				Mach no.	Dynamic pressure (psf)	Altitude (ft)	Stagnation temperature (F)
SP-3	Launch	16:56:59.52	. . .	. . .	. . .	. . .	. . .
	Test item deploy	16:57:34.27	. . .	2.70	329	78,000	515
	Initial line stretch	16:57:34.354	1543*	2.69	317	78,500	508
	Maximum load	16:57:34.441	3600*+	2.68	312	78,800	498
SP-4	Launch	12:30:00.00	. . .	. . .	. . .	. . .	. . .
	Test item deploy	12:30:32.77	. . .	1.66	328	56,300	130
	Initial line stretch	12:30:32.810	720	1.48	275	56,400	100
	Maximum load	12:30:32.918	2633+	1.42	251	56,600	90
SP-5	Launch	12:57:03.01	. . .	. . .	. . .	. . .	. . .
	Test item deploy	12:57:44.28	. . .	5.48	229	117,000	2540
	Initial line stretch	12:57:44.486	213	5.40	213	118,000	2480
	Maximum load	12:57:45.130	530+	5.23	172	121,600	2360

*Value from secondary source data

+Opening shock values 3.0, 2.2, and 1.1 times steady-state values

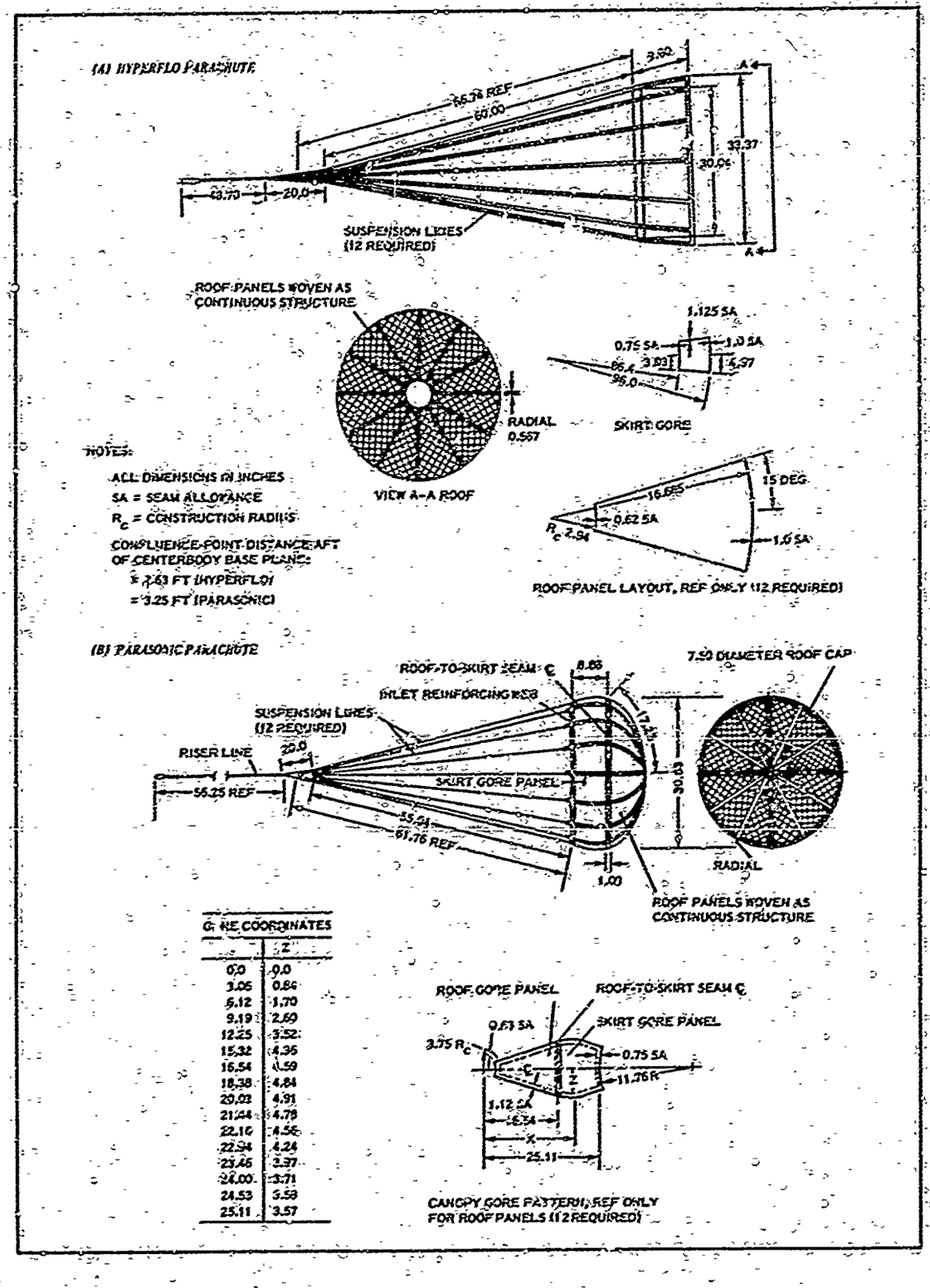

GORE COORDINATES

X	Z
0.0	0.0
3.06	0.86
6.12	1.70
9.19	2.59
12.25	3.52
15.32	4.36
16.54	4.59
18.38	4.84
20.02	4.91
21.44	4.79
22.16	4.56
22.94	4.24
23.46	3.97
24.00	3.71
24.53	3.59
25.11	3.57

Figure 21 - HYPERFLO and PARASONIC Wind-Tunnel Configurations

constructed of 0.25-in. webbing. The total porosity of this parachute was approximately 5.6 percent, and its inlet-to-exit area ratio was 7.0.

The 4-ft-diameter PARASONIC parachute for the wind-tunnel test was constructed of nylon with a Dyna-Therm coating on the canopy. The mesh roof was constructed of 0.25-in. webbing. The total porosity of this parachute was approximately 5 percent, and its inlet-to-exit area ratio was 7.0.

(2) Test Setup

The parachutes were deployed from a strut-mounted centerbody. The location of the centerbody in the wind tunnel is shown in Figure 22. The parachutes were packed in the aft end of the centerbody on a spring-loaded plate. They were held inside the center body and against the plate by retaining straps that were released by a squib-fired release-pin mechanism.

The parachute riser was connected to the centerbody by a cable with a load cell in series. A swivel was used to prevent twisting of the parachute suspension lines. A shear pin designed to protect the load cell was used to connect the riser line to the cable.

A 5000-lb capacity, double-element load cell was used to measure the drag load of the decelerators to within ±7 lb for the range of drag loads measured during these tests. A direct writing oscillograph was used to

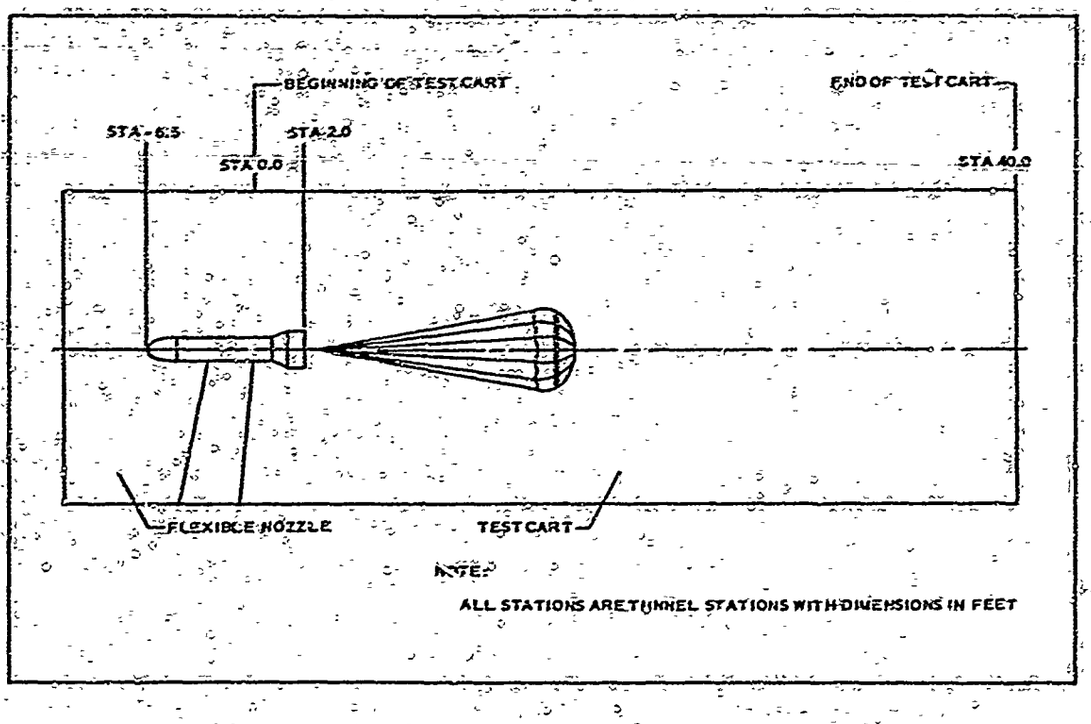

Figure 22 - Location of Small Parachute in Wind Tunnel

monitor the decelerator drag load during testing. Five motion-picture cameras and two television cameras, installed in the test section walls, were used to document and monitor the tests.

(3) Procedure

A parachute was packed in the aft end of the strut-mounted centerbody before the wind-tunnel test operation was initiated. Once test conditions were established, the decelerator was ejected from the centerbody into the airstream. Motion pictures, drag data, and dynamic pressure data were obtained during and after each deployment. When the decelerator deployment sequence was completed, a steady-state drag load was calculated by averaging the analog output signal from the strain-gage load cell over a one-second interval.

The parachutes were deployed at a nominal Mach number and free-stream dynamic pressure of 2.8 and 120 psf, respectively. After deployment, additional data were obtained at Mach numbers of 2.9 and 3.0. The centerbody was maintained at zero angle of attack and yaw for the entire test. Table XIV summarizes the test conditions (Reference 23).

(4) Results

Deployment and inflation data were obtained from the PARASONIC parachute but not from the HYPERFLO, which failed to separate completely from the deployment bag. A strap from the HYPERFLO deployment bag encircled the riser lines during deployment, thus causing the parachute to become partially reefed. Steady-state data were obtained for both decelerators at Mach 2.8 and 120-psf free-stream dynamic pressure. Additional data were obtained at Mach 2.9 and 3.0. Table XIV summarizes the test results.

The PARASONIC deployment time history is shown in Figure 23A. The snatch and opening shock forces of this configuration were 930 and 650 lb, respectively.

The drag coefficients for the parachute configurations are given in Table XIV. The effect of Mach number on parachute drag coefficient is shown in Figure 23B. In the test range, the PARASONIC drag coefficient showed little decrease with increasing Mach number, as compared with the decrease in the HYPERFLO drag coefficient. The drag coefficient of the HYPERFLO was from 45 to 50 percent higher than the PARASONIC.

Photographic coverage obtained by motion-picture cameras permitted the determination of decelerator inflation and stability characteristics. The PARASONIC parachute attained full-canopy inflation approximately 0.015 sec after full-line extension. The fully-inflated canopy exhibited an oscillation of approximately ±7.0, ±4.5, and ±8.0 deg at Mach 2.8, 2.9, and 3.0, respectively. This oscillation was in a plane that is perpendicular to the centerline of the centerbody. The frequency of oscillation was greatest at Mach 3.0. The HYPERFLO parachute, once inflated, exhibited a 17.0-deg oscillation at Mach 2.8.

TABLE XIV - WIND-TUNNEL TEST CONDITIONS AND RESULTS FOR SMALL PARACHUTES

Small parachute configuration	Canopy nominal diameter, D_o (ft)	Canopy total porosity (percent)	Ratio of inlet to exit area, A_i/A_e	Mach no. free stream, M_∞	Dynamic pressure free stream, q_∞ (psf)	Nominal surface drag coefficient, C_{D_o}	Maximum angle of oscillation about base attachment point (±deg)*	Time from deployment initiation to full inflation (sec)*	Time from full-line extension to full inflation (sec)
PARASONIC	4	5.0	7.0	2.8	120	0.135	7.0	0.73	0.015
			7.0	2.[illegible]	120	0.130	4.5	. . .	. . .
			7.0	3.0	120	0.131	8.0	. . .	. . .
HYPERFLO	4	5.6	7.0	2.8	120	0.218	17.0	+	. . .
			7.0	2.9	120	0.209	. . .	. . .	. . .
			7.0	3.0	120	0.188	. . .	. . .	. . .

*These data were obtained from photographic coverage

+No deployment data obtained

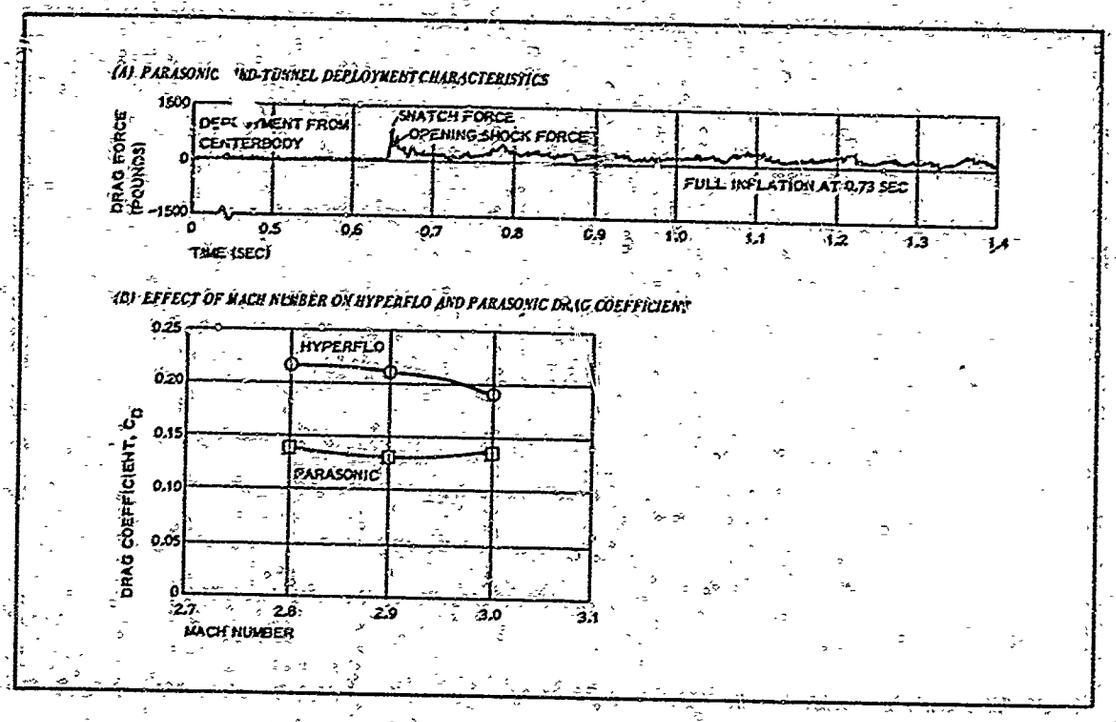

Figure 23 - HYPERFLO and PARASONIC Wind-Tunnel Test Results

Although the HYPERFLO parachute had a higher drag coefficient than the PARASONIC, the latter was selected for flight tests because of its superior stability.

c. Free-Flight Tests

(1) SP-3 Parachute

The SP-3 PARASONIC parachute was the first to be flight-tested. To obtain temperature-time records of the SP-3 canopy during flight, thermocouples were located in the positions shown in Figure 24. All the flight-tested small parachutes were equipped in this manner.

The test vehicle (C) was launched by an Honest John-Nike (HJ-N) booster combination. At 32 sec after launch, the three radars lost the vehicle in flight and could not pick it up again. A good signal from the telemetry was received throughout the flight until impact. One phototheodolite tracked the vehicle for 160 sec and another for about 90 sec. Both first and second stage booster separations were normal. Without radar tracking, the vehicle impact point could not be established. Neither the search aircraft nor the recovery boat located the vehicle.

Azimuth readings were obtained from Sites B4A, D-3, and A-11. A second aircraft and the recovery boat made another search at 14.30, but the vehicle was not located.

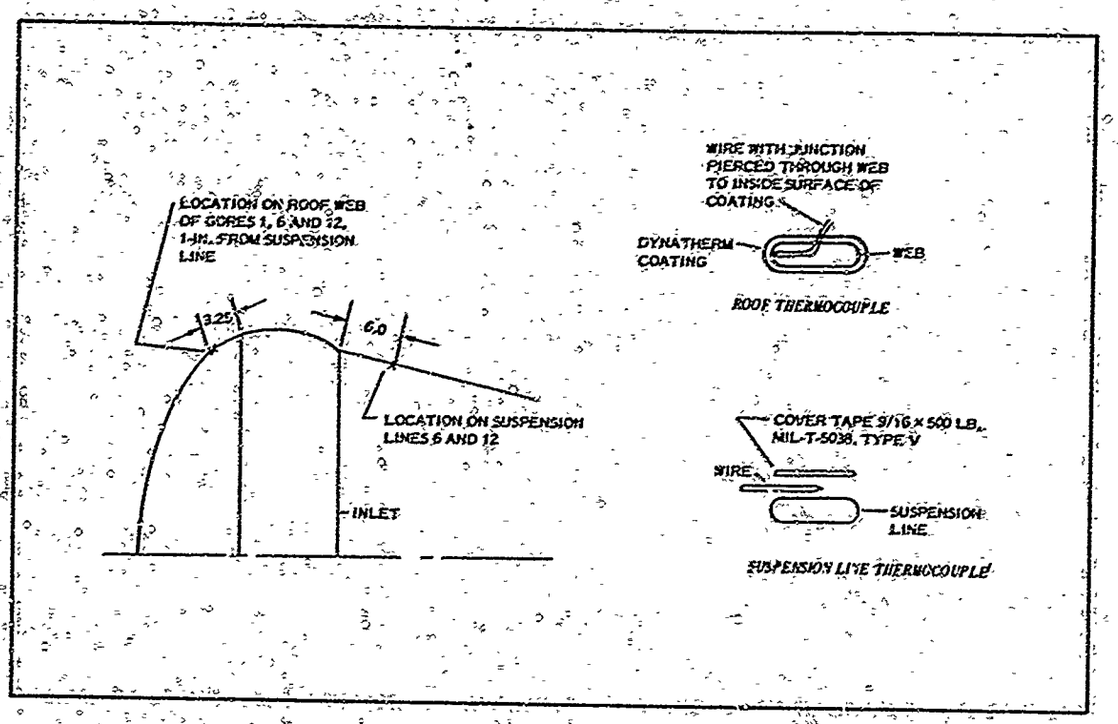

Figure 24 - Location of Thermocouples for SP-3, SP-4, and SP-5

Table XV shows the SP-3 predicted and the telemetry-recorded actual event times, as well as the range times. As indicated, the actual 284.1-sec total flight time was shorter than the 417.0-sec predicted time. All events functioned as programmed. The shorter flight time was due mostly to the short recovery parachute period.

The static pressure reading at deployment indicated an altitude of approximately 78,800 ft at 34.7 sec. The radar plots at 32 sec (where radar lost the vehicle) indicated that the altitude was approximately 74,000 ft.

The shock and drag channels dropped to zero load values 0.175 sec after the test item container ejection was initiated. Off-scale peak load values occurred, indicating broken stain gage circuits.

Loss of the test vehicle and, hence, the SP-3 test item and the test film, limited conclusions on flight performance. However, the accelerometer data gave an indication of the forces. Readings obtained from the thermocouples showed the temperature rise to be negligible as predicted. First order interpretation of the tracking data, which considered the acceleration of gravity, the dynamic pressure (q) change, and a constant drag area (C_DA), indicated a parachute drag coefficient (C_{D_o}) of 0.22 to 0.25.

Figure 25 shows a plot of usable SP-3 data from available telemetry over the opening interval. Load values were calculated from recorded accelerometer data.

TABLE XV - SP-3 EVENT TIMES

Event	Time after launch (sec)		Range time (hr:min:sec)
	Predicted	Actual	
Launch	0.0	0.00	16:56:59.60
First stage burnout	4.8	4.73	16:57:04.33
Second stage ignition	16.3	16.40	16:57:16.00
Second stage burnout	19.5	19.60	16:57:19.20
Second stage separation	21.7	22.20	16:57:21.80
Telemetry pretest calibration	27.6	27.70	16:57:27.30
Despin on	27.6	27.70	16:57:27.30
Despin off	. . .	29.40	16:57:29.00
Solenoids open	33.4	33.70	16:57:33.30
Test item deploy	34.4	34.70	16:57:34.30
Post-test calibrate	64.4	64.40	16:58:04.00
Post-test calibrate off	67.4	68.00	16:58:07.60
Solenoids closed	75.3	76.40	16:58:16.00
Separation nut	270.0	256.70	17:01:16.30
Recovery parachute ejection	270.5	257.10	17:01:16.70
Nose separation	271.5	258.00	17:01:17.60
End of transmission	417.0	284.10	17:01:43.70

(2) SP-4 Parachute

For the SP-4 flight test, Test Vehicle C was launched by an Honest John-Nike-Nike (HJ-N-N) booster combination. At liftoff the first and second stages both ignited. The second stage quickly separated from the first stage. The vehicle was then boosted at the proper time by the third stage Nike and reached a test point of Mach 1.60 and a 328-psf dynamic pressure.

Except for a premature ignition of the second stage, all flight events occurred as planned. As a result of the premature firing, the test decelerator was deployed at a time of higher dynamic pressure and a lower Mach number than planned. The dynamic pressure based on the phototheodolite data was 328 psf versus the 274 psf planned. The Mach number was 1.6 versus the 4 planned. The SP-4 test parachute remained attached to the vehicle from the time of deployment, T + 32.77 sec, to T + 217.58 sec, at which time the parachute was released and recovery was initiated.

The telemetry yielded useful data. The 70-kc (shock) and the 40-kc (drag) channels showed good agreement. Peak shock loads were in excess of

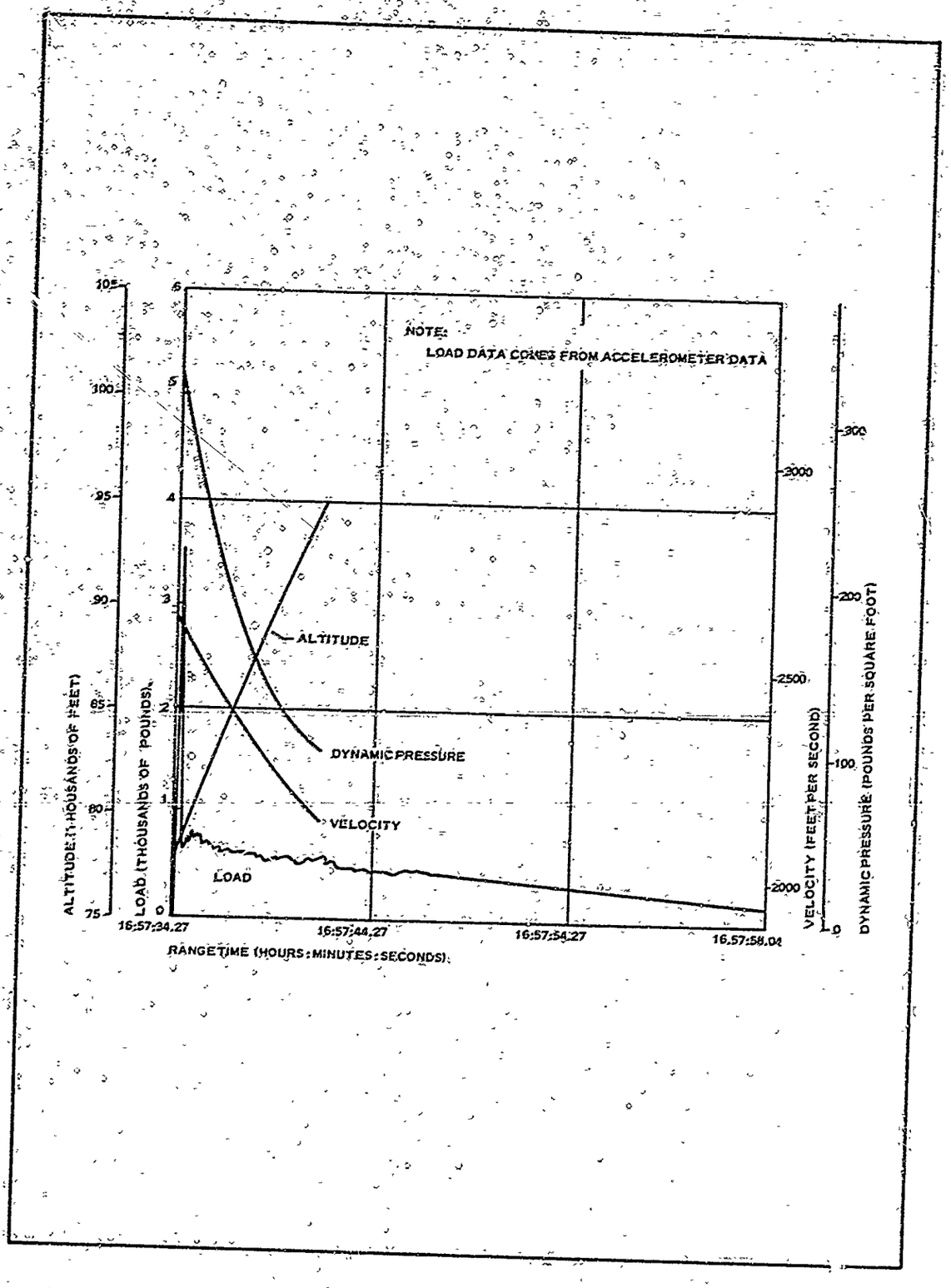

Figure 25 - SP-3 Performance Curves

2000 lb on the strain link. The 30-kc (acceleration) channel monitored booster thrusting and gave a satisfactory indication of initial deceleration by the test parachute.

One of the five thermocouples on the test parachute showed an open circuit during the vertical operational range check. One thermocouple failed during test parachute deployment. The other three thermocouples continued to operate during flight until the test parachute was released. The maximum temperature measured by the thermocouples was 103 F from the time of parachute deployment onward. The 22-kc channel recorded event markers and current pulses throughout the flight.

As indicated by Table XVI, there was an excellent agreement between the SP-4 predicted and actual event times. Recovery events initiated by barometer switches were earlier than estimated for normal staging.

TABLE XVI - SP-4 EVENT TIMES

Event	Time after launch (sec)		Range time (hr:min:sec)
	Predicted	Actual	
Launch	0.0	0	12:30:00.11
First stage burnout	4.8	. . .	. . .
Second stage ignition	10.0	0	12:30:00.11
Second stage burnout	13.2	3.5	12:30:03.61
Third stage ignition	16.0	15.97	12:30:16.08
Third stage burnout	19.2	19.35	12:30:19.45
Third stage separation	22.8	22.6	12:30:22.71
Telemetry pretest calibrate	25.0	24.35	12:30:24.46
Despin on	25.0	24.35	12:30:24.46
Despin off	. . .	25.12	12:30:25.23
Solenoids open	32.0	31.9	12:30:32.01
Test item deploy	33.0	32.77	12:30:32.88
Post-test telemetry calibrate	60.0	. . .	. . .
Post-test telemetry calibrate	60.0	. . .	. . .
Solenoids closed	70.0	69.89	12:31:10.00
Separation nut fired	320.0	217.58	12:33:37.69
Recovery parachute ejected	320.5	218.1	12:33:38.21
Nose probe separation	321.5	218.97	12:33:39.08
Recovery parachute inflated	. . .	250.8	12:34:10.91
End of transmission	460.0	259.78	12:34:19.89

The test vehicle was recovered floating in good condition. Both cameras - a high-speed, 800-frame per second unit and a 400-frame per second unit - monitored the test parachute behavior. A search was conducted for the SP-4 test parachute, which fell with the release tensiometer beam. The tensiometer beam had a pinger attached for underwater location. The pinger was heard using the hand-held, onboard listening device. The parachute was discovered 3/4 mi offshore in 35 ft of water, but it could not be retrieved. A second search was conducted, again without success. By this time, the pinger battery power had expired. Underwater currents had probably moved the parachute to an unknown position.

Figure 26 shows the phototheodolite and telemetry data of SP-4 performance during and immediately following deployment.

(3) SP-5 Parachute

For the SP-5 flight test, Test Vehicle C was launched by an Honest John-Nike-Lance (JH-N-L) booster combination. Liftoff was very stable. The second and third stages fired precisely as programmed. The test point attained was approximately Mach 5.5 at 122,000-ft altitude, very close to the predicted test point of Mach 5.59 at 121,000-ft.

The radar beacon track was reported off direction at 38 sec after launch by Sites A-20 and D-3. Skin track at Site A-20 continued until about 300 sec after launch, when the track was lost. At this time, the vehicle was descending, and the altitude was 486,000 ft.

The test vehicle was not recovered. Impact was 75 mi down range in water deeper than 600 ft. The aircraft and recovery boat searched the projected impact area for 3 hr after launch. The aircraft, directed from A-20 radar, searched a region approximately 20 mi square.

The SP-5 deployment, shock and drag loads were recorded by telemetry. Parachute thermocouples provided continuous readings on the telemetry record during the total period. During re-entry the thermocouple temperature values reached 824 F, which was band-limited for the telemetry.

As indicated by Table XVII, there was generally good agreement between the SP-5 actual event times and the predicted times.

Significant performance data were obtained for the upward trajectory test point and the bonus re-entry condition. The SP-5 test parachute did not survive the total high thermal and loading environment of the re-entry trajectory; however, the parachute did build up significant drag during re-entry, showing that SP-5 had a long term capability to withstand a high-temperature environment.

Figure 27 shows the SP-5 plots of phototheodolite and telemetry data at and immediately following deployment and during the re-entry phase. Although films of SP-5 were not recovered, the parachute operation was considered normal. This view was based on the load traces, which were very similar in shape to those recorded for the same size and type canopies during wind-tunnel testing to Mach 3.

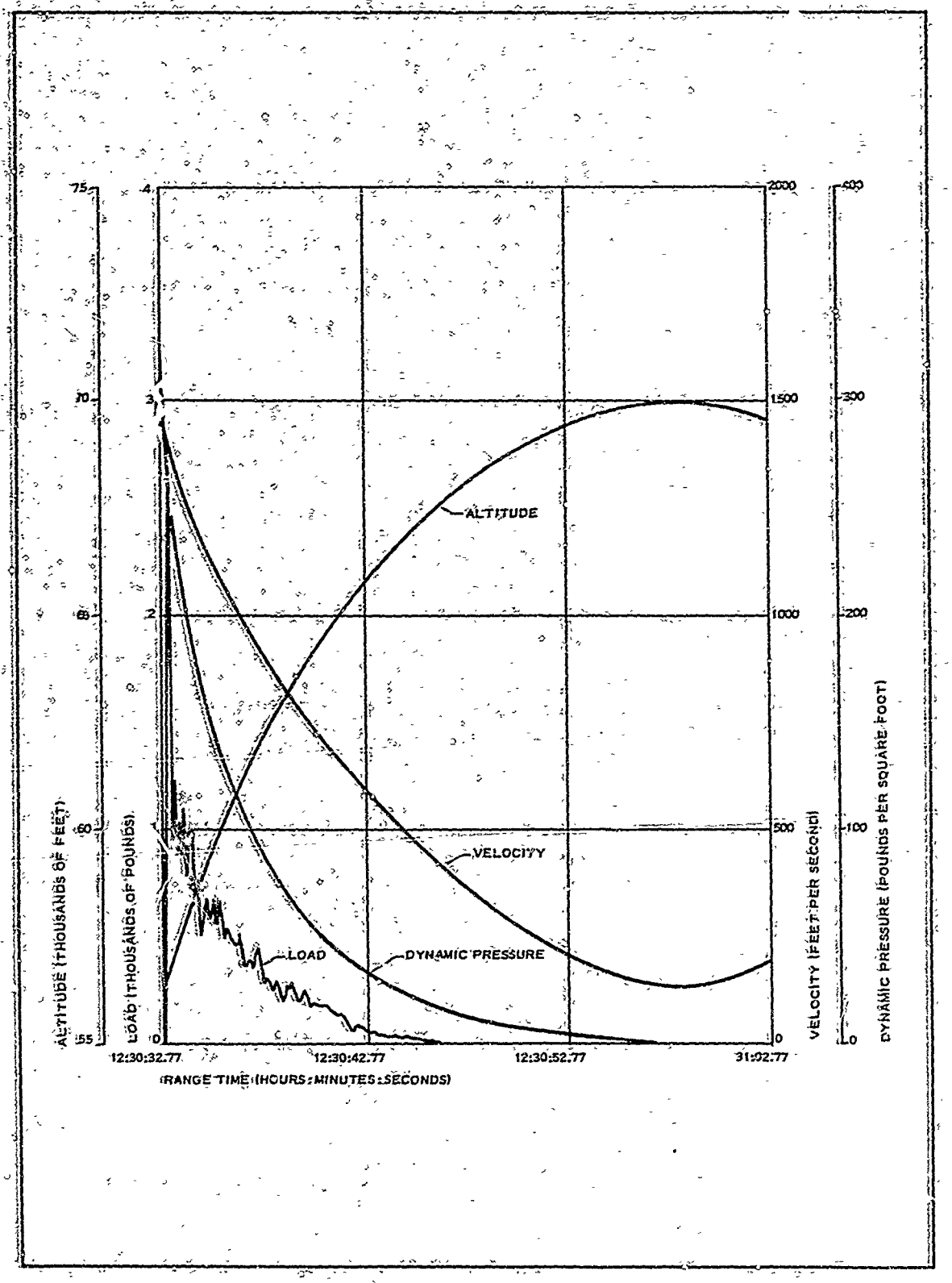

Figure 26 - SP-4 Performance Curves

SECTION IV - SMALL PARACHUTE DECELERATOR

TABLE XVII - SP-5 EVENT TIMES

Event	Time after launch (sec)		Range time (hr:min:sec)
	Predicted	Actual	
Launch	0.0	0.00	12:57:03.51
First stage burnout	4.8	4.59	12:57:08.10
Second stage ignition	9.7	9.79	12:57:13.30
Second stage burnout	12.9	13.09	12:57:16.60
Third stage ignition	26.3	24.69	12:57:28.20
Third stage burnout	32.3	39.45	12:57:33.96
Third stage separation	33.4	31.54*	12:57:35.05
Telemetry pretest calibrate	37.1	36.03	12:57:39.54
Despin on	37.1	35.83	12:57:39.34
Despin off	. . .	36.91	12:57:40.42
Solenoids open, Camera 1 and 2 on	41.0	40.37	12:57:43.88
Test item deploy (canister ejected)	42.0	41.27	12:57:44.78
Post-test telemetry calibrate	74.0	. . .	. . .
Recovery sequence initiated	90.0	88.50	12:58:32.01
Barometric switches closed	†	403.74	13:03:47.25
Separation nut fired	. . .	403.94	13:03:47.45
Recovery parachute ejected	. . .	404.49	13:03:48.00
Nose probe separation	. . .	405.42‡	13:03:48.83
Recovery parachute inflated	. . .	. . .	. . .
End of transmission	. . .	424.49	13:04:08.06

*Initiated only; separated at 41.27 sec

†11,000 ft

‡Initiated only; no separation

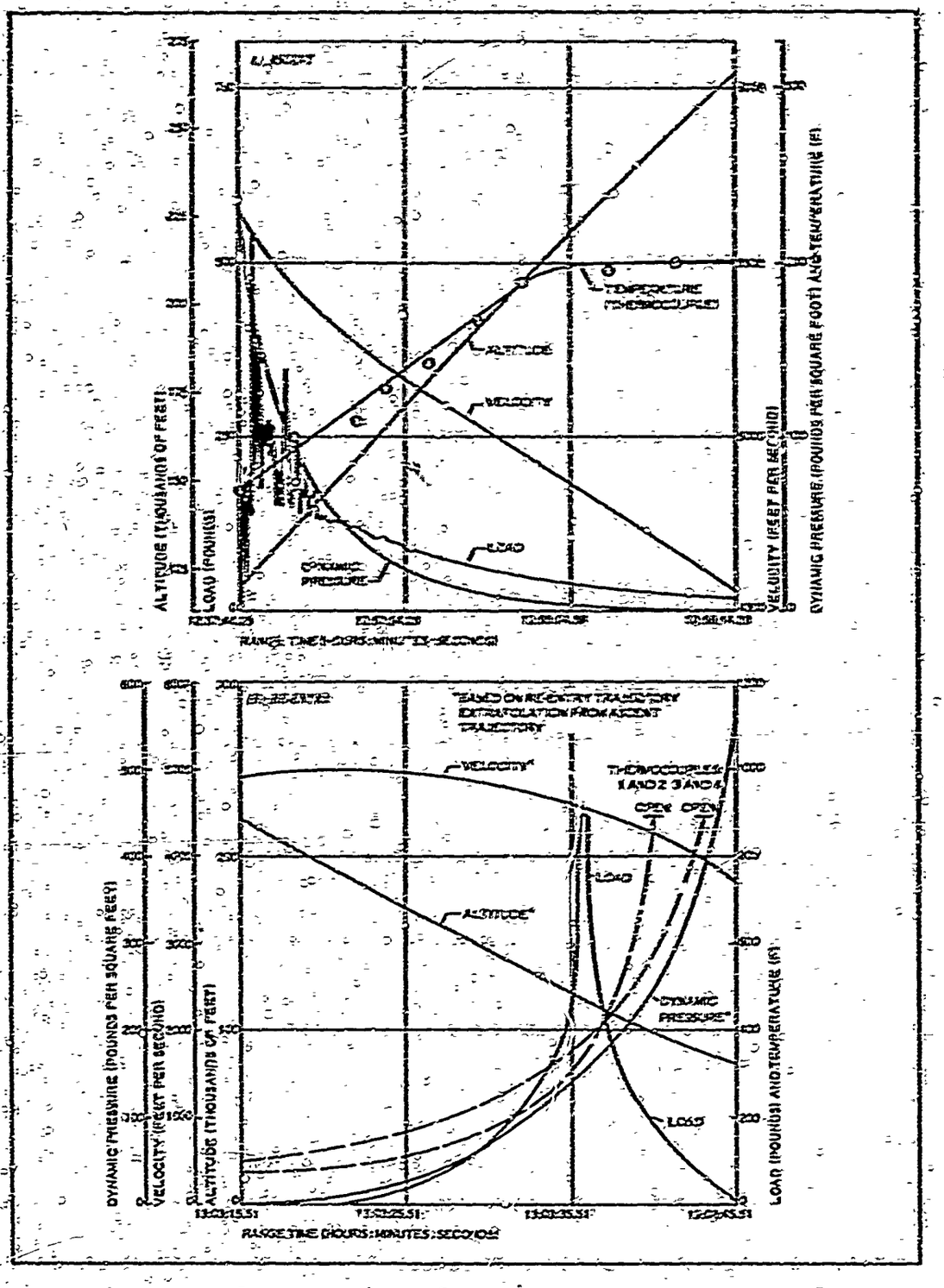

Figure 27 - SP-5 Performance Curves

SECTION IV - SMALL PARACHUTE DECELERATOR

3. AERODYNAMIC ANALYSIS

a. General

As explained earlier in this section, the small parachute configuration used for the Phase III flight tests was the same as the PARASONIC configuration (SP-3, SP-4, and SP-5) developed and preliminarily tested in Phase I (References 1). Reviewed in this analysis are the shapes that the PARASONIC configuration must have for stability, the pressure distribution analysis, the drag and filling time evaluation, and the measurement of porosity.

b. Aerodynamic Stability

The Phase III efforts demonstrated that the PARASONIC parachute shape, in conjunction with the A/A^* relationship established in Phase I, is stable behind a forebody in supersonic flow (A/A^* = area inlet/area throat at sonic condition). The experimental evidence that relates to the adequacy of the small parachute stability characteristics is the load trace and film data of the flight tests. The SP-5 load trace shows force fluctuations on the order of 50 percent from the mean value after the chute has inflated; this corresponds to earlier wind-tunnel data involving a fully-inflated, stable shape for similar parachutes at Mach 2.6 and 3.0. Films of SP-4 shown an inflated shape similar to that observed during wind-tunnel tests. Measured lateral stability was ±3 deg at Mach 1.4. Thus, it appears that the theory has yielded area relationships that allow satisfactory inflation stability based on the load traces and limited camera coverage.

c. Pressure Distributions

Methods established in Phase I were used to calculate the values of the pressures acting on the canopy. These methods are based on free-stream conditions. The type of pressure coefficient distribution predicted is shown in Figure 28 (References 24, 25, and 26). Mach number M_1 is from predicted trajectory conditions; M_2 is from flow following a bow shock (normal shock); and M_3 is from isentropic relationships to sonic velocity for an area ratio of 7 to 1, respectively. The internal pressure coefficients are related to the inside canopy surface and consider the total pressure after the bow shock and the local velocities. The external base and skirt pressure coefficients are derived from free-stream conditions and are based on Reference 24, and References 1 and 25, respectively. The values versus Mach number are presented in Figures 29A and 29B. The value of the skirt pressure coefficient is calculated using:

$$C_{p_{2c}} = \frac{2}{\beta}\left(\frac{a}{b}\cos\alpha_c\right) \qquad (15)$$

Where:

$$\beta = \sqrt{M_1^2 - 1}$$

M_1 = Mach number, free-stream conditions ahead of vehicle

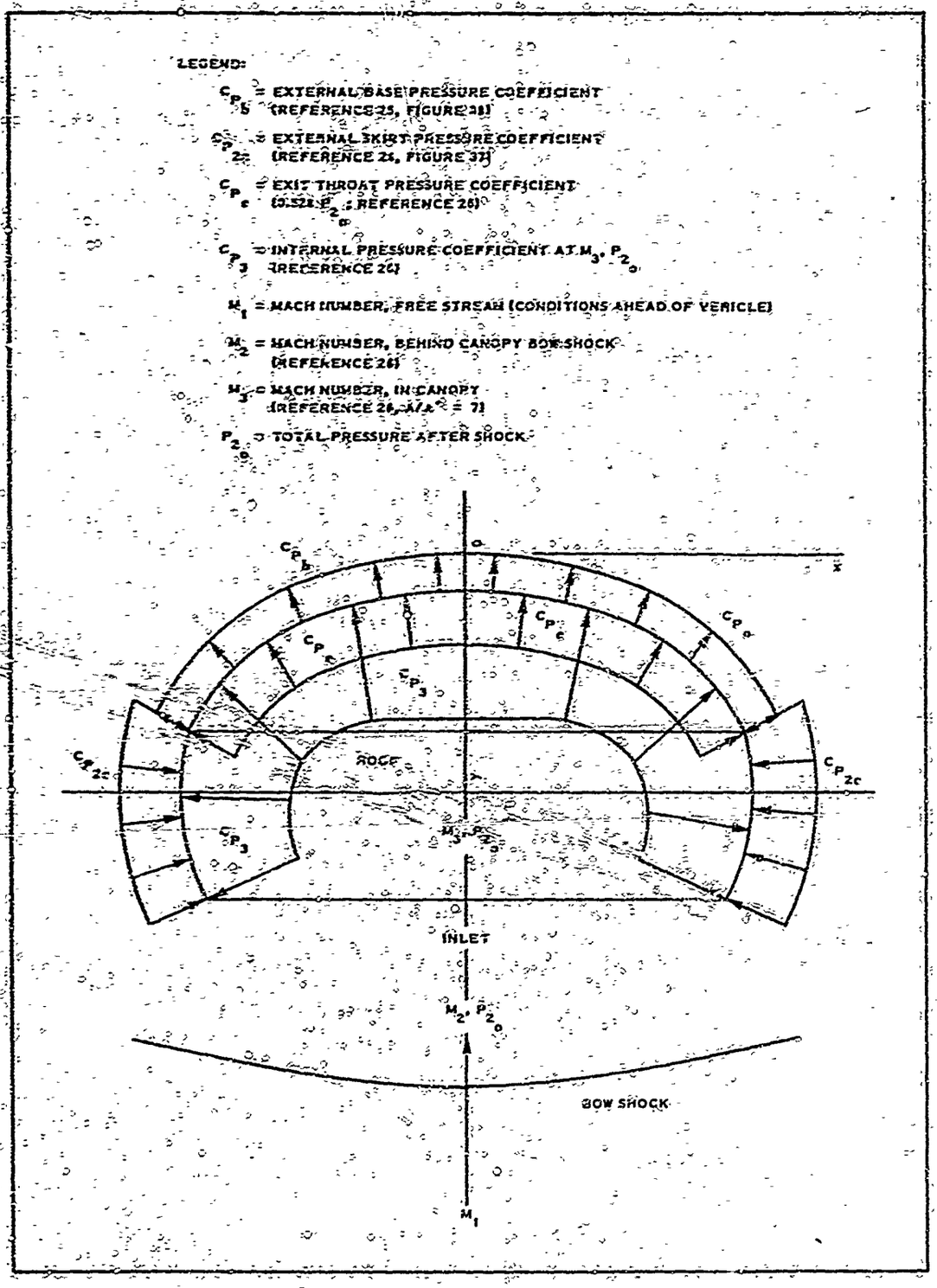

Figure 28 - Steady-State Pressure Coefficients

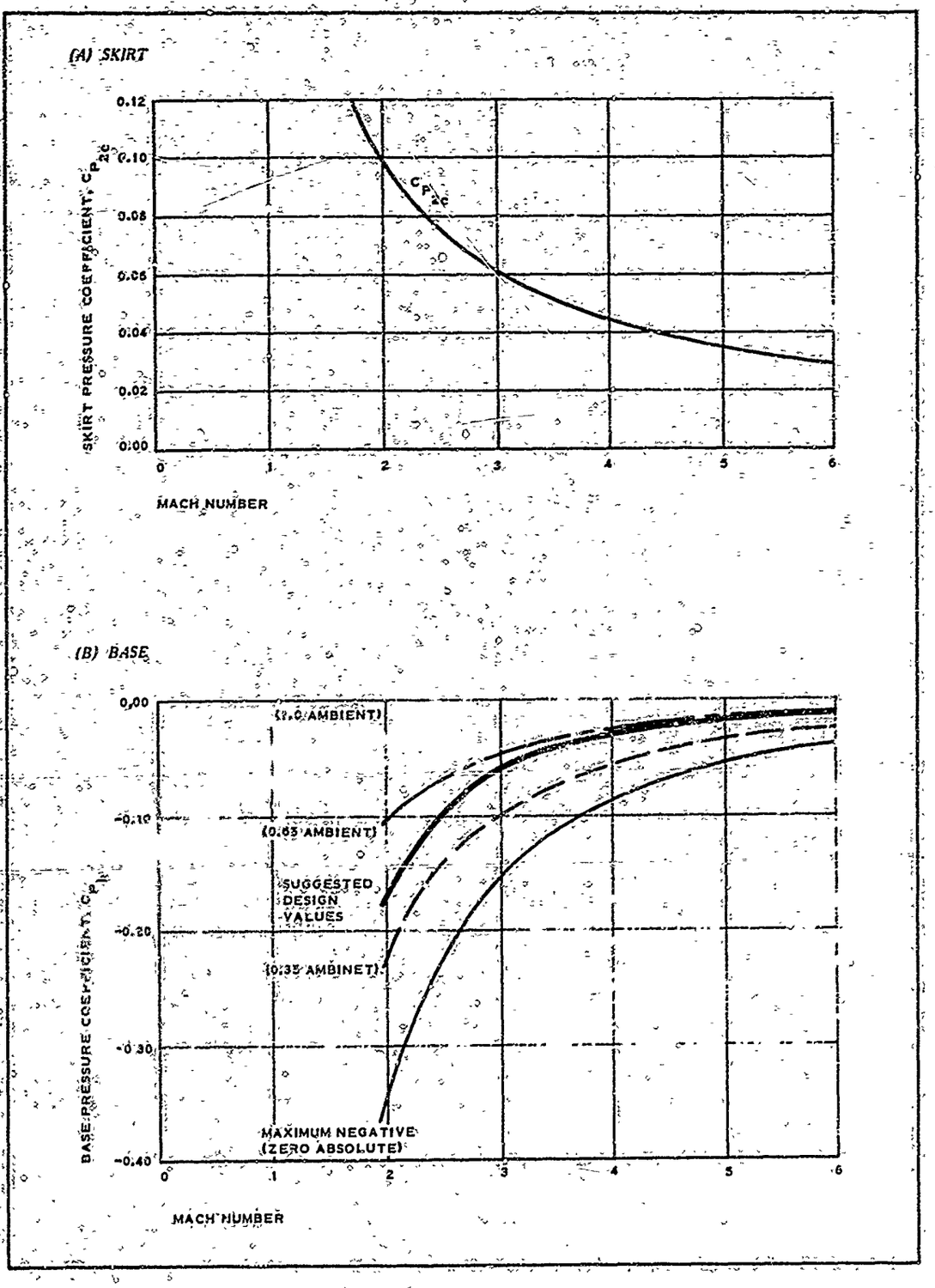

Figure 29 - Predicted External Pressure Coefficients

a = camber

b = chord

a/b = 0.175 based on geometry

α_o = conical angle of attack = 5 deg = 0.0874 rad

The negative value of the external base pressure coefficient is limited by the local static pressure being zero absolute in the equation:

$$C_P = \frac{P - P_1}{0.7 M_1^2 P_1}$$

$$= \frac{-P_1}{0.7 M_1^2 P_1} = \frac{-1.43}{M_1^2} \qquad (16)$$

Where P_1 = ambient static pressure. These values are presented for reference in Figure 29, along with 0.65 and 0.30 of the maximum negative value. The 0.65 values ($C_P = -0.98/M_1^2$) correspond closely with the wind-tunnel data obtained over the base of solid BALLUTE models where the porosity is zero (Reference 1, p 144). Because increased porosity should increase the values of the abolute pressures at the base, the values corresponding to a solid base (0.65 of the maximum negative pressure coefficient) should be a realistic negative limit.

To estimate the effects of area-to-area at sonic condition ratio (A/A^*) on the base pressure values, the pressure ratio values available and the value required to fill the mesh from the throat to the surface area must be determined. The total-mesh-to-inlet area ratios vary between 0.88 and 1.24 depending on the type and construction of the parachute. With an $A/A^* = 7$, expansion ratios in the mesh are possible from 6.15 to 8.7. The corresponding pressure ratios required to follow the expansion ratios are 67 to 111 times base pressure. The ratio of the total pressure after the shock to the ambient pressure varies from 8.5 to 40 as the Mach number increases from 2.5 to 5.6 (Reference 26). The greatest pressure ratios are available by using the solid base pressure corresponding to the 0.65 of the maximum negative C_P, which is equivalent to 0.35 of ambient pressure. The pressure ratios vary from 24 to 114. Thus, comparing these values with 67 to 111 times the base pressure based on geometry, it appears that an over-expanded nozzle is provided for the low Mach number; and depending on the parachute configuration, the correct expansion ratio to a slightly under-expanded nozzle is provided for the highest Mach number.

With an over-expanded nozzle, the flow will separate and have an exit static pressure approaching base pressure. The maximum pressure ratio available (Mach 5.6) applied to minimum area ratio pressure ratio requirements (i.e., 114/67) will result in a jet static pressure of approximately twice P_b for a solid or 0.70 of ambient pressure. At low Mach numbers, the jet area will be small compared to the total base area

because of separation; at the maximum Mach number, the jet area will approach the total mesh area. At low Mach numbers the average base pressure should approach the nonporous values because of the small jet areas, and they should approach twice the solid base pressure or 0.7 ambient at Mach 5.6.

Thus, a curve is suggested that favors 0.65 of the maximum negative pressure coefficient at Mach 2.5 and 0.35 of the maximum negative pressure coefficient at Mach 5.6. These values were compared with extrapolated data to Mach 3.6 (reported in Reference 25) for boosters with varying (jet-booster) diameter ratios and (jet/ambient) pressure ratios. While these data are not directly comparable with the parachute roof mesh case, the predicted values are comparable to the suggested design value in Figure 29.

d. Drag and Filling Times

The pressure distribution analysis served as a basis for calculating loads. Figure 30 shows the reported and predicted nominal surface drag coefficients versus Mach number (References 10, 11, 20, 21, 27, and 28). Table XVIII summarizes the pressure coefficients around the canopy based on deployment conditions, as well as the drag coefficients based on wind-tunnel data. The conditions of the bottom row of Table XVIII resemble closely the conditions of the SP-5 test. From these values, the parachute force was calculated to be 428 lb. The corresponding average force indication from performance of the SP-5 test was about 300 lb. Filling times were slow, based on the force data as compared to wind-tunnel data of similar parachutes at Mach 2.8 (Reference 23). The force trace shows that SP-5 required 0.65 sec from line stretch to fill completely, as opposed to 0.015 sec for the PARASONIC discussed in Reference 23.

The measured drag coefficients, based on nominal surface area, were:

1. For SP-3, 0.306 at Mach 2.68
2. For SR-4, 0.377 at Mach 1.42
3. For SP-5, 0.145 at Mach 5.23

These compare with the predicted nominal surface drag coefficients that were based on full-scale wind-tunnel tests of 0.242 at Mach 2.68; 0.32 at Mach 1.42; and 0.17 at Mach 5.23 (Figure 30). The test values are considerably less than drag values based on predicted pressure distributions over the canopy (see Table XVIII), which do not consider the loss in total pressure due to the wake of a forebody.

e. Porosity Measurement

The aerodynamic theory discussed thus far, depends heavily on the value of roof porosity. To establish this theory more firmly, a method was used for determining the parachute porosity by airflow tests. This method is detailed below, and the test setup shown in Figure 31.

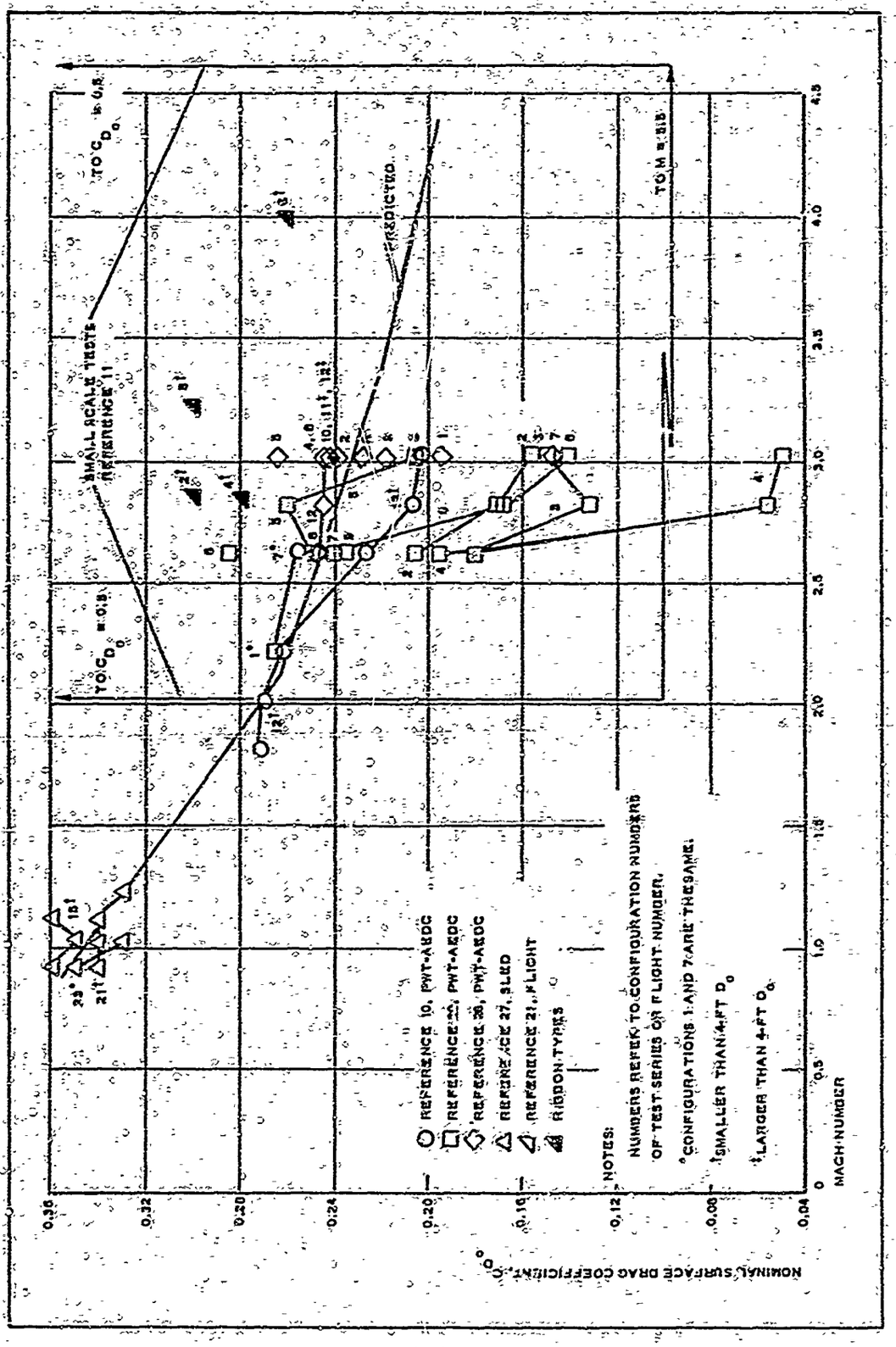

Figure 30 - Reported and Predicted Drag Coefficients versus Mach Number

TABLE XVIII - PREDICTED SMALL PARACHUTE PRESSURE AND DRAG COEFFICIENTS

Test item SP	Free stream Mach number, M_1	Altitude (10^3 ft)	Dynamic pressure, q (psf)	Reynolds number, Re (10^6)	Pressure coefficients					Nominal surface drag coefficient, C_{D_o}	
					Internal stagnation $C_{P_{2o}}$	Internal static C_{P_2} (based on M_3 = 0.083)	Exit throat, C_{P_e}	External skirt, $C_{P_{2c}}$ (Figure 29A)	External base, C_{P_b} (Figure 29B)	Based on pressure distributions	Extrapolated from PWT data
3	2.50	85.3	200	1.34	1.72	1.71	0.445	0.077	-0.100	0.50	0.25
6	5.60	160.0	43	0.10	1.82	1.80	0.936	0.031	-0.011	0.58	0.17
4	3.35	98.0	200	0.998	1.79	1.78	0.880	0.054	-0.047	0.52	0.22
5	5.60	121.2	200	0.55	1.82	1.80	0.936	0.031	-0.011	0.58	0.17

The small parachute canopy was mounted on the outlet of a diverging duct. Flow into the duct was produced by a two-horsepower blower. A screen evened the flow across the duct throat, and an anemotherm was used to measure the mean flow through the duct. Inserted through the roof mesh and into the canopy interior was a total pressure probe that was connected to an inclined tube manometer.

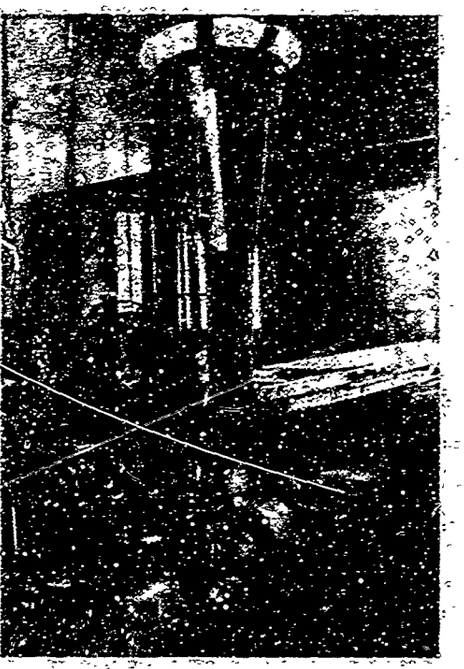

Figure 31 - Air-Flow Test Setup

The quantity of airflow was calculated from the duct throat area and the duct throat velocity. The parachute inlet area was determined by measurement. The pressure (P) drop across the mesh (total pressure inside less total pressure ambient) was used to determine the mesh orifice velocity (V) by means of the relationship $\Delta P = 1/2\rho V^2$ (where ρ = density). From the known flow quantity and velocity through the orifices, the area of the orifices was calculated. Appendix IV develops the area relationship made from two sets of measurements. These results agree within 1.5 percent. They show an inlet area-to-exit area ratio of 7.7 to 7.8 for SP-5.

4. SMALL PARACHUTE GEOMETRY

The inlet area-to-exit area variations between the SP-3, SP-4, and SP-5 PARASONIC small parachutes were limited to manufacturing tolerances. The resultant geometric differences in porosity were small. This was determined by calibration tests that were performed to establish the ratio of inlet area to exit area based on the flow at a pressure of one-half inch of water. A typical coated mesh roof is shown in Figure 32.

5. STRUCTURAL LOADS AND MATERIAL SELECTION

Using the canopy aerodynamic theory presented in Item 3 of this section, the structural loads were calculated by considering that the isotensoid shape of the canopy allows the radial line loads and canopy stresses to be uniform throughout the structure.

The method of optimizing and analyzing parachutes for static loading is detailed in References 1, 29, 30, and 31. In addition, a procedure for determining the gore pattern for the small parachute design of Phase I is given in References 1 and 29. The basic method of construction (biased gores of a single-ply fabric and a set of equally spaced meridian cords) was retained from Phase I of ADDPEP. Thus, the static load analysis and the gore pattern determination procedure apply to the drag devices of Phase III.

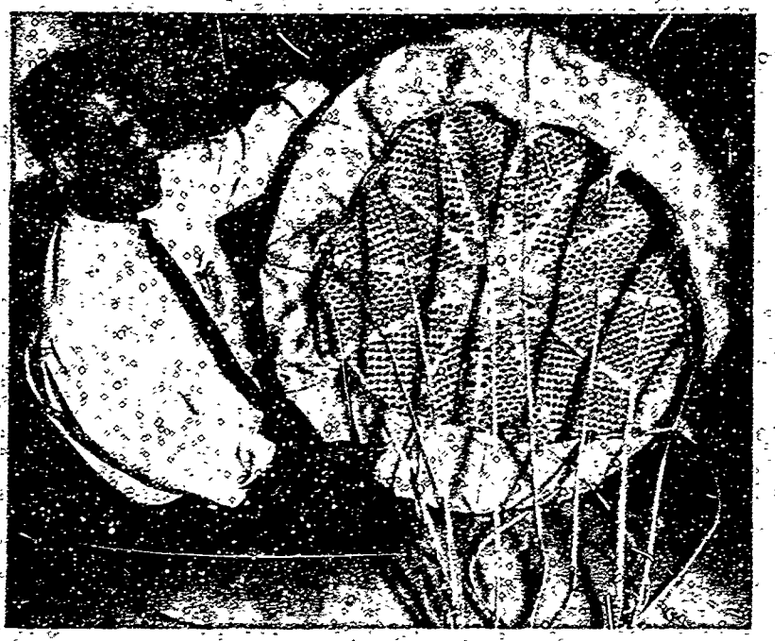

Figure 32 - PARASONIC Parachute with Coated Mesh Roof

The equilibrium equations for the stresses in the fabric and the forces in the meridian straps at any point y are as follows (see Figure 33):

$$F = 2\pi x N_{\phi} \sin\phi + nF_{ms} \sin\phi$$

$$= P\pi x^2 \tag{17}$$

$$N_{\phi} = \frac{Pr}{2} \tag{18}$$

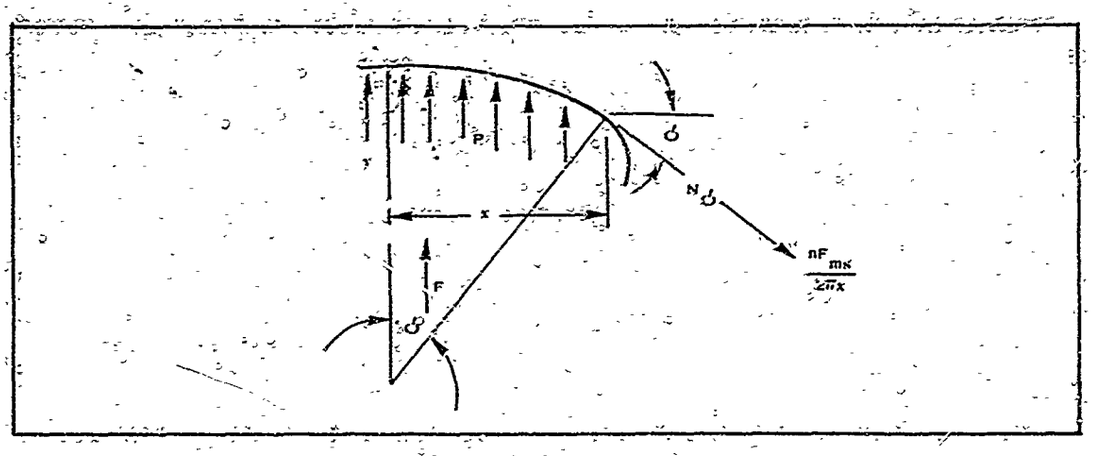

Figure 33 - Structural Load Definitions

In Equations 17 and 18:

x = shape coordinate and radius of parallel circle

ϕ = coordinate angle defining parallel circle

n = number of meridian straps

F_{ms} = force in meridian strap

N_ϕ = meridian fabric stress

N_θ = circumferential fabric stress

y = shape coordinate defining parallel circle

r_g = radius of gore lobe

The quantities x and ϕ were calculated from the profile of the parachute. Since the parachute lobes outward between meridian straps, the radius of the gore lobe (r_g) is used rather than the principal curvature radius (if the parachute were considered a perfect surface of revolution). The r_g radius was calculated as 6.4 in using the methods presented in Appendix III of Reference 1. The amount of additional cloth used for the lobe can be determined by comparing the dimension of a gore to the dimension of a perfect surface of revolution.

Since the gores are on the bias, the membrane stresses, N_ϕ and N_θ, are assumed equal. Given the small strains and little racking of the small parachute configuration, this is a reasonable assumption.

The pressures were computed from the following pressure coefficients:

$$C_{P_2} = 1.80 \tag{19}$$

$$C_{P_e} = 0.94 \tag{20}$$

$$C_{P_b} = -0.011 \tag{21}$$

$$C_{P_{2c}} = 0.032 \tag{22}$$

As the pressures differ between the inside and the outside, the pressures can be obtained from the value of q and the appropriate pressure coefficient. Using a porosity of 11.6 percent for the roof material:

$$\text{Internal pressure on roof} = 1.8\,q(1 - 0.116) + 0.94\,q(0.116)$$

$$= 1.70\,q \text{ above ambient} \tag{23}$$

Therefore:

$$\text{Resultant pressure on roof} = 1.70\,q \text{ above ambient} \tag{24}$$

$$\text{Resultant pressure on skirt (back of equator)} = 1.81\,q \tag{25}$$

$$\text{Resultant pressure on skirt (front of equator)} = 1.77\,q \tag{26}$$

Using a 200-psf dynamic pressure, the values for stresses and forces are obtained as shown in Table XIX. The y coordinate is measured from the back of the parachute. The suspension line load, calculated from the pressure drag value is:

$$D = 1482 \text{ lb} \tag{27}$$

TABLE XIX - SMALL PARACHUTE COORDINATES AND LOADS

Point	Coordinate (in.)		Fabric stress, N_ϕ or N_θ (lb/in.)	Meridian load, F_m (lb)
	x	y		
0	0.00	0.00	0.0	0.0
1	1.00	0.03	1.3	13.8
2	2.00	0.08	2.4	26.3
3	3.00	0.19	3.3	37.6
4	4.00	0.33	3.9	47.9
5	5.00	0.52	4.6	55.5
6	6.00	0.77	5.2	61.1
7	7.00	1.08	5.5	65.7
8	8.00	1.48	5.7	68.3
9	9.00	1.97	5.9	70.6
10	10.00	2.56	5.8	73.6
11	11.00	3.31	6.5	74.1
12	12.00	4.29	6.2	71.8
13	12.78	5.29	6.3	74.3
14	13.44	6.29	5.9	78.5
15	13.92	7.29	5.9	77.3
16	14.22	8.29	6.7	71.5
17	14.45	9.29	6.7	72.2
18	14.55	10.29	7.1	69.4
19	14.56	11.29	7.1	69.3
20	14.54	12.29	7.3	67.9
21	14.49	13.29	6.9	70.3
22	14.37	14.29	7.0	70.1
23	14.17	15.29	7.9	61.2
24	13.93	16.29	8.1	70.0
25	13.84	16.60	8.5	84.0

This predicted drag value, based on free stream conditions forward of the parachute, results in a nominal drag coefficient of 0.585, as compared to 0.17 estimated from wind-tunnel data using small parachute models behind a forebody (Figure 30). With a suspension line angle of 13 deg, the load on one suspension line is:

$$\frac{1482}{12 \cos 13 \text{ deg}} = 127 \text{ lb} \qquad (28)$$

The load on the inlet loop is calculated from the equilibrium equation, where the suspension line attaches to the inlet loop. The force in the inlet loop is:

$$F = 144 \sin 31 \text{ deg} - 127 \sin 13 \text{ deg} = 45.6 \text{ lb} \qquad (29)$$

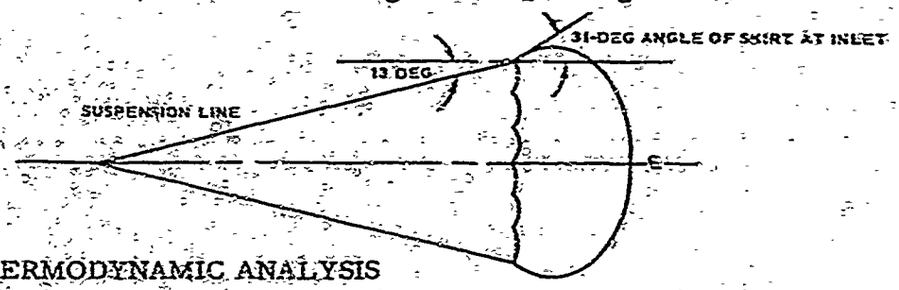

6. THERMODYNAMIC ANALYSIS

a. General

This thermodynamic analysis concerns a PARASONIC small parachute decelerator trailing in the wake of a leading body in a supersonic stream along a trajectory path. The analysis is largely dependent on the capability to define the flow properties existing immediately in front of the decelerator.

A schematic of the probable flow field around the two vehicles (shown in Figure 34) was composed on the basis of experimental wind-tunnel

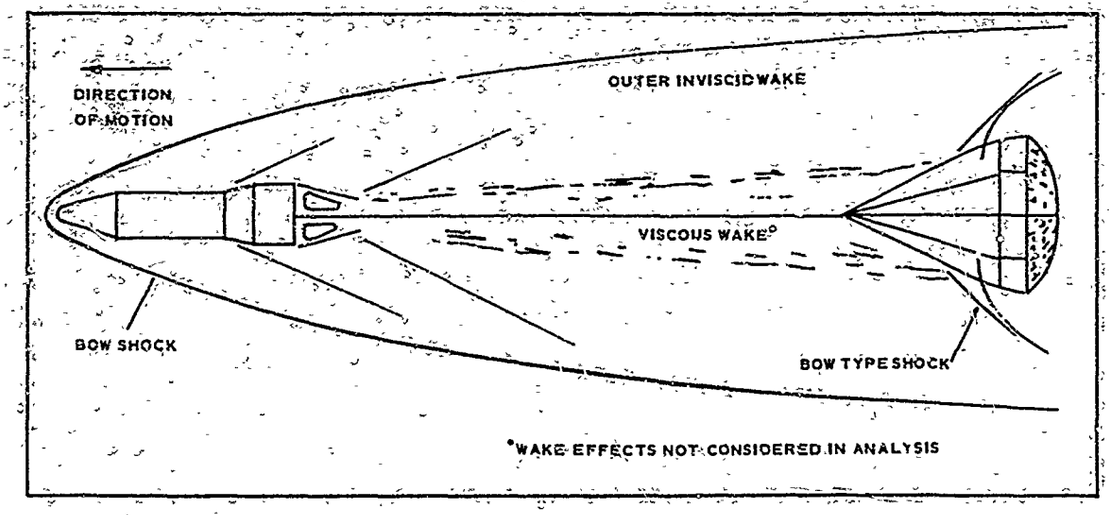

Figure 34 - Flow Field Schematic of PARASONIC Decelerator

investigations conducted on BALLUTE decelerators in the wake of a leading body (ADDPEP, Phase II, Reference 2). In Figure 34, the two bodies are immersed in a flow field bounded by the leading body bow shock. The parachute decelerator itself is subjected to a flow field consisting of a viscid and inviscid wake region resulting from the flow over the leading body. A portion of the parachute riser lines leading to the confluence point is partially submerged in the viscous region of the leading body wake. In the vicinity of the skirt, a bow type of shock is formed. In the suspension line region, which is exposed to the inviscid portion of the leading body wake, oblique type shocks are formed. Some evidence that such a flow situation does exist has been experimentally determined and reported on in Reference 32.

This type of flow field is not readily amenable to engineering thermal analysis, since only limited experimental data are available regarding such a flow field. Thus, in lieu of experimental evidence of a particular type of flow field, the decelerator is assumed to be exposed to the same free stream conditions that the leading body is subjected to along the trajectory path. This in essence was the primary assumption made in describing a thermal analysis method for parachute decelerators trailing in the wake of a leading body (ADDPEP, Phase ., Reference 1). An outline of this method is described below. Consideration of the more realistic flow field is deferred until more definitive experimental data become available on flow characteristics over a parachute decelerator in the wake of a leading body.

b. Analytic Methods

The physical elements of the PARASONIC parachute decelerator are the suspension lines, the leading edge of the skirt, the skirt surface, and the canopy or roof. These elements are shown schematically in Figure 35. The heat transfer rates to the suspension lines and skirt surface can be analyzed on the basis of flow over a flat plate, and the skirt leading edge can be analyzed on the basis of flow over a cylinder normal to the flow. In each case, the local flow properties must be evaluated as functions of the upstream flow conditions existing in front of the decelerator. These flow properties can then be used in conjunction with the equations for evaluating the heat transfer rates that pertain to these surfaces (presented in Reference 1 and not repeated here).

In the case of the canopy or roof, the calculation of the heat transfer rates requires a special consideration. The supersonic speed range parachutes considered under ADDPEP require a porous roof to function effectively in this flight regime. As a consequence, a flow rate through the small openings of the roof results that is a function of (1) total pressure inside the parachute canopy and (2) static pressure acting on the outside of the canopy roof. When the ratio of pressures becomes critical, sonic flow occurs through these orifices.

For purposes of thermal analysis of the roof elements, it is assumed that the heat flux rates to an element of the roof forming a section of a typical orifice could be calculated by using a heat transfer coefficient obtained from an evaluation of the following equation (see List of Symbols in the preliminary pages of this report):

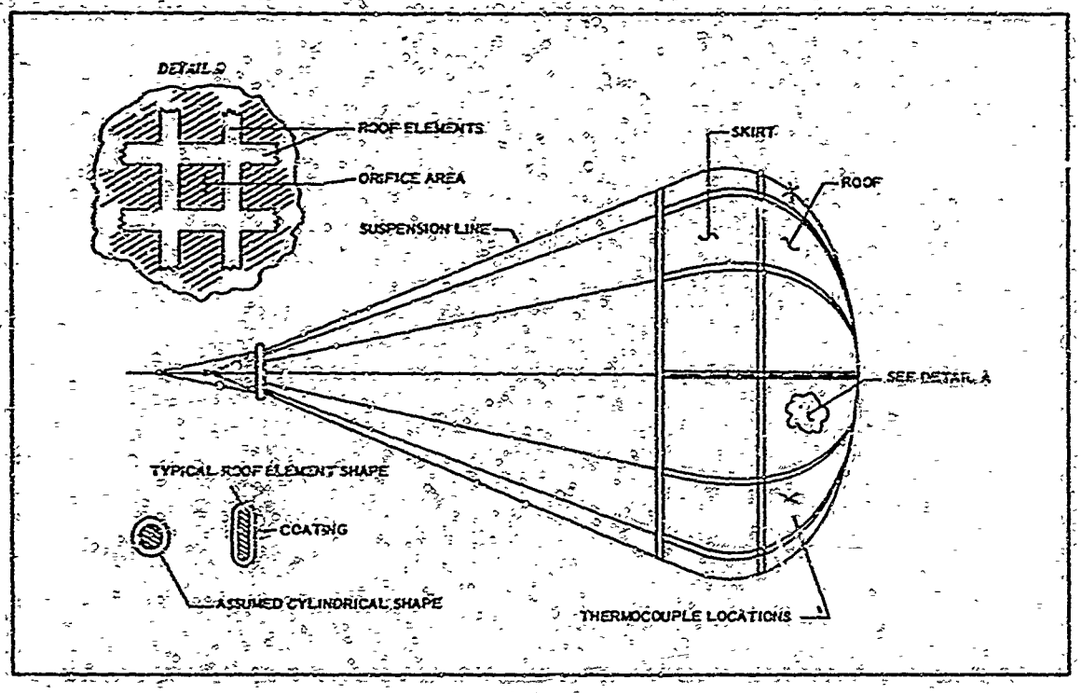

Figure 35 - Schematic of PYKASONIC Test Parachute

$$h_c = \left[\frac{0.026}{(D^*)^{0.2}}\left(\frac{C_P \mu^{0.2}}{Pr^{0.6}}\right)\left(\frac{P_t g}{c^*}\right)\left(\frac{D^*}{r_e}\right)^{0.1}\right]\left(\frac{A^*}{A}\right)^{0.9}\sigma \qquad (30)$$

This equation is developed in Reference 33 for calculating the heat transfer coefficient to a nozzle wall. It is easily adaptable to the conditions inside the parachute roof provided that the geometry of the roof surface is specified and the flow around and into the parachute is assumed or described.

Once the heat transfer coefficient is evaluated, the heat flux rate into the roof element can be described as:

$$\dot{q} = h_c(T_{aw} - T_w) \qquad (31)$$

Since this rate is dependent on the surface temperature, the method of heat balance must be defined to complete the thermal analysis method.

c. Heat Balance Methods

Once the heating rates are defined, the temperature response of any of the decelerator components may be calculated on the basis of either a quasisteady state equilibrium heat balance or a transient heat conduction. The fact that useful life of a decelerator occurs during a highly transient phase of the flight suggests that the heat balance be solved on a similar

basis. Hence, in the case of a cylindrical element of the roof, the partial differential equation may be applied for heat conduction in a solid cylinder:

$$\frac{\partial T}{\partial \tau} = \alpha\left(\frac{\partial^2 T}{\partial r^2} + \frac{1}{r}\frac{\partial T}{\partial r}\right) \qquad (32)$$

For slab like elements, the heat conduction method outlined in Reference 2 may apply. This equation may be converted to a finite difference equation so that the heat-in minus the heat-out is equal to the heat stored. If it is assumed that the material is divided into a number of nodes, then for any i^{th} node, the heat balance is:

$$\frac{k_i(T_i - T_{i+1})}{r_{i+1}\ln\left(\frac{r_i}{r_{i+1}}\right)} = \frac{\rho_i c_i}{\Delta\tau}\left(\frac{r_i + r_{i+1}}{2r_{i+1}}\right)\left(\frac{r_i - r_{i+1}}{2}\right)(T_{i+1}' - T_{i+1}) +$$

$$\frac{\rho_{i+1} c_{i+1}}{\Delta\tau}\left(\frac{r_{i+1} - r_{i+2}}{2}\right)(T_{i+1}' - T_{i+1}) + \frac{k_{i+1}(T_{i+1} - T_{i+2})}{r_{i+1}\ln\left(\frac{r_{i+1}}{r_{i+2}}\right)} \qquad (33)$$

At the outer surface, the following boundary conditions apply:

$$h_c(T_{aw} - T_1) - \epsilon\sigma(T_1^4 - T_3^4) = \frac{\rho_i c_i}{\Delta\tau}\left(\frac{r_1 - r_2}{2}\right)(T_1'^4 - T_1) + \frac{k_1(T_1 - T_2)}{r_1\ln\left(\frac{r_1}{r_2}\right)} \qquad (34)$$

These equations are readily adaptable to digital computer language so that they can be solved as a function of the trajectory path. An example solution is described next.

d. Calculated and Measured Values, SP-5

The thermal analysis methods set forth above were used to analyze the SP-5 flight test results. The SP-5 PARASONIC parachute was designed to be deployed at Mach 5.6 and an altitude of 120,000 ft. The flight test was completed near these planned deployment test conditions, as shown earlier in Figure 27.

Typical thermal properties assumed for roof elements are given in Table XX. Since the roof elements were subjected to the most critical heating environment, the results of the calculation for these elements are presented here. The other elements have been analyzed as suggested in Reference 1.

TABLE XX - THERMAL PROPERTIES OF SP-5 MATERIALS IN FLIGHT TEST

Material	Position	Thickness (in.)	Density (lb/ft^3)	Specific heat (Btu/lb-F)	Thermal conductivity (Btu/hr-ft-F)
D-65	Coating	0.025	68.6	0.25	0.053
Nomex	Roof element	0.10 diam	42.0	0.35	0.032

The heat transfer coefficients were calculated using Equation 30 as a function of time. The thermal environment inside the canopy is that due to free stream conditions subjected to a normal shock at the inlet face. The heat flux rates resulting from the calculations are shown in Figure 36 as a function of time from launch. The initial peak heat flux rate on a roof element occurs immediately after deployment; it was calculated to be about 24 Btu/ft^2-sec. The heating rate decays rapidly as the vehicle gains altitude. About 15 sec after deployment, the heating was calculated to be negligible. About 360 sec after launch, aerodynamic heating increases as the vehicle re-enters the sensible atmosphere. The maximum heat flux rate to a roof element was calculated to be about twice that experienced during exit flight deployment (or about 50 Btu/ft^2-sec). Thereafter, the heating decreases as the vehicle decelerates to terminal conditions.

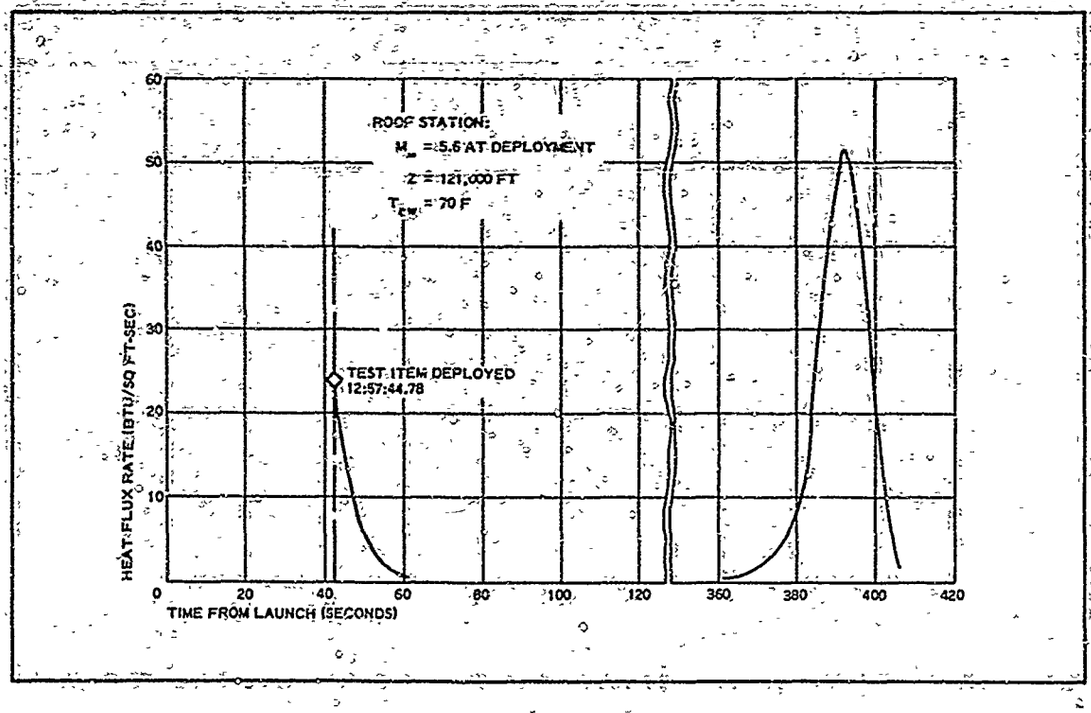

Figure 36 - Calculated Cold Wall Heat Flux Rates

The predicted temperature rise in the Nomex roof material, calculated using Equations 32, 33, and 34, is shown in Figure 37. Also shown is the predicted recovery temperature calculated on the basis of the trajectory computed for this flight test case. Superimposed on these predicted temperature variations are the (1) telemetered total temperature data taken from the vehicle nose probe and (2) Nomex roof temperature data received from thermocouples mounted in the roof elements. The shape of the predicted recovery temperature variation following deployment of the test item closely follows the telemetered, total-temperature, vehicle-probe data. However, there is a 1000-F difference in the two temperatures. Evidently, this difference is due to the inability of the vehicle total temperature pr[illegible] to measure temperatures in excess of 2000 F. The total temperatures expected during flight test should have ranged only slightly higher than 2000 F. Although the two temperatures (T_{t2} and T_{aw}) are not the same quantity, the difference is much greater than can be accounted for in applying a recovery factor to the total temperature to obtain the adiabatic wall temperature (T_{aw}).

The predicted Nomex surface temperature rise for laminar and for turbulent flow are in excess of that actually experienced shortly after deployment. The analysis, based on existing turbulent flow, is too conservative, whereas the temperature rise calculated on the basis of laminar flow is more reasonable.

The re-entry portion of the flight is shown on the right-hand side of Figure 37. In the re-entry case, an offset in the calculated adiabatic wall and measured parachute temperature profiles may be caused by one of

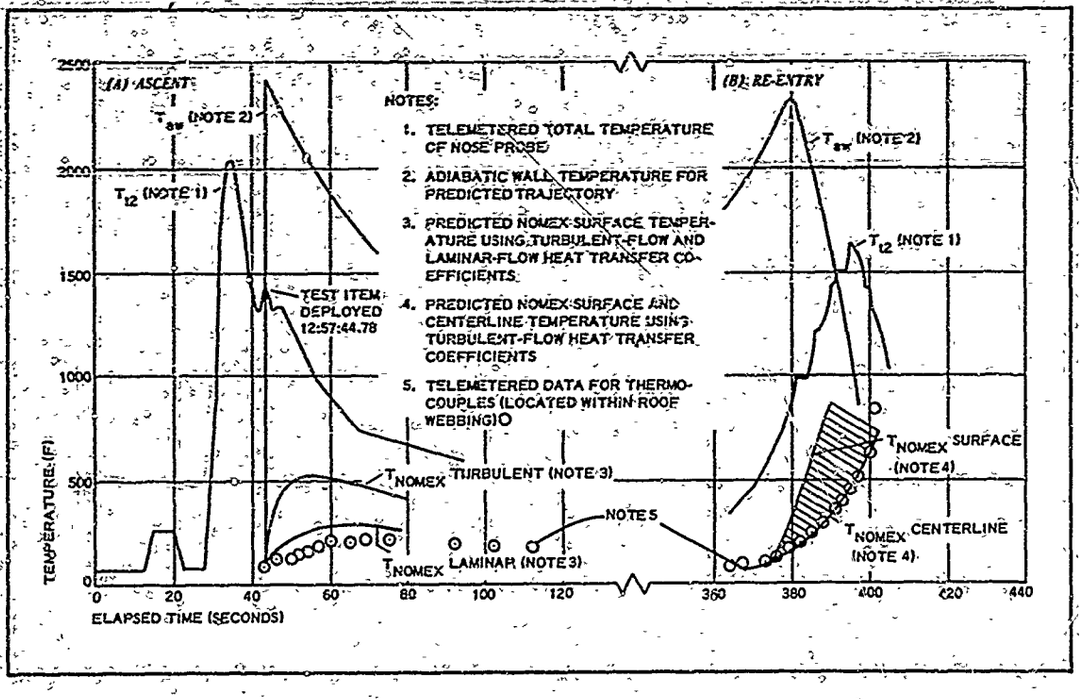

Figure 37 - SP-5 Flight Test: Predicted and Measured Temperature Data

two factors: (1) a slight mismatch in time between the actual flight test trajectory and the calculated re-entry trajectory upon which the predicted temperatures are based; (2) a time delay in the nose probe readings. It is also noted that a temperature differential again exists between the predicted adiabatic wall temperatures and the telemetered nose probe temperatures.

The time offset is not obvious in the case of the values for the Nomex material. Two predicted temperature histories are shown in Figure 37. The first, rising steeply above the telemetered data, was calculated for a position at the interface of the coating material and the Nomex roof element; a temperature rise to 700 F is predicted in 15 sec at this location. The second temperature history matches the telemetered data almost exactly; this history was calculated for a node inside the assumed cylindrical roof element shown in Figure 35. The exact location of the thermocouples is between the webbing surface and its centerline. Other calculated nodal temperature histories would have straddled the data of the two curves and are not shown here. It is significant to note that a fair amount of correlation exists between these temperature histories during the re-entry phase, which tends to verify the assumed turbulent flow nozzle analogy method for calculating heat flux rates upon which the temperature rise histories are based.

In conclusion, a fair degree of correlation exists between the predicted temperature rise in a roof element and that actually experienced during aerodynamic heating exposure. Since the temperature rise is ultimately a function of the accuracy of establishing the heat flux rates to be experienced, it is evident that these must be predicted accurately. In the analysis presented, a flow field refinement would have resulted in predicting a less severe thermal environment inside the parachute canopy and thereby lowering heat flux rates to the roof elements. The method of analysis developed in this program, however, yields results that are within the limits of engineering accuracy of determining the test environment. These results may be used for thermal design of parachute decelerators with a fair degree of confidence.

7. MATERIAL, SEAM, AND JOINT TESTING

a. General

A major Phase III goal was to extend the performance capability of the coated Nomex parachutes to their maximum potential. Accomplishment of this goal hinged on applying the thermodynamic theory (detailed in the Phase I final report, Reference 1) to the best coating system found in the Phase I laboratory tests and verifying this construction with an instrumented flight test. Additional laboratory testing of the optimum Phase I coating system applied to the small parachute design is described below, and the theoretical thermal behavior is compared with that shown by the SP-5 tests.

b. Material Selection

Selection of materials to be used for construction of small supersonic parachutes was based upon effects of probable test conditions more severe

than the design, static and dynamic loadings, seam efficiency, temperature, and safety. After basic materials and required strengths were determined, the parameters of weight, thickness, porosity, flexibility, and weave were considered together with fabricating and coating techniques.

Material selection for flight test parachutes SP-3, SP-4, and SP-5 was based on analysis as described in Item 6 of this section.

c. Materials Test Data

A series of tests were conducted to extend and evaluate earlier data on coated Nomex materials obtained at low heat flux rates. The latest data were obtained using heated air accelerated to Mach 7 to 8 in a heat tunnel. The Nomex samples were held perpendicular to the airstream and loaded to approximately 5 percent of their quick break, room temperature strength. (Quick break refers to strain rates of approximately 1 in. per minute on 12-in. samples.)

The tested samples included Nomex webbing similar to MIL-W-5625 and MIL-W-4088 (see Table XXI). The test conditions varied from a cold wall heat flux rate of 8.8 to 12.7 Btu/ft^2-sec (see Table XXII). The test results varied from short lift times (approximately 2 sec) for the uncoated samples to long life periods for coated samples (20 to 30 sec). It is important to note that doubling the thickness of the Nomex webbing (1 and 2 versus 1A) increased the lifetime only a fraction of a second. This can

TABLE XXI - TEST SAMPLES OF NOMEX

No.	Specification	Width bare (in.)	Total length (in.)	Length coated (in.)	Thickness bare (in.)	Thickness coated (in.)	Weight	
							Bare (gr)	Coated (gr)
1	MIL-W-5625	1/2	24	0	0.058	0.058	7.4612	7.4612
2	MIL-W-5625	1/2	24	0	0.058	0.058	7.4064	7.4064
3	MIL-W-5625	1/2	24	0	0.058	0.058	7.4638	7.4638
4	MIL-W-5625	1/2	24	6	0.058	0.101 to 0.110	7.4601	9.095
5	MIL-W-5625	1/2	24	6	0.058	0.116 to 0.126	7.4154	9.1020
6	MIL-W-5625	1/2	24	6	0.058	0.096 to 0.110	7.4534	9.3732
7	MIL-W-5625	1/2	24	6	0.058	0.121 to 0.131	7.4466	9.8196
8	MIL-W-5625	1/2	24	6	0.058	0.102 to 0.115	7.4495	9.9930
9	MIL-W-5625	1/2	24	6	0.058	0.107 to 0.115	7.4960	10.0725
10	MIL-W-5625	1/2	24	6	0.058	0.118 to 0.134	7.5871	11.1564
11	MIL-W-5625	1/2	24	6	0.058	0.110 to 0.116	7.4958	10.7269
12	MIL-W-5625	1/2	24	6	0.058	0.110 to 0.130	7.4394	11.0750
1A	MIL-W-4088	9/16	24	0	0.029	0.029	4.3968	4.3968
2A	MIL-W-4088	9/16	24	0	0.029	0.029	4.3914	4.3914
3A	MIL-W-4088	9/16	24	0	0.029	0.029	4.5377	4.5377

TABLE XXII - TEST CONDITIONS AND RESULTS FOR NOMEX SAMPLES

Test (by sample no.)	Conditions									Results	
	Angle of attack (deg)	Tunnel static pressure, P_2 (mm Hg abs)	Plenum pressure, P_o (psi, gage)	Weight flow, W (lb/min)	Plenum air temp, T_o (F)	Stream stagnation temp, T_2 (F)	Stream pitot pressure, P_2' (mm Hg abs)	Load, L (lb)	Heat flux ratio, q_{cw} (Btu/sq ft-sec)	Time to failure (sec)	Effective heat capacity, Q_{eff} (Btu/lb)
1	90	1.40	141	1.45	. . .	1390	81.0	80	12.70	2.78	178
2	90	1.40	138	1.47	1600	1310	82.5	82	12.70	2.76	174
3*	. . .	. . .	. . .	. . .	. . .	. . .	. . .	. . .	. . .	. . .	. . .
4	90	0.75	54	0.68	1660	1310	38.0	80	8.80	41.60	1680
5	90	0.77	55	0.69	1670	1195†	39.3	80	8.80	17.90	720
6	90	0.79	57	0.68	1680	1440†	41.0	80	8.80	22.80	904
7	90	1.40	137	1.47	1560	1298	81.3	80	12.70	17.60	700
8	90	1.05	97	1.05	1650	1270	62.4	80	10.82	18.90	890
9	90	0.95	90	1.08	1695	1295	58.0	80	10.82	23.50	1088
10	90	1.30	135	1.48	1600	1310	82.4	82	10.82	24+	. . .
11	90	0.95	90	1.08	1680	1300	59.0	80	10.82	26.90	1212
12	90	1.30	136	1.48	1600	1310	83.0	82	12.70	28.24	1470
1A	90	1.40	138	1.47	1590	1295	82.0	80	12.70	2.20	270

*Not tested

†No. 5 twisted wire received broken thermocouple; No. 6 twisted wire bent up

be compared to the many time increase in lifetime duration for the same weight increase using the coating. The effective heat capacity (Q_{eff}) ranged from 174 to 1680 Btu/lb (see Table XXII and Figure 38). The methods used to calculate these values follow.

To calculate effective heat capacity:

$$Q_{eff} = \frac{\int \dot{q}_{cw}\, d\tau}{\rho t} \qquad (35)$$

Where:

$\dot{q}_{cw}$ = measured cold wall heat flux rate (Btu/sq ft-sec)

τ = time of exposure (sec)

ρ = density of material (pcf)

t = thickness of material (ft)

$W = \rho A t$

W = weight of material (lb)

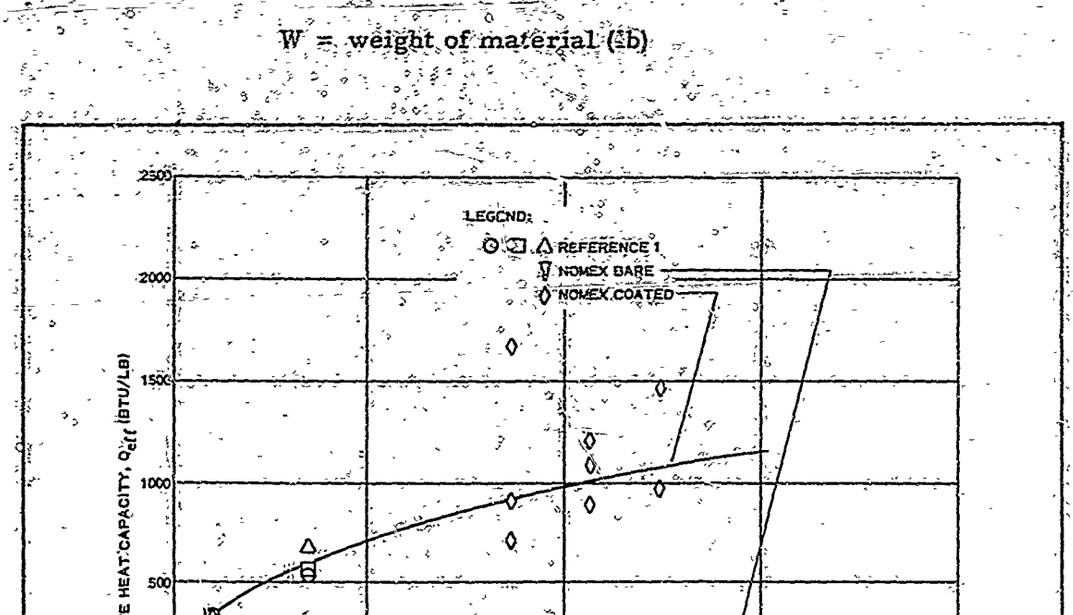

Figure 38 - Heat Capacity versus Heat Flux Rate

A = area of specimen (sq ft)

$\rho t = W/A$

The specimen provided were 2 ft long and approximately 0.5 in. wide. They were weighed before and after coating. Therefore, the weight of the specimen per unit area was readily calculated.

The calculations for Specimen 1 are:

$$A = (24)\left(\frac{1}{2}\right) = 12 \text{ sq in.} = 0.0835 \text{ sq ft} \tag{36}$$

$$\rho t = \frac{W_1}{A} = \left(\frac{7.4612 \text{ gm}}{453.6 \text{ gm/lb}}\right)\left(\frac{1}{0.0835 \text{ sq ft}}\right) = 0.197 \text{ psf} \tag{37}$$

$$Q_{eff} = \frac{(12.7)(2.775)}{0.197 \text{ Btu/sq ft}} = 178 \text{ Btu/lb} \tag{38}$$

The calculations for coated Specimen 7 are:

$$W_7 = \frac{7.4466}{453.6} = 0.0164 \text{ lb} \tag{39}$$

$$W_c = \frac{9.8198 - 7.4466}{453.6} = \frac{2.3732}{453.6} = 0.00523 \text{ lb} \tag{40}$$

Using one-half W_c (since it is questionable whether the aft side is useful):

$$W_{7T} = W_7 + \frac{W_c}{2} = 0.0164 + 0.00261 = 0.019 \text{ lb} \tag{41}$$

$$\rho t = \frac{W}{A} = \frac{0.019}{0.0835} = 0.228 \text{ psf} \tag{42}$$

$$Q_{eff} = \frac{(12.7)(17.6)}{0.228} = 980 \text{ Btu/lb} \tag{43}$$

The calculations for coated Specimen 12 are:

$$W_{12} = \frac{7.4394}{453.6} = 0.0164 \text{ lb} \tag{44}$$

$$W_c = \frac{3.6356}{453.6} = 0.008 \text{ lb} \tag{45}$$

$$W_{12T} = 0.0204 \text{ lb} \tag{46}$$

$$\rho t = \frac{0.0204}{0.0835} = 0.244 \text{ psf} \tag{47}$$

$$Q_{eff} = \frac{(12.7)(28.24)}{0.244} = 1470 \text{ Btu/lb} \tag{48}$$

The results of the Phase I and III laboratory tests, in conjunction with the thermodynamic heating predictions, indicated that 0.100 in. thick Nomex, coated with 0.025 in. thick Dynatherm D-65, meets the maximum heating case requirements for Phase III.

8. DESIGN AND FABRICATION

a. General

The principal factors that shaped the design and influenced the fabrication procedure of the Phase III PARASONIC small parachute configuration were as follows:

1. The canopy was shaped for good structural efficiency.
2. The canopy roof elements were relatively heavy and were coated for good thermal performance.
3. The canopy skirt had a catenary shape for efficient canopy-suspension line load transfer.

Described below are the design and the fabrication techniques that were generated to incorporate these features.

b. Design

The PARASONIC design was a refinement of the HYPERFLO configurations. (The two designs are presented in Drawings 530A005-300 and 530A005-301.) The materials used in the construction of both units were identical except in the region of the roof gore-to-skirt gore seam reinforcement, where webbing was used for the HYPERFLO and bias tape was used for the PARASONIC. Other design differences between the two types were the lack of verticals on the PARASONIC and the treatment of the inlet reinforcement. Both canopies had 12 gores and radials. The PARASONIC radials were formed by six continuous pieces of webbing over the canopy. The radials were sewed to the gore seams and maintain the spacing of the roof gore webbing.

The inlet reinforcing tape and forward edge of the PARASONIC skirt were arranged in a scalloped pattern forming a catenary between suspension lines to balance the fabric stresses near the inlet. The HYPERFLO inlet was constructed as a hoop.

The suspension lines were folded and stitched into a rounded cross-section to minimize the effects of the lines on the flow into either canopy. The confluence point was formed by the use of a keeper ring that constrains and spaces the suspension lines. A single hard confluence point, formed by sewing the lines together, was abandoned based on wind tunnel tests of a similar parachute. Line failures occurred at the single hard point after 90 sec of wind tunnel testing.

c. Fabrication

The principal fabrication development consisted of finding a method of

weaving a three-dimensional mesh roof for the PARASONIC. The thermodynamic heating predictions and the in-plant test results indicated that 0.100 in. thick Nomex, coated with 0.025 in. thick Dynatherm D-65, met the maximum heating case requirements. Woven and flat mesh cloth and integral weaving approaches were reviewed as were the width of the elements.

Fabrication of parachute roof panels from coated yarns 0.15-in. thick presented mesh or grid weaving problems, as well as problems in seaming between the gores and between the roof and skirt portions of the canopy. Attempts to stitch components woven from this stiff and heavy yarn proved futile. Efforts to interweave the roof gores by looping the yarns together at the gore edges also were unsatisfactory (see Appendix V). The final approach was to hand-weave the entire roof as a unit, using a continuous yarn that was always oriented at 45 deg to the gore centerline. A three-dimensional surface was developed upon which the roofs were woven.

Assembly alignment was controlled as follows. The skirt gore seams were matched by providing match marks along the centerline of the seam lap. These marks were transferred from the gore template to the cloth with an ink-marking pen. The marks were spaced at convenient intervals of one to four inches, depending on the degree of curvature of the gore seam. The meridional straps were correctly located by premarking the straps with station marks while they were in a straight and lightly tensioned position for matching with corresponding station marks on the gores. The station marks were transferred to the gores from the gore template while in a flat position.

9. DEPLOYMENT SEQUENCE AND PACKING PROCEDURE

a. General

Packing and, to a lesser extent, deployment of the PARASONIC small parachutes were influenced by the stiffness that the coating introduced. Figure 39 shows the deployment sequence. Figure 40 presents photographs of packing the parachute into the deployment bag.

b. Deployment Sequence

The Phase III deployment system approach was the same as that used previously in ADDPEP Phase I for small parachutes (References 29 and 34) and also for the BALLUTE flight tests (Reference 2). Deployment was from within a deployment bag and occurred with lines first. The test item container was thrust rearward from Test Vehicle C at a relative speed of approximately 25 fps. The parachute was contained within the deployment bag, which was accelerated to the rear by a bridle to the container. Movement of the bag rearward several feet straightened the riser forward of the bag and caused a knife attached to the riser to cut the forward closure cord of the bag; this allowed the balance of the riser line and suspension lines to be extracted in an orderly manner from the deployment bag. The line extraction sequence was controlled by ties to the bag. The canopy was extracted last by the lines opening the locking loop through the internal bag loops holding the canopy. The canopy unfolded

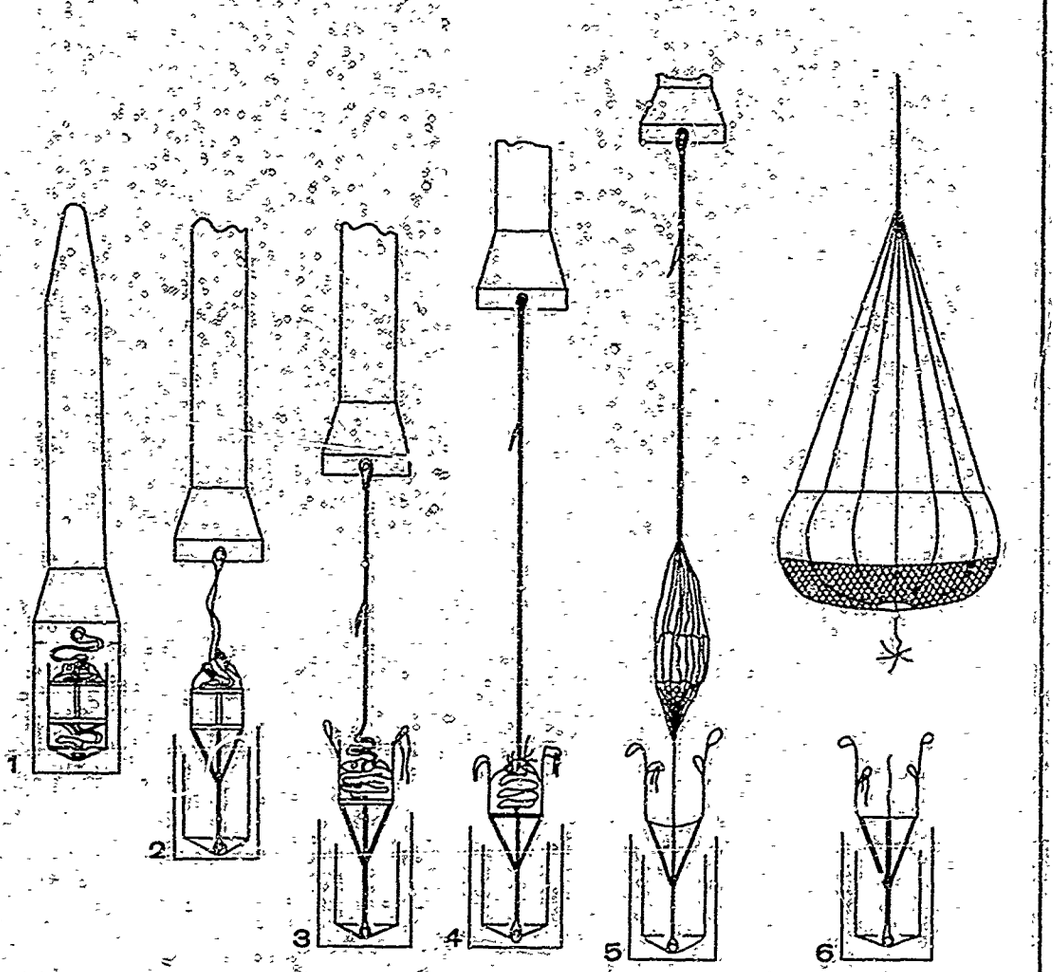

1. VEHICLE IN FLIGHT BEFORE DEPLOYMENT BEGINS. PARACHUTE PACKAGED IN DEPLOYMENT BAG. RISER ATTACHED TO VEHICLE. BAG-BRIDLE LINE ATTACHED TO AFT SECTION OF CANISTER.

2. CANISTER SEPARATED FROM VEHICLE. DEPLOYMENT BAG OUT OF CANISTER, BEING ACCELERATED BY CANISTER THROUGH BRIDLE LINES. RISER LINES SLIGHTLY EXTENDED. ONE RISER LINE HAS METAL CORD-CUTTER KNIFE. NYLON CORD LACED THROUGH OUTER LOCK LOOPS OF DEPLOYMENT BAG AND THROUGH KNIFE. CORD CLOSES END OF BAG, RETAINING PARACHUTE AND RISER IN DEPLOYMENT BAG, WHEN ACCELERATING LOADS ARE APPLIED TO BAG BY CANISTER.

3. CANISTER AND DEPLOYMENT BAG FURTHER AFT OF MISSILE. KNIFE HAS CUT LOCK CORD, ALLOWING RISER LINES TO DEPLOY.

4. FOUR INNER LOCK LOOPS SEWED INSIDE BAG JUST FORWARD OF CANOPY INLET HELD TOGETHER BY A LOCKING LOOP. THIS ARRANGEMENT HOLDS CANOPY IN BAG UNTIL LINES ARE FULLY EXTENDED.

5. DEPLOYMENT BAG OFF PARACHUTE. APEX OF CANOPY IS STILL ATTACHED TO BAG WITH LIGHT NYLON BREAK CORD TO ENSURE FULL CANOPY EXTENSION.

6. PARACHUTE FULLY INFLATED. BREAK CORD BROKEN. DEPLOYMENT BAG AND CANISTER ENTIRELY SEPARATED.

Figure 39 - PARASONIC Small Parachute Deployment Sequence

(A) FOLDED CANOPY AND DEPLOYMENT BAG

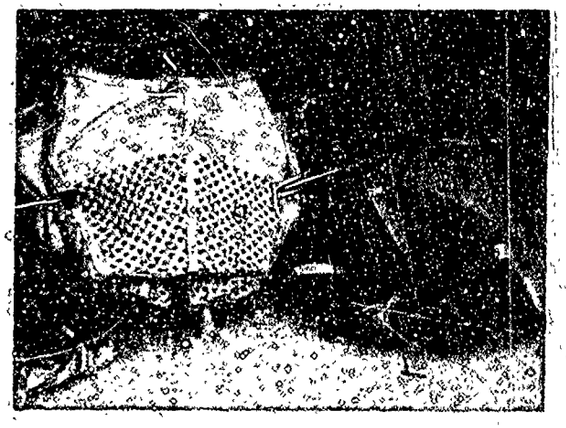

(B) CANOPY IN BAG, LINES TUCKED INTO CANOPY LOCK

(C) SUSPENSION LINES ATTACHED TO BAG

(D) BAG CLOSED, KNIFE INSTALLED

Figure 40 - Packing the PARASONIC Parachute

and then was aligned by a tie cord to the bag. When the tie cord broke, the parachute inflated.

c. Packing SP-3 Into Deployment Bag

The parachute was placed on the folding table. The mesh portion of the canopy was stiff as a result of the coating. Accordingly, the pattern shown in Figure 41 was used. The apex was doubled forward and made even with the roof/skirt seam, as the sectional view in Figure 41 indicates. Then the roof was folded into six lobes, as the plan view shows. To complete the canopy folding, the skirt was pleated and turned into the center or outside the roof (not shown in the plan view). The result was a loose pack approximately 12 in. in diameter by 9 in. high.

The apex cord was Type I, 100-lb nylon, doubled to give a 200-lb gross capability. The cord was attached to the bag with clove hitches and two half-hitches. The locking loop that held the inside bag loops together adjacent to the skirt consisted of a 25-in. circumference of 1-in, 2500-lb webbing closed with a 3-point, 3-in. long splice sewn with FF thread. To protect the fold of suspension lines in the end of the locking loop, the fold was wrapped in a 6- by 6-in. piece of Nomex cloth before being inserted. Four 35-lb cotton tie cords held the suspension lines and riser to the bag. One was placed around the folded suspension lines, one at the confluence ring, and two along the riser. The cord that closed the bag consisted of two turns of 550-lb cord.

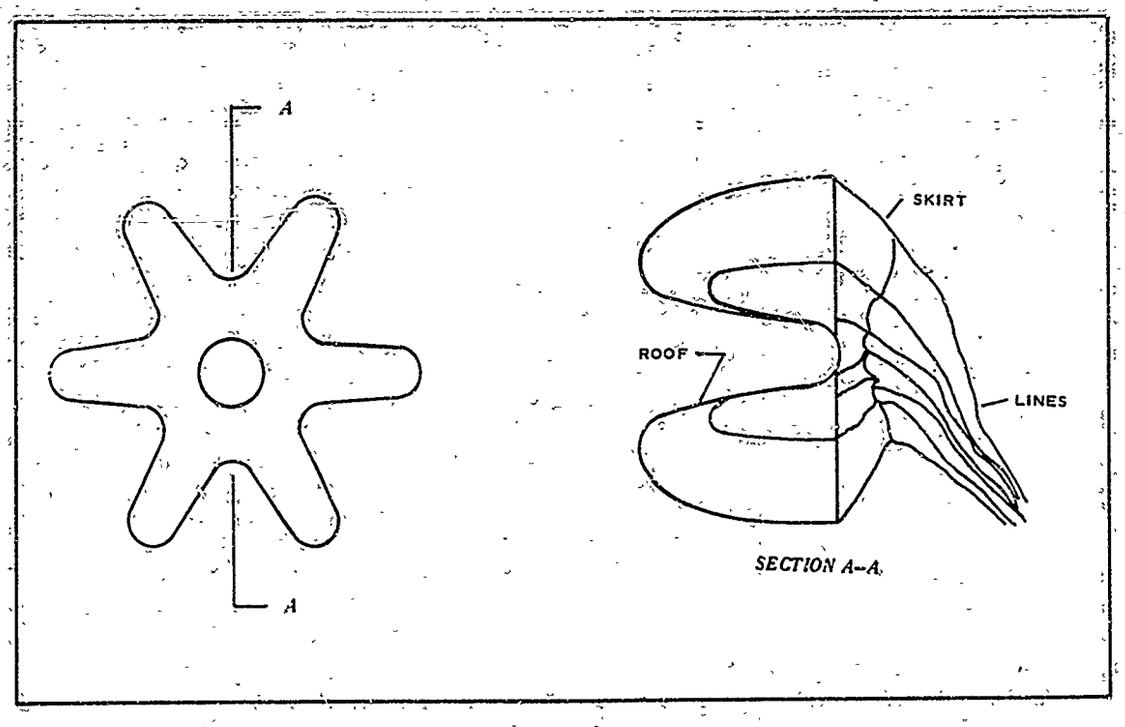

Figure 41 - PARASONIC Small Parachute Canopy Folding Pattern

SECTION IV - SMALL PARACHUTE DECELERATOR

10. SUMMARY AND CONCLUSIONS

a. Configuration

Phase I information (Reference 1), supported by more recent wind tunnel results (Reference 23), was used in generating the small parachute (SP) flight test configuration. The free-flight stability results, based on drag link data (Figures 26 and 27) and SP-4 camera data, were similar to the results obtained with similar full-scale units (4-ft D_o) in the PWT facility at AEDC (Figure 23A). The lateral stability measured by the SP-4 film was ±3 deg at Mach 1.4.

b. Aerodynamic Loadings

During free-flight and wind-tunnel tests, the parachute was observed to take its design shape under load. The drag values measured for full-size units in the wind tunnel and in free flight agree within the accuracy of the data. Based on these limited correlations, full-scale tests in the wind tunnel are recommended for establishing parachute drag and stability characteristics to Mach 3 and dynamic pressures greater than 120 psf, which are the limit values of the wind-tunnel facility. Reported small-scale wind-tunnel data were not consistent enough for design use (Figure 30).

The measured nominal surface area drag coefficients were:

1. For SP-3, 0.306 at Mach 2.68
2. For SP-4, 0.377 at Mach 1.42
3. For SP-5, 0.145 at Mach 5.23

These values compare favorably with the predicted drag coefficient values that were based on full-scale wind-tunnel tests of 0.242 at Mach 2.68, 0.32 at Mach 1.42, and 0.17 at Mach 5.23 (Figure 30). However, the test values are considerably less than the drag values that stemmed from predicted pressure distributions over the canopy (see Table XVIII), which do not consider the loss in total pressure due to the wake of a forebody.

c. Structure

On the basis of the drag link and camera data, it is concluded that the parachutes are more than structurally adequate for the design conditions. The re-entry case for SP-5 indicated the parachute could withstand more severe heating and loading environments than the design values. Peak loads of 1000 lb, after being subjected to a cold wall pulse of 337 Btu pulse, were withstood, as compared to a design load of 1482 lb and a cold wall heat pulse of 121 Btu (Figure 36).

d. Thermodynamic Analysis

A thermodynamic analysis was performed to (1) compare the predicted material temperatures with the measured temperature values for the

SP-5 flight test and (2) evaluate the predicting technique. The prediction technique is considered acceptable for engineering design. Figure 37 presents the values for comparison.

The measured maximum 200-F temperature value during ascent can be compared with 300 F for laminar flow and 500 F for turbulent flow heat transfer rates. The measured temperature values to 800 F during re-entry can be compared with the predicted temperature values to 800 F for turbulent flow heat transfer rates. These comparisons suggest that the heat transfer coefficients during SP-5 ascent should be based on laminar flow values. The re-entry values agree with the turbulent heat transfer values.

e. Materials

The selected materials, which performed as required, included Nomex cloth and webbing coated with Dynatherm D-65. Heat-tunnel tests indicated that the coating offered a much more efficient heat protection approach than increasing the mass of the Nomex (Figure 38).

f. Design and Fabrication

The structural design evolved from analysis performed during Phases I and III. The basic changes from the Phase I designs were associated with the higher temperature predicted for the SP-5 flight test conditions. These conditions required the development of fabrication techniques for the mesh roof (Appendix V). These included establishing (1) a three-dimensional "saddle" shape form for weaving the roof accurately, (2) weaving techniques, (3) attachments to the skirt, and (4) coating methods.

g. Deployment System and Packing Procedure

The Phase III deployment and packing procedure is similar to that used for the small parachutes in Phase I. A bag was used to obtain lines-first deployment and limit the snatch force.

(Reverse is blank)

SECTION V

CONCLUSIONS

1. GENERAL

During the concluding Phase III of ADDPEP (Aerodynamic Deployable Decelerator Performance-Evaluation Program), wind-tunnel and free-flight tests results were used to evaluate decelerator design methods and testing techniques. The main conclusions stemming from these evaluations are drawn together in this section.

2. FREE-FLIGHT TEST CAPABILITY

From tests of the free-flight test vehicle/booster systems, it is concluded that:

1. The performance of Test Vehicle A/Booster can be predicted with confidence. The data system is adequate, except that the exterior camera becomes unreliable at the higher Mach numbers above 2.2. As a whole, recovery and reusability of the system exceed the design goals. However, the reliability of the cameras is unacceptable with more than one reuse.
2. The performance of Test Vehicle C/Booster also can be predicted with confidence. The data transmission range is excellent. Tracking beacon drop-out occurred just prior to launch during the SP-3 test and at Lance ignition during the SP-5 test. When recovered, the Test Vehicle C meets design goals for reusability.

3. LARGE PARACHUTE DECELERATOR

From free-flight tests of the large, supersonic, hemisflo parachute design, it is concluded that:

1. The flight tests confirm the strong inflation characteristics of the canopy when the inlet is reefed to low area ratio values (0.15 to 0.20) in the transonic and supersonic regime (Mach 2.7).
2. Phase III free-flight drag values are consistent with Phase II results and significantly higher than results obtained from wind-tunnel tests of similar models.
3. In the case of parachutes having less than 0.25 line twist values, the measured opening times decrease with increasing flight Mach numbers and dynamic pressures. Phase II efforts indicate that 1.5 turns of line twist lengthens the opening time.
4. Calculated values for opening shock indicate that these values decrease with increasing Mach number

and dynamic pressure. The largest opening shock value occurs at the lowest Mach number, dynamic pressure, and reefing size.

5. An analytical approach is needed to predict reefing line loads. A new approach is presented in Appendix I.

6. Reduced reefing line loads or a much stronger reefing line is required for dynamic pressures greater than approximately 2500 psf.

7. Changes to the suspension line materials should be considered because of the damage to the lines.

8. The deployment approach is satisfactory, as demonstrated by the fact that the snatch loads are much less than the opening loads and the lack of deployment bag damage. However, damage to the nylon lines still occurs.

4. SMALL PARACHUTE DECELERATOR

From wind-tunnel and free-flight tests of the small supersonic parachute design, designated PARASONIC, it is concluded that:

1. The PARASONIC design demonstrates similar inflation and system stability characteristics during wind-tunnel and free-flight tests. The stability is better than that of a HYPERFLO design that was also investigated.

2. There is a good correlation between the drag characteristics of the free-flight tested and wind-tunnel tested full-scale parachutes. At Mach 2.68, 1.42, and 5.23, the nominal surface drag coefficients are 0.306, 0.377, and 0.145, respectively, based on free-flight data; and 0.242, 0.32, and 0.17, based on wind-tunnel data and extrapolations. The small-scale data obtained are not consistent enough for design use.

3. The parachutes are structurally adequate for the design test conditions.

4. The thermal analysis approach is acceptable for design. Good correlation occurs for the re-entry case where turbulent flow conditions exist.

5. The coated Nomex materials used are more than adequate for the design heating and drag loads.

6. The deployment system, which is similar to normal lines-first approaches, is adequate.

APPENDIX I

ESTIMATING MAXIMUM REEFING LINE LOADS FOR LARGE PARACHUTES

An analytical approach is presented here for estimating the maximum reefing line loads of large supersonic paraclutes. The approach considers the work done by the dynamic pressure from the line stretch configuration to the reefed configuration. It is assumed that the work is stored in the canopy as strain energy. The values calculated using this approach are compared with results obtained from free-flight tests of six large parachutes, designated LP-3, -4, -5, -7, -8, and -9. All the parachute canopies are characterized by a nominal diameter of D_o = 16 ft, and by a suspension line length of L_S = 32 ft.

Two basic simplifying assumptions are made:

1. The flow is incompressible.

2. The external flow is at ambient conditions.

With these assumptions, the pressure difference across the canopy is constant and equal to the dynamic pressure, and the canopy shape becomes spherical at maximum conditions. Thus, two energy factors are ignored: (1) the energy reduction due to the higher external pressures acting on the forward canopy surface and (2) the energy increase due to lower external pressure at the base of the canopy.

The following equation gives the work, W, done by the dynamic pressure, q, on the parachute configuration of Figure 42A to bring it to the configuration of Figure 42B:

$$W = q(V_F - V_i) \tag{49}$$

Where:

V_F = volume of air bounded by canopy and inlet plane

V_i = volume of air enclosed in reefed parachute

This work is stored as strain energy in the canopy. Assuming that a uniform biaxial stress, N_1, due to opening shock exists in the canopy, the strain energy stored per unit area of canopy is:

$$w = \frac{W}{S_R} = 2\left(\frac{1}{2}\right)N_1 \epsilon_M = N_1 \epsilon_M \tag{50}$$

Where S_R is the surface area of a partially opened parachute and where ϵ_M, the strain in the canopy, is assumed at the maximum value of:

$$\epsilon_M = 0.14 \text{ ft/ft} \tag{51}$$

APPENDIX I

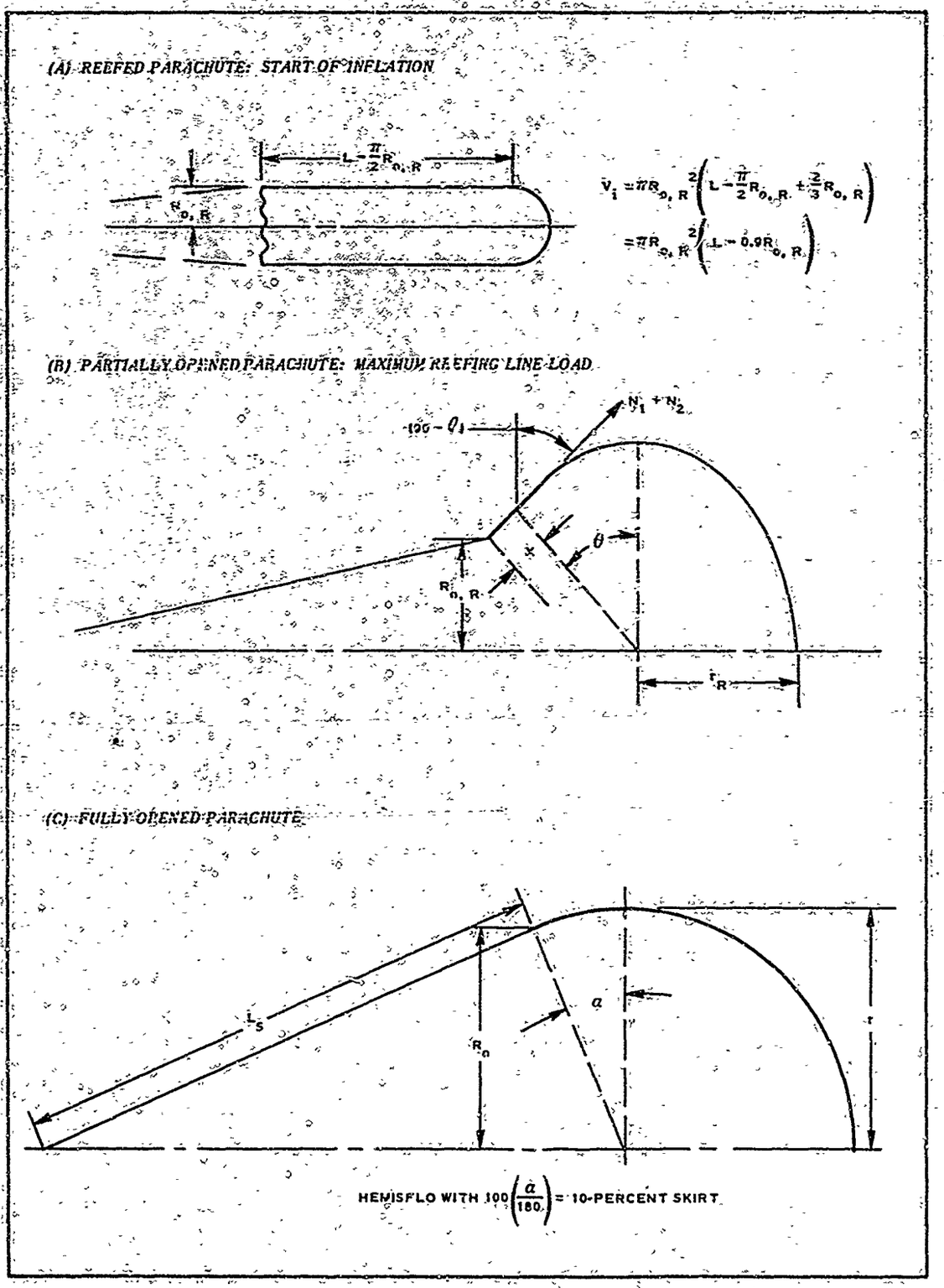

Figure 42 - Reefed, Partially Opened, and Fully Opened Large Parachute

APPENDIX I

It is noted that (see Figures 42A and B):

$$V_F \cong \frac{4}{3}\pi r_R^3 \tag{52}$$

$$S_R \cong 4\pi r_R^2 \tag{53}$$

$$V_i \cong \pi R_{o,R}^2 (L - 0.9R_{o,R}) \tag{54}$$

Where:

L = length from apex to skirt along meridian

r_R = opening parachute radius (assumed spherical)

$R_{o,R}$ = reefed parachute inlet radius

$= kR_o$, $0 \leqq k \leqq 1$

R_o = fully inflated parachute inlet radius

Now Equation 50 solved for N_1 gives:

$$N_1 = \frac{W}{S_R C_M} = \frac{q}{0.14}\left[\frac{1}{3}r_R - \frac{1}{4}(L - 0.9R_{o,R})\left(\frac{R_{o,R}}{r_R}\right)^2\right] = 7.143Cq \tag{55}$$

Where:

$$C = \frac{1}{3}r_R - \frac{1}{4}(L - 0.9R_{o,R})\left(\frac{R_{o,R}}{r_R}\right)^2$$

In addition to N_1, the canopy is subjected to the familiar stress due to dynamic pressure:

$$N_2 = \frac{qr_R}{2} \tag{56}$$

Considering the meridional stress, $N_1 + N_2$, around the inlet and projecting it in the plane of the inlet gives an outward radial loading on the periphery of the inlet. The total drag, D, is given by:

$$D = C_D S_P q \tag{57}$$

Where:

C_D = drag coefficient = 1.5

S_P = opening parachute frontal area

The drag is resisted around the inlet by the suspension lin s. The load per unit length of inlet periphery (N_3) is D/L_R. The following equation gives the inward radial component of this load, which relieves the outward component $(N_1 + N_2) \sin \theta$ (see Figure 42B):

$$N_3 = \frac{D}{L_R} \frac{R_{o,R}}{L_S} \tag{58}$$

Where:

L_R = inlet perimeter

L_S = length of suspension lines

Note that:

$$L_R = 2\pi R_{o,R} \tag{59}$$

$$L_S = 32 \text{ ft} \tag{60}$$

Now Equation 58 becomes:

$$N_3 = \frac{D}{64\pi} = \frac{1.5\pi r_R^2 q}{64\pi} = 0.02344 r_R^2 q \tag{61}$$

Consequently, the net outward radial load per unit length of the inlet periphery is:

$$N_R = (N_1 + N_2) \sin \theta - N_3 \tag{62}$$

And the hoop tension is:

$$P_R = N_R R_{o,R} = \left[(N_1 + N_2) \sin \theta - N_3\right] R_{o,R} \tag{63}$$

The angle θ and the radius r_R may be determined from the geometry of Figure 42B for $X = 0$. In fact:

$$(\theta + \tfrac{\pi}{2}) r_R = L \tag{64}$$

$$r_R \cos \theta = R_{o,R} \tag{65}$$

Dividing Equation 64 by 65 results in:

APPE. DIX I

$$\frac{\theta + \frac{\pi}{2}}{\cos\theta} = \frac{L}{R_{o,R}} = \frac{9.316}{R_{o,R}} \tag{66}$$

From Figure 42C:

$$S_o = 2\pi r^2(1 + \sin\alpha) = \frac{\pi D_o^2}{4} = 0.7854(16)^2 = 201.06 \tag{67}$$

Where:

S_o = fully inflated canopy surface area

D_o = canopy nominal diameter

Hence:

$$r = \sqrt{\frac{201.06}{2\pi(1.309)}} = 4.942 \text{ ft} \tag{68}$$

$$L = \left(\frac{\pi}{2} + \frac{\pi}{10}\right) r = \frac{6\pi}{10} r = 4.942(0.6\pi) = 9.316 \text{ ft} \tag{69}$$

The angle θ may be found for Equation 66 from standard tables. (Letting $\phi = \theta + \pi/2$, Equation 66 reduces to $\sin\phi/\phi = R_{o,R}/316$, from which ϕ can be found from tables that give values of $\sin\phi/\phi$ versus ϕ.) Then, the radius r_R may be found from either Equation 64 or 65.

Using the equations derived above, the values of P_R were calculated as shown in Tablex XXIII and XXIV for the test parachutes. Allowable values of P_R are given in Table XXIV for comparison.

Results of the tests indicated the reefing lines were broken for the LP-3, LP-7, and LP-9 parachutes. The analytical values predict the results of LP-7 and LP-9 by almost a factor of two. Parachutes LP-3, LP-4, and LP-5 appear marginal, with only LP-3 breaking, and that occurred approximately 1/10 of a second after the initial reefed shape.

From the results of this analysis (which requires only knowledge of the parachute size, materials, and the test conditions), a reefing line strength can be predicted within engineering requirements. Further refinements would include the use of compressible flow, vehicle wake, and estimates of the external flow for the various stages of opening.

TABLE XXIII - GEOMETRY OF CANOPIES*

Parachute	q (psf)	L_R (ft)	$R_{o,R}$ (ft)	θ (deg)	$\sin\theta$	r_R (ft)	$S_R = \pi r_R^2$	$\frac{1}{4}(L - 0.9R_{o,R})$	$C = \frac{1}{3}r_R - \frac{1}{4}(L - 0.9R_{o,R})\left(\frac{R_{o,R}}{r_R}\right)^2$
LP-3	1350	20.5	3.26	38.4	0.62115	4.16	54.37	1.596	0.41
LP-4	1640	15.5	2.47	50.0	0.76604	3.84	46.33	1.773	0.55
LP-5	2410	15.5	2.47	50.0	0.76604	3.84	46.33	1.773	0.55
LP-7	3270	13.1	2.08	55.6	0.82511	3.68	42.55	1.861	0.64
LP-8	850	11.0	1.75	60.4	0.80949	3.54	39.37	1.935	0.71
LP-9	4560	11.0	1.75	60.4	0.86949	3.54	39.37	1.935	0.71

*Canopy and suspension lines geometry: D_o = 16 ft; L = 9.316 ft; L_S = 32 ft

TABLE XXIV - CANOPY STRESSES AND CRITICAL HOOP TENSION AROUND INLET PERIPHERY

Parachute	$N_1 = 7.143Cq$ (lb/ft)	$N_2 = \frac{1}{2}qr_R$ (lb/ft)	$N_1 + N_2$ (lb/ft)	$(N_1 + N_2)\sin\theta$ (lb/ft)	$D = 1.55S_Pq$ (lb)	$N_3 = D/(64\pi)$ (lb/ft)	$N_R = (N_1 + N_2)\sin\theta - N_3$ (lb/ft)	Hoop tension around inlet: Calculated $P_R = N_R R_{o,R}$ (lb)	Hoop tension around inlet: Allowable P_{All} (lb)
LP-3	3,954	2808	6,762	4,200	110,100	548	3,652	11,905	12,000
LP-4	6,444	3149	9,593	7,349	113,782	566	6,783	16,754	18,000
LP-5	9,469	4627	14,096	10,798	167,482	833	9,965	24,614	18,000
LP-7	14,950	6017	20,967	17,300	208,708	1038	16,262	33,825	18,000
LP-8	4,311	1505	5,816	5,057	50,197	250	4,807	8,412	24,000
LP-9	23,585	8071	31,656	27,525	269,291	1339	26,186	45,826	24,000

APPENDIX II

DROGUE PARACHUTE SIZE AND REEFING SIZES FOR LARGE PARACHUTES

1. GENERAL

This appendix presents the approach for determining the drogue size that was used to deploy the LP-7, LP-8, and LP-9 large supersonic parachutes at a constant acceleration.

2. ASSUMPTIONS

The basic assumptions are:

1. Weight of test item and bag = 140 lb
2. Weight of drogue parachute = 5 lb
3. Desired acceleration = 40 g
4. Nominal surface drag coefficient, C_{D_o} = 0.09 to 0.26 (References 11 and 20)
5. Calculated test conditions: Mach, M = 2.2, = 2.6, and = 3.0 for dynamic pressure, q = 5440, = 7450, and = 9900 psf, respectively.

3. CALCULATIONS OF PARACHUTE SIZE

The drag requirements are:

$$(40)(145) = 5800 \text{ lb} \tag{70}$$

The C_DA requirements for Mach 3 → 2.2 are:

$$\frac{5800}{9900} \text{ to } \frac{5800}{5440} = 0.585 \text{ to } 1.07 \text{ sq ft} \tag{71}$$

Depending on the reefing ratio,

$$C_{D_o} \text{ at Mach 2.2} = 0.1 \text{ to } 0.26 \tag{72}$$

$$C_{D_o} \text{ at Mach 3.0} = 0.09 \text{ to } 0.26 \tag{73}$$

The nominal surface areas (S_o) corresponding to the C_{D_o} values are:

$$S_o \text{ at Mach 2.2} = \frac{1.07}{0.26} = 4.1 \text{ sq ft (no reefing)} \tag{74}$$

APPENDIX II

$$S_o \text{ at Mach } 3 = \frac{0.583}{0.09} = 6.5 \text{ sq ft (maximum reefing)} \quad (75)$$

The choice of a drogue, with an S_o between these two values, can be reefed for the desired range of drag areas. A 30-in. diameter (D_o) parachute (S_o = 4.91 sq ft) with various degrees of reefing was chosen.

Reefing size at maximum dynamic pressure (q) is based on required C_{D_o}:

$$C_D A \text{ at Mach } 3.0 = 0.585 \quad (76)$$

$$C_{D_o} = \frac{0.585}{4.91} = 0.119 \quad (77)$$

To obtain this 0.119 value, the reefing area is equal to 20 percent of the constructed inlet area (based on data in Reference 11). The reefed inlet size is also equal to the square root of 0.20 or 0.466 times the constructed inlet diameter. These values are compared with those of Reference 20, Configuration R-1, where the nominal surface drag coefficient is 0.09 to 0.12 for an 11.6-percent, and 0.18 for a 26.2-percent, reefed-to-constructed inlet area ratio. The larger scale results predict larger drag values for the same reefing size at Mach 1.8 to 2.2.

These reefing ratios can also be compared with the maximum reefed condition of the test parachute for the flight case of LP-5. Here the reefed canopy inlet diameter was 1.225 ft versus a constructed diameter of 2.355 ft. The corresponding area ratio was 26 percent. The nominal surface drag coefficient was 0.25, which is above the 0.10 for small-scale and 0.17 for large-scale wind-tunnel data. The drag force based on all three coefficients is:

$$D = (0.25,\ 0.10,\ \text{and } 0.17)(3383)(12.566) = 10,625,\ 4250,\ \text{and } 7220 \text{ lb} \quad (78)$$

4. WAKE CONSIDERATIONS

The small-scale data were taken behind a 2-in. forebody diameter, and the parachute projected diameter was 13 in., a ratio of 6.5 to 1. The large-scale data were taken behind a 1.47-ft forebody diameter, and the parachute constructed diameter was 6.67 ft, a ratio of 4.5 to 1. For LP-3, LP-4, and LP-5, the flight test drogue was behind a 15-in.-diameter test item deployment bag, and the constructed diameter of the drogue parachute was 32 in., a factor of approximately 2. For LP-7, LP-8, and LP-9, the construction diameter of the drogue was 20 in., a factor of 1.33. The films indicated full inflation of the drogue reefed to a 14.7-in. inlet diameter for the LP-5 test at 8-bag diameters aft. It was anticipated that full inflation of the smaller parachute at the same position would be attained because the reefed inlet diameter of the smaller 30-in. D_o parachute was 17.67 in., compared to 14.70 in. for the 48-in. D_o parachute used during the LP-5 test.

APPENDIX III

GROMMET TEST RESULTS: LARGE PARACHUTE DEPLOYMENT BAG

Listed below are the results of pull tests conducted on samples that were based on the grommet lacing approach used for the large parachute deployment bag:

1. No. 1 sample of deployment bag constructed to Drawing 530A005-017
   a. Material
      Lacing webbing: 1500 lb, 9/16 in.
      Lacing grommets: four no. 2
   b. Results (total for four grommets)
      Grommets began to pull out at 1500 lb
      Cloth failure at 2480 lb

2. No. 2 sample of deployment bag constructed to Drawing 530A005-017
   a. Material
      Identical to no. 1 sample
   b. Results (total for four grommets)
      Grommets began to pull out at 1500 lb
      Cloth failure at 2390 lb

3. No. 3 sample of deployment bag constructed to Drawing 530A005-017 using heavier bag cloth
   a. Material
      Lacing webbing: 1500 lb, 9/16 in.
      Lacing grommets: five no. 2
      Bag material: Stern and Stern, no. 2823, 20.5 oz
   b. Results (total for five grommets)
      Grommets began to pull out at 3700 lb
      Grommets badly bent at 4000 lb
      Jaw slippage at 4830 lb

4. No. 4 sample (no. 3 sample modified)
   a. Material
      No. 3 sample with no. 3 lacing grommets replacing the smaller no. 2 grommets; and with 1800-lb 5/8-in. webbing replacing the 1500-lb, 9/16-in. webbing
   b. Results (total for five grommets)
      Webbing failed at 4950 lb near center
      Grommets elongated, but in place
      Bag cloth undamaged

5. No. 5 sample (no. 3 sample modified)
   a. Material
      No. 3 sample with new no. 3 grommets replacing the previously elongated no. 3 grommets in the no. 4 sample; and keeping the 1500-lb, 9/16-in. webbing

b. Results (total for five grommets)
Webbing failed at 4925 lb
Grommets elongated, but in place
Bag cloth undamaged

Based on the above test results, the deployment bag design for LP-8 and LP-9 included the heavier No. 3 grommets in place of the No. 2 grommets and the heavier Stern and Stern No, 2823 bag cloth in place of MIL-C-7219 Type III cloth.

APPENDIX IV

POROSITY CALCULATIONS FOR SMALL PARACHUTE SP-5

1. GENERAL

This appendix presents the method used to measure the overall porosity of the SP-5 small parachute. This was done using the air flow test setup shown schematically in Figure 43; a photograph of the setup is shown earlier in Figure 31.

2. AVERAGE PRESSURE DIFFERENCE OF 0.35 IN. OF WATER

The velocity, diameter, area, and flow volume are:

$$\text{Velocity in pipe} = 3000 \text{ fpm} = 50 \text{ fps} \tag{79}$$

$$\text{Diameter of pipe} = 8\text{-}15/16 \text{ in.} = 8.9375 \text{ in.} \tag{80}$$

$$\text{Area of pipe} = \frac{\pi D^2}{4} = \frac{3.1416(8.9375)^2}{4} = 62.6 \text{ sq in.} \tag{81}$$

Flow volume per second = mean velocity times area

$$= 50\left(\frac{62.6}{144}\right) = 21.80 \text{ cfs through pipe and system} \tag{82}$$

To calculate velocity (V) through the area exit based on the pressure differential (ΔP) across the roof:

$$\Delta P = \frac{1}{2}\rho V^2 = 0.35 \text{ in. of water across roof}$$

$$= 0.35\left(\frac{62.4}{12}\right) = \frac{0.002378}{2} V^2 \tag{83}$$

$$V^2 = 1531 \tag{84}$$

$$V = 39.2 \text{ fps} \tag{85}$$

The roof exit area (A_e) is based on volume through the system and velocity through the roof:

$$A_e = \frac{\text{Volume}}{V} = \frac{21.80}{39.2} = 0.556 \text{ sq ft}$$

$$= 80 \text{ sq in.} \tag{86}$$

The measured inlet area (A_i) is:

APPENDIX IV

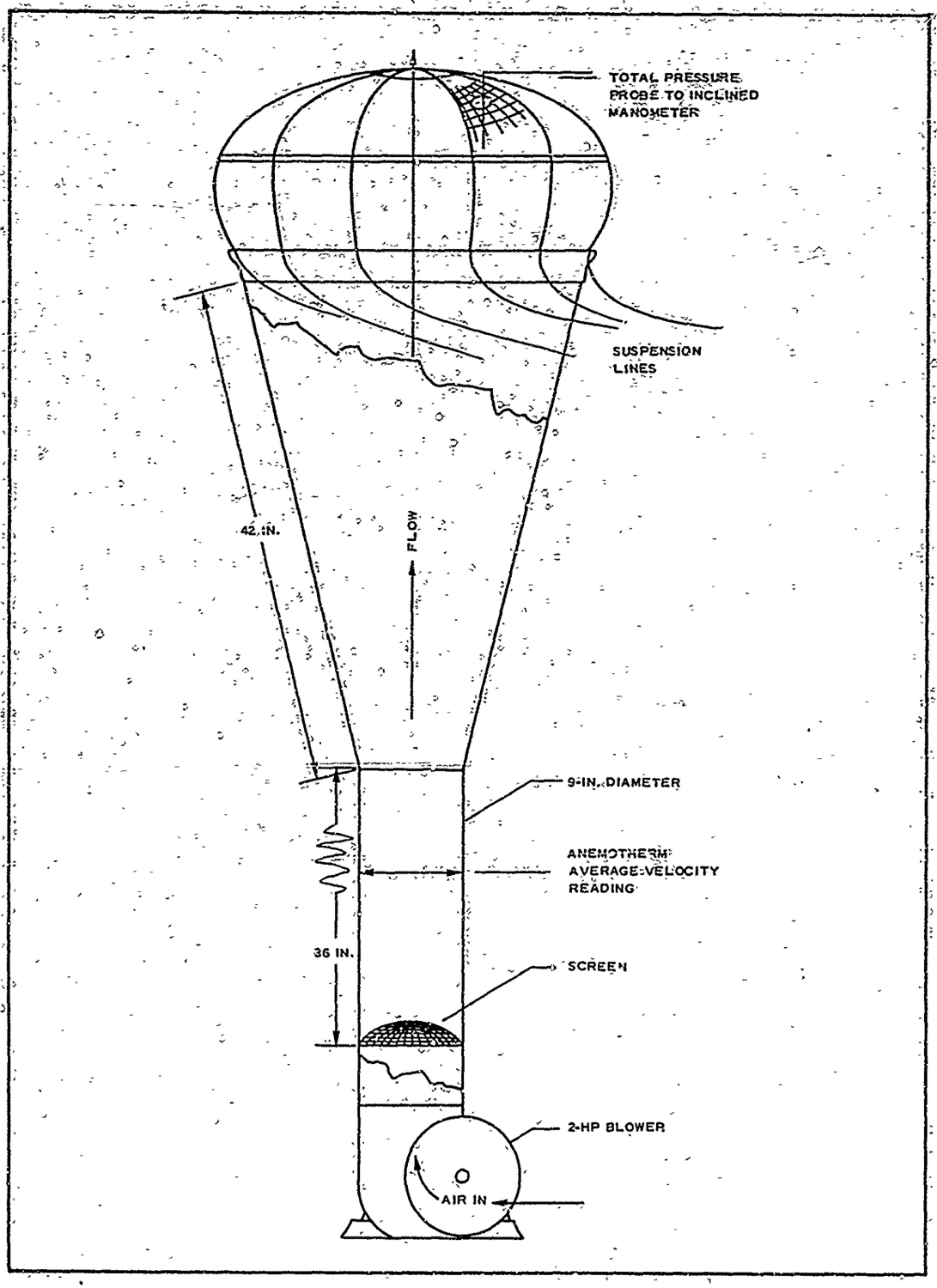

Figure 43 - Schematic of Air Flow Test Setup

APPENDIX IV

$$A_i = \frac{\pi D^2}{4} = \frac{\pi(28.15)^2}{4} = 624 \text{ sq in.} \quad (87)$$

The ratio of A_i to A_e is:

$$\frac{A_i}{A_e} = \frac{624}{80} = 7.8 \quad (88)$$

This compares with the desired ratio of 7.

3. AVERAGE PRESSURE DIFFERENCE OF 0.20 IN. OF WATER

The velocity, diameter, area, and flow volume of the pipe are:

$$\text{Velocity in pipe} = 2300 \text{ fpm} = 38.3 \text{ fps} \quad (89)$$

$$\text{Diameter of pipe} = 8\text{-}15/16 \text{ in.} = 8.9375 \text{ in.} \quad (90)$$

$$\text{Area of pipe} = \frac{\pi D^2}{4} = \frac{3.1416(8.9375)^2}{4} = 62.6 \text{ sq in.} \quad (91)$$

Flow volume per second = mean velocity times area

$$= 38.3\left(\frac{62.6}{144}\right) = 16.69 \text{ cfs through pipe and system} \quad (92)$$

To calculate velocity (V) through the roof exit based on the pressure differential (ΔP) across the roof:

$$\Delta P = \frac{1}{2}\rho V^2 = \frac{1}{2}0.002378V^2 = 0.2 \text{ in. water}$$

$$= 0.001189V^2 = 0.2\left(\frac{62.4}{12}\right) \quad (93)$$

$$V^2 = \frac{1.04}{0.001189} = 875 \quad (94)$$

$$V = 29.6 \text{ fps} \quad (95)$$

The roof exit area (A_e) is based on volume through the system and velocity through the roof:

$$A_e = \frac{\text{Volume}}{V} = \frac{16.69}{29.6} = 0.564 \text{ sq ft or } 80 \text{ sq in.} \quad (96)$$

The measured inlet area (A_i) is:

$$A_i = 624 \text{ sq in.} \quad (97)$$

APPENDIX IV

The ratio of A_i to A_e is:

$$\frac{A_i}{A_e} = \frac{624}{81} = 7.7 \qquad (98)$$

This compares favorably with the desired ratio of 7.

APPENDIX V

FABRICATION TECHNIQUES FOR PARASONIC PARACHUTES

This appendix presents the approach used to construct the coated mesh roof of the SP-3, SP-4, and SP-5 PARASONIC parachutes.

Calculated thermal dynamic requirements necessitated that the roof mesh be made of 0.100-in.-diameter Nomex coated with 0.25 in. thick Dyna-Therm D-65. The resulting thickness of the roof structure, as compared to that of the skirt fabric, meant that normal sewing methods would not suffice. Gore-to-gore attachments also imposed unique problems in sewing the thick mesh together.

After several efforts to obtain efficiently sewn seams between the roof and skirt, the roof and cap, and the roof gores, it was concluded that sewing would result in a stiff, lumpy roof. Therefore, other approaches were investigated. These included weaving separate gores and weaving the roof as a unit.

Weaving the roof as a unit provided the most flexible flight units. The following procedure was used: The weaving pattern was laid out to obtain a bias pattern in each gore. A predetermined weaving path was then followed to minimize the number of joints (see Figure 44). The weaving pattern required each of 33 lengths of webbing to pass completely around the roof in a zig-zag path and then be sewed to itself. The 33 joints were distributed so that no more than three occurred in one gore. The webbing length paths were: (1) Numbers 1-4 pass from the gore around a webbing hoop at the roof cap to form a finished edge; (2) Numbers 5-13 and 25-33 pass from gore edge to gore edge and change direction at the gore edge; and (3) Numbers 14-24 pass from the gore around a webbing hoop at the mouth of the roof to form a finished edge.

A weaving fixture was used to aid in fabricating and accurately positioning the mesh webbing during weaving. Pegs were located at all gore-to-gore webbing intersections. The fixture was developed by cutting out 12 stiffened gore patterns and attaching them together along the radial centerlines. Because of the fullness in gore widths, a saddle shaped surface was created. The surface was rigidized by backing it with foam. Since the surface of the fixture was convex, the mesh webbing laid against the surface was true length.

To facilitate weaving, only light coats of D-65 were applied to the mesh webbing before the weaving began. When the weaving was completed, sewing between the mesh and the hoops located the mesh webbing. Additional coats were applied to obtain the required porosity.

The weaving approach provided structural continuity to the roof mesh at the cap and skirt. The major structural loads between the roof and skirt cloth were carried by sewing through the roof mouth webbing hoop and the skirt cloth. Gore-to-gore loads generally were carried by the webbing of one gore interlocking with the webbing of the adjacent gore. Sewing between the radials and the gores maintained the woven positions and carried a portion of the load.

APPENDIX V

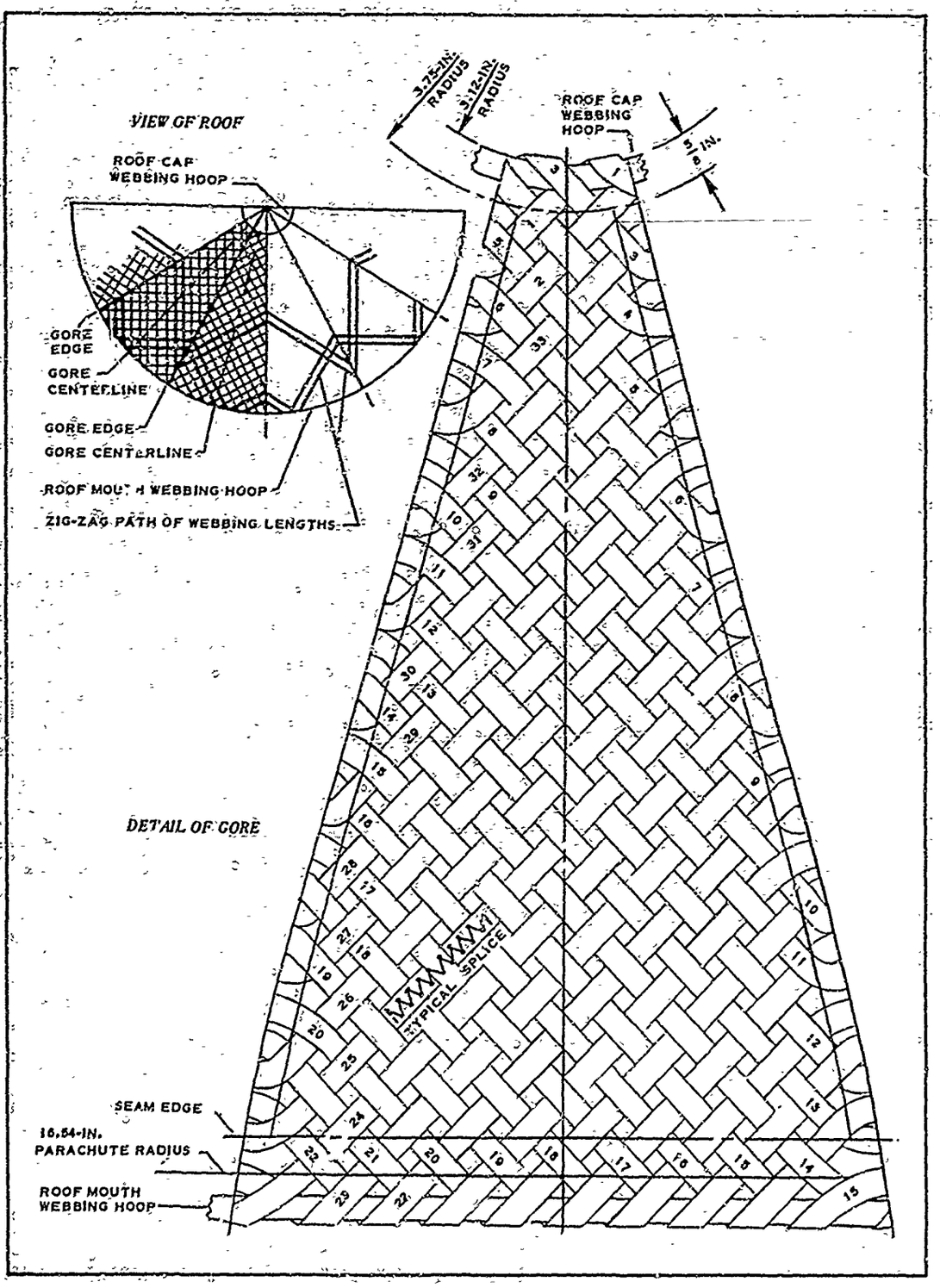

Figure 44 - Gore Weaving Pattern

LIST OF REFERENCES

1. Nebiker, F. R.: Aerodynamic Deployable Decelerator Performance-Evaluation Program. ADDPEP Phase I Technical Report. AFFDL-TR-65-27. Wright-Patterson Air Force Base, Ohio, Air Force Flight Dynamics Laboratory, Research and Technology Division, Air Force Systems Command, prepared by Goodyear Aerospace Corporation, Akron, Ohio, under Contract AF33(657)-10955, May 1965.

2. Bloetscher, F.: Aerodynamic Deployable Decelerator Performance-Evaluation Program. ADDPEP Phase II Technical Report. AFFDL-TR-67-25. Wright-Patterson Air Force Base, Ohio, Air Force Flight Dynamics Laboratory, Research and Technology Division, Air Force Systems Command, prepared by Goodyear Aerospace Corporation, Akron, Ohio, under Contract AF33(615)-1513, April 1967.

3. Trachta, G. S.: Supersonic Parachutes - LP-7. DR-N-8771. White Sands Missile Range, N.M., U.S. Army, 25 March 1966.

4. Trachta, G. S.: Supersonic Parachutes - LP-7. DR-N-8698. White Sands Missile Range, N.M., U.S. Army, 8 March 1966.

5. Trachta, G. S.: Supersonic Parachutes - LP-8. DR-N-8796. White Sands Missile Range, N.M., U.S. Army, 7 April 1966.

6. Trachta, G. S.: Supersonic Parachutes - LP-8, Volumes 3 and 6. DR-N-8797. White Sands Missile Range, N.M., U.S. Army, 4 April 1966.

7. McCracken, S. L.: Supersonic Parachutes - LP-9. DR-N-8871. White Sands Missile Range, N.M., U.S. Army, 26 April 1966.

8. Martinelli, E.: Supersonic Parachutes - LP-9, Volumes 1, 2, and 3. DR-N-8856. White Sands Missile Range, N.M., U.S. Army, 21 April 1966.

9. Deitering, J. S.: Wind Tunnel Investigation of Flexible Parachute Model Characteristics at Mach Numbers 1.5 to 5. AEDC-TDR-63-263. Arnold Air Force Station, Tenn., Arnold Engineering Development Center, Air Force Systems Command, January 1964.

10. Lowry, J. F.: Aerodynamic Characteristics of Various Types of Full Scale Parachutes at Mach Numbers from 1.8 to 3.0. AEDC-TDR-64-120. Arnold Air Force Station, Tenn., Arnold Engineering Development Center, Air Force Systems Command, June 1964.

11. Deitering, J. S.; and Hilliard, E. E.: Wind Tunnel Investigation of Flexible Aerodynamic Decelerator Characteristics at Mach Numbers 1.5 to 6. AEDC-TR-65-110. Arnold Air Force Station, Tenn., Arnold Engineering Development Center, Air Force Systems Command, June 1965.

12. Adkisson, B. N.: Supersonic Parachutes - LP-3. DR-N-7296. White Sands Missile Range, N.M., U.S. Army, 1 March 1965.

LIST OF REFERENCES

13. Adkisson, B. N.: Supersonic Parachutes - LP-3. DR-N-7294 and Addendum. White Sands Missile Range, N.M., U.S. Army, 17 March 1965.

14. Adkisson, B. N.: Supersonic Parachutes - LP-4. DR-N-7350. Vol I and II. White Sands Missile Range, N.M., U.S. Army, 15 March 1965.

15. Adkisson, B. N.: Supersonic Parachutes - LP-4. DR-N-7323. White Sands Missile Range, N.M., U.S. Army, 5 March 1965.

16. Martinelli, E.: Supersonic Parachutes - LP-5. DR-N-7423. White Sands Missile Range, N.M., U.S. Army, 2 April 1965.

17. Martinelli, E.: Supersonic Parachutes - LP-5. DR-N-7394. White Sands Missile Range, N.M., U.S. Army, 26 March 1965.

18. Binder, R. C.: Fluid Mechanics. New York, Prentice-Hall, Inc., 1949.

19. [illegible] ASD [illegible] Air Force [illegible] Command, [illegible] L.

20. Reichenau, David E. A.: Aerodynamic Performance of Various Hyper-flo and Hemisflo Parachutes at Mach Numbers from 1.8 to 3.0. AEDC-TR-65-57. Arnold Air Force Station, Tenn., Arnold Engineering Development Center, Air Force Systems Command, March 1965.

21. Nickel, W. E.; and Sims, L. W.: Study and Exploratory Free-Flight Investigation on Deployable Aerodynamic Decelerators Operating at High Altitudes and at High Mach Numbers. FDL-S-TDR-64-35. Wright-Paterson Air Force Base, Ohio, Air Force Flight Dynamics Laboratory, Research and Technology Division, Air Force Systems Command, July 1964.

22. Deitering, J. S.: Performance of Flexible Aerodynamic Decelerator at Mach Numbers from 1.5 to 6. AEDC-TDR-63-119. Arnold Air Force Station, Tenn., Arnold Engineering Development Center, Air Force Systems Command, July 1963.

23. MacLanahan, D. A., Jr: An Investigation of Various Types of Decelerators at Mach Number 2.8. AEDC-TR-66-136. Arnold Air Force Station, Tenn., Arnold Engineering Development Center, Air Force Systems Command, July 1966.

24. Mirels, H.: Theoretical Wave Drag and Lift of Thin Supersonic Ring Airfoils. NACA-TN-1678. 1948.

25. Boren, T. C.; and Hatalsky, W.: Jet Effects upon Base Drag. Pomona, Calif., General Dynamics Corporation.

26. NACA-R-1135: Equations, Tables, and Charts for Compressible Flow. Moffet Field, Calif., Ames Research Staff, 1953.

LIST OF REFERENCES

27. Federson, P. R.: Study of Parachute Performance and Design Parameters for High Dynamic Pressure Operation. FDL-TDR-64-66. Wright-Patterson Air Force Base, Ohio, Air Force Flight Dynamics Laboratory, Research and Technology Division, Air Force Systems Command, May 1964.

28. Reichenau, David E. A.: Investigation of Various Full-Scale Parachutes at Mach Number 3.0. AEDC-TR-65-241. Arnold Air Force Station, Tenn., Arnold Engineering Development Center, Air Force Systems Command, December 1965.

29. GER-11317: Analysis and Design of Hyperflo Test Item SP-3 (ADDPEP). Akron, Ohio, Goodyear Aerospace Corporation, November 1963.

30. GER-11279: Analysis and Design of BALLUTE Test Item B-1 (ADDPEP). Akron, Ohio, Goodyear Aerospace Corporation, October 1963.

31. GER-10770: The Application of Isotensoid Membranes to the Design of Inflatable Drag Bodies. Akron, Ohio, Goodyear Aerospace Corporation, July 1962.

32. Haak, E. L.; and Niccum R. J.: The Effects of Mass Accommodation on Shock Wave Stability for Ribbon Parachutes in Supersonic Flow. Houston, Tex., AIAA Aerodynamic Deceleration Systems Conference, September 1966.

33. Bartz, D. F.: A Simple Equation for Rapid Estimation of Rocket Nozzles Convective Heat Transfer Coefficient. Pasedena, Calif., Jet Propulsion Laboratory, January 1957, pp. 49-51.

34. GER-11415: Analysis and Design of Hyperflo Test Item SP-5 (ADDPEP). Akron, Ohio, Goodyear Aerospace Corporation, January 1964.

(Reverse is blank)

UNCLASSIFIED
Security Classification

DOCUMENT CONTROL DATA - R&D

(Security classification of title, body of abstract and indexing annotation must be entered when the overall report is classified)

1. ORIGINATING ACTIVITY (Corporate author) Goodyear Aerospace Corporation Akron, Ohio	2a. REPORT SECURITY CLASSIFICATION UNCLASSIFIED 2b. GROUP

3. REPORT TITLE
Aerodynamic Deployable Decelerator Performance-Evaluation Program, Phase II

4. DESCRIPTIVE NOTES (Type of report and inclusive dates)
Final Report, Phase III, April 1965 to July 1967

5. AUTHOR(S) (Last name, first name, initial)
Bloetscher, Frederick
Arnold, William V.

6. REPORT DATE October 1967	7a. TOTAL NO. OF PAGES 130	7b. NO. OF REFS 34
8a. CONTRACT OR GRANT NO. AF33(615)-2541 b. PROJECT NO. 5065 c. Task No. 606507 d.	9a. ORIGINATOR'S REPORT NUMBER(S) GER-12909 9b. OTHER REPORT NO(S) (Any other numbers that may be assigned this report) AFFDL-TR-67-60	

10. AVAILABILITY/LIMITATION NOTICES
This document is subject to special export controls, and each transmittal to foreign governments or foreign nationals may be made only with prior approval of the Air Force Flight Dynamics Laboratory.

11. SUPPLEMENTARY NOTES	12. SPONSORING MILITARY ACTIVITY Air Force Flight Dynamics Laboratory Wright-Patterson AFB, Ohio 45433

13. ABSTRACT

The Aerodynamic Deployable Decelerator Performance-Evaluation Program (ADDPEP) has aimed to advance the state of the art by developing the most effective analytical and empirical techniques for designing aerodynamic deployable decelerators and for evaluating these engineering techniques through wind-tunnel and free-flight tests. During the third and concluding phase of ADDPEP, two types of decelerators were investigated: large reefed supersonic parachutes and small supersonic parachutes. The areas investigated by tests included analytical and engineering design methods, material capabilities, and fabrication techniques.

Three large parachutes were built that had the same basic configuration: hemisflo, 16-ft diameter canopy, 10-percent extended skirt, 10-percent porosity. These parachutes were designed for 200,000-lb opening loads. Free-flight tests were performed at deployment Mach numbers of 2.22, 1.20 and 2.70; at altitudes of 18,050, 9,370, and 19,700 ft; and at dynamic pressures of 3697, 1514, and 5155 psf, respectively. The tests confirmed the predicted drag area. However, reefing line loads were underestimated; improved analytical methods are needed to predict this hoop-type load under dynamic conditions at the higher Mach numbers.

Three small parachutes were built that had the same basic configuration, designated PARASONIC: 4-ft-diameter, 5-percent total porosity. Wind-tunnel tests confirmed that this PARASONIC design, when constructed of materials that are compatible with the flight environments investigated, has better stability than a HYPERFLO design that was also investigated in both Phases I and III. Free-flight tests were performed at deployment Mach numbers of 2.70, 1.60, and 5.48; at altitudes of 78,000, 56,300, and 117,000 ft; and at dynamic pressures of 329, 328, 229 psf, respectively. The flight tests confirmed the stability predictions and the adequacy of the construction for the performance range investigated.

This document is subject to special export controls, and each transmittal to foreign governments or foreign nationals may be made only with prior approval of the Air Force Flight Dynamics Laboratory.

DD FORM 1 JAN 64 1473

UNCLASSIFIED
Security Classification

UNCLASSIFIED
Security Classification

14. KEY WORDS	LINK A		LINK B		LINK C	
	ROLE	WT	ROLE	WT	ROLE	WT
Supersonic Decelerators High Dynamic Pressure Supersonic Parachutes Supersonic Parachutes "PARASONIC" Parachutes Aerodynamics Aerodynamic Heating						

INSTRUCTIONS

1. ORIGINATING ACTIVITY: Enter the name and address of the contractor, subcontractor, grantee, Department of Defense activity or other organization *(corporate author)* issuing the report.

2a. REPORT SECURITY CLASSIFICATION: Enter the overall security classification of the report. Indicate whether "Restricted Data" is included. Marking is to be in accordance with appropriate security regulations.

2b. GROUP: Automatic downgrading is specified in DoD Directive 5200.10 and Armed Forces Industrial Manual. Enter the group number. Also, when applicable, show that optional markings have been used for Group 3 and Group 4 as authorized.

3. REPORT TITLE: Enter the complete report title in all capital letters. Titles in all cases should be unclassified. If a meaningful title cannot be selected without classification, show title classification in all capitals in parenthesis immediately following the title.

4. DESCRIPTIVE NOTES: If appropriate, enter the type of report, e.g., interim, progress, summary, annual, or final. Give the inclusive dates when a specific reporting period is covered.

5. AUTHOR(S): Enter the name(s) of author(s) as shown on or in the report. Enter last name, first name, middle initial. If military, show rank and branch of service. The name of the principal author is an absolute minimum requirement.

6. REPORT DATE: Enter the date of the report as day, month, year, or month, year. If more than one date appears on the report, use date of publication.

7a. TOTAL NUMBER OF PAGES: The total page count should follow normal pagination procedures, i.e., enter the number of pages containing information.

7b. NUMBER OF REFERENCES: Enter the total number of references cited in the report.

8a. CONTRACT OR GRANT NUMBER: If appropriate, enter the applicable number of the contract or grant under which the report was written.

8b, 8c, & 8d. PROJECT NUMBER: Enter the appropriate military department identification, such as project number, subproject number, system numbers, task number, etc.

9a. ORIGINATOR'S REPORT NUMBER(S): Enter the official report number by which the document will be identified and controlled by the originating activity. This number must be unique to this report.

9b. OTHER REPORT NUMBER(S): If the report has been assigned any other report numbers *(either by the originator or by the sponsor)*, also enter this number(s).

10. AVAILABILITY/LIMITATION NOTICES: Enter any limitations on further dissemination of the report, other than those imposed by security classification, using standard statements such as:

(1) "Qualified requesters may obtain copies of this report from DDC."

(2) "Foreign announcement and dissemination of this report by DDC is not authorized."

(3) "U. S. Government agencies may obtain copies of this report directly from DDC. Other qualified DDC users shall request through _____."

(4) "U. S. military agencies may obtain copies of this report directly from DDC. Other qualified users shall request through _____."

(5) "All distribution of this report is controlled. Qualified DDC users shall request through _____."

If the report has been furnished to the Office of Technical Services, Department of Commerce, for sale to the public, indicate this fact and enter the price, if known.

11. SUPPLEMENTARY NOTES: Use for additional explanatory notes.

12. SPONSORING MILITARY ACTIVITY: Enter the name of the departmental project office or laboratory sponsoring *(paying for)* the research and development. Include address.

13. ABSTRACT: Enter an abstract giving a brief and factual summary of the document indicative of the report, even though it may also appear elsewhere in the body of the technical report. If additional space is required, a continuation sheet shall be attached.

It is highly desirable that the abstract of classified reports be unclassified. Each paragraph of the abstract shall end with an indication of the military security classification of the information in the paragraph, represented as *(TS)*. *(S)*. *(C)*. *or (U)*

There is no limitation on the length of the abstract. However, the suggested length is from 150 to 225 words.

14 KEY WORDS: Key words are technically meaningful terms or short phrases that characterize a report and may be used as index entries for cataloging the report. Key words must be selected so that no security classification is required. Identifiers, such as equipment model designation, trade name, military project code name, geographic location, may be used as key words but will be followed by an indication of technical context. The assignment of links, rules, and weights is optional